論文 / 著書情報
Article / Book Information

題目(和文)	高力ボルト摩擦接合継手の耐荷性能評価における不確定要因の定量化
Title(English)	Quantification of uncertain influential parameters affecting structural performance evaluation of high strength bolted friction joints
著者(和文)	平尾賢生
Author(English)	Kensho Hirao
出典(和文)	学位:博士（工学）, 学位授与機関:東京工業大学, 報告番号:甲第12218号, 授与年月日:2022年9月22日, 学位の種別:課程博士, 審査員:佐々木 栄一,廣瀬 壮一,岩波 光保,千々和 伸浩 ,WIJEYEWICKREMA ANIL,伊藤 裕一,小林 裕介,鈴木 啓悟
Citation(English)	Degree:Doctor (Engineering), Conferring organization: Tokyo Institute of Technology, Report number:甲第12218号, Conferred date:2022/9/22, Degree Type:Course doctor, Examiner:,,,,,,,
学位種別(和文)	博士論文
Type(English)	Doctoral Thesis

Doctoral Dissertation

Quantification of Uncertain Influential Parameters Affecting Structural Performance Evaluation of High Strength Bolted Friction Joints

Tokyo Institute of Technology

Department of Civil Engineering

Supervised by Professor Eiichi SASAKI and Professor Yuichi ITO

Kensho HIRAO

Contents

List of Figures

Chapter 1: Introduction

Chapter 2: Analytical Study on Effect of Uncertain Parameters in Structural Performance

Chapter 3: Establishment of Non-Destructive Bolt Axial Force Measurement

Chapter 4: Evaluation of Faying Surface Contact Condition

List of Tables

List of Symbols

A_t	Real contact area [mm^2]
C	Ultrasonic velocity in materials [$\mathrm{mm}/\mu\mathrm{s}$]
C_r	Chirp ratio
d	Diameter of the bolt [m]
d_h	Bolt hole diameter [mm]
E	Young's modulus
F	Bolt axial force [N], [kN]
F_l^R	Parasitic filter of real part
F_l^I	Parasitic filter of imaginary part
k	Torque coefficient
L	Bolt length [mm]
M	Dimensional space
m	Number of faying surfaces
N_0	Design bolt axial force [kN]
n	Number of bolts
n_w	Number of waves
P_{l-1}^R	Real part
P_{l-1}^I	Imaginary part
$P_{\bar{y}}$	Average yield pressure [N/mm^2]
p	Bolt pitch [mm]
R	Frequency ratio
R_s	Design Slip resistance [kN]
R_y	Design Yield resistance [kN]
r	Bolt hole diameter [mm]

T	Tightening torque [N · m]
T_p	Ultrasonic propagation time inside the probe (one way) [μs]
T_u	Ultrasonic propagation time (one way) [μs]
T_B	Base plate thickness [mm]
T_S	Splice plate thickness [mm]
t	Steel plate thickness [mm]
t_1	Time [μs]
υ	Ultrasonic velocity [mm/μs]
W	Steel plate width [mm]
W_v	Vertical force [N]
β	Ratio of design slip resistance to design yield resistance
β_0	Constant term
β_m	Partial regression coefficient
Δ_n	n raps time [μs]
Δ_{TOF}	Time of Flight [μs]
μ	Slip coefficient
μ_0	Design slip coefficient
ρ	Density in the material [g/mm^3]
σ_y	Yield stress [N/mm^2]
ψ^R	Real signal mother wavelet

Acknowledgements

I would like to express my sincere gratitude to my supervisor, Associate Professor Eiichi Sasaki, for his kind support, advice and encouragement. I would like to thank my advisor, Associate Professor Eiichi Sasaki, for his enthusiastic guidance, extremely constructive criticism, and kind advice throughout my research.

I would also like to express my sincere gratitude to my associate advisor, Specially Appointed Professor Yuichi Ito, for his kind support and encouragement. His appropriate advice from the perspective of a person with field experience helped me a lot in my research.
I am always amazed by their attitude toward research, and I would like to learn from them and apply it to my future research life.

I would also like to express my sincere gratitude to Specially Appointed Associate Professor Kouichi Takeya, Assistant Professor Ayako Akutsu, and Postdoctoral Researcher Porjan Tuttipongsawat for their kind support and advice. I would like to express my deepest gratitude to them for their kind support and advice. They have always been there for me, and they have provided me with a wealth of knowledge and advice from their experience in the doctoral program.

I would also like to thank Adjunct Associate Professor Yusuke Kobayashi, Associate Professor Hiroshi Tamura, Dr. Atsushi Tanabe, and Dr. Hisatada Suganuma for their accurate advice and kind encouragement. I would also like to thank Adjunct Associate Professor Yusuke Kobayashi, Associate Professor Hiroshi Tamura I would also like to express my sincere gratitude to them for their sincere and constructive comments on many issues related to this research. I am also very grateful to Ms. Ishihara for her help in other aspects of my research. She helped me with many administrative tasks.

I have been indebted to Associate Professor Keigo Suzuki at the University of Fukui since I was an undergraduate student. I would like to express my deepest gratitude to him for his willingness to accept me for my experiments at the University of Fukui.
I would also like to express my gratitude to the graduates of Sasaki Laboratory: Dr. Hiroshi Iwabuki, Dr. Natdanai Sinsamutpadung, Dr. Cao, Dr. Piseth Doung, Dr. Sanzma Vazracharya,

and Mr. Ando for their many advices. I would like to express my gratitude to all of them. In particular, I would like to express my sincere gratitude to those who were international students for their language support.

I spent a lot of time with my classmates Mr. Iizuka, Ms. Irie, and Mr. Mishima. We competed and helped each other in a good way, which enriched my research life.

I would like to thank Ms. Rodthong, Mr. Keerthi, Mr. Isozumi, and Mr. Hirai, my junior students in Sasaki Lab, for their support in my research and experiments. It was also a good experience for me to help them with their research.

I am also very grateful to Ms. Scorupski for her advice on English.

Finally, I would like to thank my father, mother and grandmother, Mr. Noriaki Hirao, Ms. Hitomi Hirao and Ms. Mieko Hirao for their understanding and support over the years.

Abstract

Steel structures maintenance is a topic that is gaining more and more significance in the field of civil engineering. The structural performance of high strength bolted friction joints used in steel structures is expected to decrease due to various effects during service, and it is necessary to accurately evaluate the structural performance of bolted joints. However, it is difficult to evaluate the structural performance of bolts in existing joints due to uncertain influential parameters such as variations in bolt axial forces, misalignment between washers and bolts in bolt holes and faying surface contact conditions. Therefore, in this study, the effects of uncertain influential parameters on the structural performance of bolted joints were first clarified. Next, by combining ultrasonic measurements, signal processing and machine learning, a quantitative evaluation method was proposed for the bolt axial force and the faying surface contact condition, which have the greatest influence on the structural performance of bolted joints.

Keywords*: bolt axial force, faying surface contact condition, high strength bolted friction joint, structural performance, ultrasonic testing*

Chapter 1
Introduction

1.1. Background

The joining methods for steel bridges are riveted joints, welded joints, and high strength bolted joints, and riveted joints were applied until the late 1950s [1, 2]. Since JIS1186 on high-strength bolts for friction joints was established in 1964, high-strength bolted friction joints have rapidly replaced riveted joints [3]. When using a bolt joint, the surface treatment of the faying surface was initially a rough surface without mill scale. Inorganic zinc-rich paint has been applied to the faying surface since the 1990s [4, 5]. Nowadays, there are bridges with high strength bolted joints that have been erected for 50 years. Some cases have been observed where the structural performance of bolted joints has been compromised by earthquakes [6]. In **Figure 1.1**, slipping was occurred at the splice plate of the bolted joint. In **Figure 1.2**, peeling was confirmed at the splice plate of the bolted joint, which is considered to have caused the slip. The structural performance evaluation of the bolted joints is considered to be indispensable for the structural performance evaluation of the entire bridge.

Thus, there is a need to accurately evaluate the structural performance of bolted joints with uncertain influential parameters for the maintenance of steel bridges. The uncertain influential parameters of bolted joints include the bolt axial force, the faying surface contact condition, displacement of bolts and washers, joint geometry (dimensions, over-sized bolt holes, bolt arrangement), bolt shape, elapsed time, and type of load (tension, compression [7], bending, shear) [8].

Current bolted joints are designed with slip occurrence as the ultimate limit state [9]. For this reason, slip resistance has been adopted as an important index of the structural performance of bolted joints. The slip resistance R_s is described by

$$R_s = N_0 \cdot \mu_0 \cdot m \cdot n \tag{1-1}$$

where, N_0 is the design bolt axial force, μ_0 is the design slip coefficient, m is number of faying surfaces, and n is number of bolts. Hence, since the number of faying surfaces m and the number of bolts n are clear, it can be seen that the important parameters for evaluating the slip resistance are the bolt axial force and the slip coefficient. The formula for calculating the slip resistance is very simple. However, in reality, many more parameters may be involved in the slip resistance because the bolted joints contain uncertain influential parameters.

Amonton-Coulomb Friction Law [10] defines that “the faying surface is independent of the apparent contact surface”, but recent research results have shown that there are exceptions to this law, with small slip occurring before the slip load is reached [11]. For the cases that are exceptions, the effect of uncertain parameters is considered to be particularly significant. Although many studies have been reported on the uncertain influential parameters of bolted joints, there are few considerations on structural performance evaluation that consider methods for quantitatively evaluating uncertain influence parameters.

The bolt axial force is affected by the variation of the introduced bolt axial force depending on the tightening method [12, 13], loosening of bolts tightened in the first half of the tightening order [14, 15], relaxation due to initial loosening [16, 17], and the effects of vibration and earthquake [18-21]. It has been reported that the bolt axial force may decrease after service due to the effects described above [22-27]. It has been confirmed that the slip coefficient depends on the skin clearance of the contact surface [28], filler plate [29], over-sized bolt holes [30, 31], multi-row arrangement of bolts [32-35], and the condition of the faying surface treatment [36-39]. In other words, the actual parameters of each bolted joints are difficult to monitor due to the setting condition of bolted joints, age, and earthquake among other things. In particular, recently, inorganic zinc-rich paint has been increasingly applied to faying surfaces, which increases the number of uncertain parameters about the faying surface contact condition. Therefore, it is required to develop a measurement method for existing bolt joints coated with inorganic zinc-rich paint that takes these uncertain influential parameters into consideration.

Many studies have proposed several evaluation methods using NDT [40-54]. However, many of them are not compatible with bolts in existing joints and applicability remains a problem. Accordingly, this study proposes an evaluation method for existing bolts by extracting characteristic signals that show invariant phenomena with few individual differences. Characteristic signals are extracted by applying signal processing to the measurement data.

On the other hand, in recent years, several studies have been conducted in the field of civil engineering to evaluate defects and loosening of the bolt axial force by applying machine learning using measured waveforms, captured images, and features as training data [55-62]. In machine learning, algorithms need to be selected appropriately according to the application, for example, decision tree [55, 63], random forest [56, 64], neural network (NN) [57-61, 65-69], and support vector machine (SVM) [70, 71] have been applied. In the evaluation of the bolt axial force by the

impact acoustics method, there is a report [62] that compared several algorithms. However, the evaluation method of the bolt axial force by combining ultrasonic waves and machine learning has not been established so far.

Therefore, in this study, the uncertain influential parameters in bolted joints were first clarified on the basis of analysis. Next, a quantitative evaluation method for the uncertain influential parameters, bolt axial force and faying surface contact condition, was proposed by combining ultrasonic testing, signal processing and machine learning. Evaluation methods with high accuracy, practicality, and applicability to bolts in existing joints was considered.

1.2. Related Research

This study targets uncertain influential parameters that are difficult to see and whose current condition cannot be clearly ascertained. Hence, the parameters influencing the structural performance of bolted joints were clarified. These parameters were evaluated quantitatively. In such a case, the structure must not be destroyed in practice. For this reason, the use of ultrasonic waves for NDT was proposed. In addition, the application of signal processing was considered to extract invariant characteristic signals from the ultrasonic data measured to evaluate uncertain parameters. As the waveform data extracted by signal processing contains minute characteristic signals that cannot be evaluated by humans, the application of machine learning was attempted. Therefore, NDT, signal processing and machine learning, which have attracted much attention in recent years, were considered through the following related research. Based on these methods, original evaluation methods were constructed.

1.2.1. Effect of Uncertain Influence Parameters on Structural Performance of Bolted Joints

There are various uncertain influential parameters that affect the structural performance of bolted joints. At present, the structural performance evaluation of bolted joints has not been established considering the uncertain influential parameters included in bolted joints. Hence, in order to evaluate the structural performance of bolted joints, many studies have been reported investigating uncertain influential parameters of bolted joints. In addition, most of the studies are

on the bolt axial force or the slip coefficient, which are considered to affect the slip resistance. In the following, some of these studies will be introduced.

Nishimura et al. [12] proved that the introduced bolt axial force varied depending on the tightening method of the bolts for the bolted joints used in actual construction sites. It was also clarified that the variation of the bolt axial force was caused by the tightening position of the upper and lower flanges and web. It is also reported that the bolt axial force varies depending on the order in which the bolts are tightened. You et al. [14] found that the bolt axial force varied depending on the tightening order of the bolts based on the design codes for bolt tightening order in Europe, China and the United States (**Figure 1.3**) for bolted joints arranged in a 4 by 4 arrangement. Due to the effect of relaxation, the bolt axial force decreases rapidly after the bolt is tightened. Minami et al. [16] and Abid et al. [17] experimentally investigated the residual bolt axial force after bolt tightening and showed the residual bolt axial force for each elapsed time after bolt tightening. As a result, Minami [16] et al. recommended that the initial value of the bolt axial force should be set at 3 seconds after bolt tightening in the bolt relaxation test. Ishihara et al. [18] investigated the bolt axial force of bolted joints damaged by the 1995 Southern Hyogo Prefecture Earthquake. As a result, it was reported that the bolt axial force was reduced by 10-30% from the design bolt axial force. In addition, cyclic slip experiment on bolted joints was conducted, and it was shown that the bolt axial force and slip coefficient decreased with increasing cycle number in the case of inorganic zinc-rich paint surface treatment. In order to improve the slip resistance of bolted joints, the number of bolts is increased. On the other hand, it has been shown that the slip coefficient decreases when the number of bolt rows in the loading direction is too large [35]. Besides, research on the slip coefficient [36-38] proposed appropriate design slip coefficients for various types of faying surface treatments, each based on the results of experiments.

1.2.2. Non-Destructive Evaluation Method for Considered Parameter in Bolted Joints

Maintaining the safety of bolted joints is a critical issue that is directly related to the safety of the entire steel structure. However, the condition of looseness of bolts and faying surfaces is difficult to ascertain, and developing a convenient method of monitoring the integrity of bolted joints is important for safe maintenance. Therefore, many studies have been conducted to evaluate the structural performance of bolted joints nondestructively, and methods using ultrasonic waves, impact acoustics, eddy currents, and piezoelectric ceramics have been investigated.

There are many reports that propose a method for evaluating the bolt axial force using the propagation velocity or propagation time of ultrasonic waves. Jhang et al. [41] focused on the relationship between stress and ultrasonic velocity. Since the bolt axial stress due to the introduction of the bolt axial force has a linear relationship with the ultrasonic velocity, the bolt axial force can be evaluated by transmitting ultrasonic waves from the bolt head and receiving them at the bottom of the bolt shank. However, there is no mention of individual differences in the bolts, and further study is needed on the application to existing bolts. Minakuchi et al. [42], Joshi et al. [43] and Sakai et al. [44] evaluated the bolt axial force considering the high correlation between bolt elongation and the bolt axial force. In these ultrasonic studies, the bolt axial force is evaluated from the time of flight (TOF) between the case of no bolt axial force (0kN) and the case of introducing the bolt axial force (**Figure 1.4**). The υ in **Figure 1.4** is the ultrasonic velocity. However, it is necessary to measure the TOF of each target bolt before the bolt axial force is introduced because the initial length of the bolt varies due to manufacturing errors. In addition, the tip of the bolt shank needs to be machined smooth [72], which makes it difficult to use for evaluating the bolt axial force of existing bolts. For the method corresponding to the existing bolts, Takahashi et al. [45] focused on the fastening force between the bolt and nut using the ultrasonic transmission method. Measurements were made with two probes on the nut as shown in **Figure 1.5**. In this method, the relationship between the fastening force of the bolt and the magnitude of the transmitted ultrasonic pulse is determined in advance, allowing the evaluation of the bolt axial force without initial values. However, two probes need to be installed on the side of the nut, which is difficult to apply in construction sites.

Other studies have been conducted to evaluate the condition of bolted joints by evaluating the faying surface contact condition. Tao et al. [49] propose a simple health monitoring method of bolt joints because the large number of bolts are involved in bolted joints. This is measured by sandwiching steel plates of the bolted joints with the faying surface unpainted between two piezoelectric transducers (PZT). It is reported that it is possible to detect the contact condition and contact pressure between two steel plates by analyzing the amplitude of the measured signal. In the case of impact tests, Hosoya et al. [50] proved by analysis and experiment that a strong correlation occurs between the variation of the bolt axial force and the natural frequency of the bolt/nut assembly for bolts with small diameters. Akutsu et al. [54] focused on the property that eddy currents capture the change in permeability of steel plate due to stress change. Since the stress

at the bolt head changes when the bolt axial force is introduced, an eddy current probe was installed on the bolt head, and the output signal was measured and analyzed to evaluate the bolt axial force.

1.2.3. Signal Processing for the Extraction of Characteristic Signals

Zhang et al. [74] applied the parasitic discrete wavelet transform (P-DWT), which is a conventional discrete wavelet transform (DWT) with a parasitic filter, to abnormal signal detection in cars. It was shown that by defining the parasitic level and designing the parasitic filter, an abnormal signal can be detected without affecting the calculation of the conventional DWT. Tsunoda et al. [75, 76] applied the above P-DWT to ultrasonic measurement waveforms to extract characteristic frequency bands from defects in order to identify concrete intrinsic defects. In this dissertation, the application of a low-frequency parasitic filter to the P-DWT is considered. This enabled the defect part to be imaged.

These research results suggest that the wavelet transform is suitable for extracting characteristic signals from waveform data such as ultrasonic waves. Hence, the authors have previously attempted to apply signal processing to the measured ultrasonic data in order to detect defects in concrete slabs [76]. Here, an own mother wavelet was created from the reflected waves from the defects and the continuous wavelet transform (CWT) using the mother wavelet was considered. It was confirmed that the characteristic signals of the defects could be extracted.

Based on the above, the application of DWT is considered for the extraction of characteristic signals in this dissertation.

1.2.4. Structural Performance Evaluation of Bolt Joints Using Machine Learning

Machine learning has become a technology that has been attracting more and more attention since the 1956 Dartmouth Conference [77, 78]. Recently, the decrease in the number of workers in the construction industry has become a problem, and the use of machine learning is expected in the field of civil engineering in order to solve the shortage of human resources and improve productivity [79]. Therefore, there are many research reports on machine learning for evaluating the structural performance of bolted joints as follows.

Kong et al. [55] proposed a method to evaluate the level of the bolt axial force by tapping the bolts of bolted joints with a hammer. Bolted joints produce a unique sound when excited by the impact of hammer tapping because of the different interfacial properties between the bolt, nut and

steel plate. The sound was discriminated by a decision tree, a machine learning algorithm, to estimate the loosening level of the bolt axial force.

Wang et al. [56] proposed a method to evaluate the overall loosening level of a group of bolts for multi-row bolted joints. PZT patches was attached to each of the splice plate and the base plate of the single-sided friction bolted joint specimen, excited by a linear swept sinusoid wave (frequency range: 30–50kHz) from the PZT patch on the splice plate side, and captured by the PZT patch on the base plate side. A feature set of measured data was fed to a random forest classifier to detect looseness in multi-row bolt joints.

Yuan et al. [57] and Mikami et al. [59] used CNN to quantitatively evaluate the measurement data obtained by hammering the bolts of a bolted joint. Tran et al. [66] focused on the relationship between the real contact area of the bolt head and the guided wave energy lost during the transmission of laser ultrasonic wave. In order to evaluate bolt looseness, the evaluation performance of deep convolutional neural network (DCNN), K-nearest neighbor, support vector regression, and deep artificial neural network for regression were compared. In addition, many studies have applied CNNs to evaluate bolt looseness, which deal with vast amounts of image data, including extended data. Zhao et al. [58], Huynh et al. [60], Zhang et al. [61], Cha et al. [67], applied image data to CNN and reported their results. Similarly, Cha et al. [71] used a combination of image-based method and SVM to evaluate bolt looseness.

As described above, machine learning is often applied to evaluate bolt looseness, however there remains an issue in quantitatively evaluating the bolt axial force and the faying surface contact condition.

1.3. Purpose and Objectives

The aim of this study was to identify uncertain influential parameters affecting the structural performance of high-strength bolted friction joints and to evaluate quantitatively the bolt axial force and faying surface contact condition, which were considered to be the most important. This study focuses on slip resistance, which is one of the indicators of structural performance. For this purpose, firstly, analyses were conducted by varying various parameters in order to identify the uncertain parameters affecting the structural performance of bolted joints. Secondly, a quantitative

evaluation method for bolt axial force, which has a significant effect on the structural performance of bolted joints, was proposed. Here, it is shown that the proposed method can be applied to existing bolts by combining ultrasonic waves, signal processing, and machine learning. Thirdly, in order to evaluate the slip coefficient, which indicates the faying surface contact condition, a method was proposed to evaluate the distribution of contact pressure by combining ultrasonic measurements and machine learning. In addition, the possibility of evaluating the coating thickness of inorganic zinc-rich paint was demonstrated. To achieve the purpose of this research, the three main research objectives considered are as follows:

I. To clarify the effects of bolt axial forces, misalignment of washers and bolts, and faying surface contact conditions on the structural performance of bolted joints by the numerical analysis.
II. To propose a non-destructive evaluation method of bolt axial force of bolted joints by applying machine learning.
III. To propose an evaluation method for contact pressure distribution and coating thickness of inorganic zinc-rich paint.

1.4. Outline of this Dissertation

The research objectives are discussed in three main chapters, Chapters 2 to 4 respectively. Outlines of all chapters are shown below (**Figure 1.6**).

Chapter 1: Introduction

Background, purpose and objectives and related researches have been discussed.

Chapter 2: Analytical Study on Effect of Uncertain Parameters in Structural Performance

Bolted joints contain many uncertain influential parameters that affect their structural performance. This chapter considers the effects of bolt axial forces, misalignment of washers and bolts, and bolted joint faying surface contact conditions on the structural performance of bolted joints. As the effects of these uncertain influential parameters on bolted joints are difficult to

visualise experimentally, numerical analyses were carried out by varying various parameters. The load transfer mechanism, slip resistance and faying surface contact condition were identified in the analysis, and the most important parameters affecting the structural performance of bolted joints - bolt axial forces and faying surface contact condition - are quantitatively evaluated in Chapters 3 and 4.

Chapter 3: Establishment of Non-Destructive Bolt Axial Force Measurement

The most significant parameter affecting the structural performance of bolted joints is considered to be the bolt axial force. However, a method that can evaluate the bolt axial force of an bolts in existing joints coated with inorganic zinc-rich paint with high accuracy has not been established. Therefore, ultrasonic testing from the bolt head was carried out to propose a simpler method of evaluating the bolt axial force in consideration of practicality. By applying the original signal processing technology to the measured waveform, it became possible to extract the characteristic signals. Furthermore, by feeding characteristic signals to machine learning, quantitative evaluation of the bolt axial force became possible.

Chapter 4: Evaluation of Faying Surface Contact Condition

It is extremely difficult to evaluate the faying surface contact condition that affects the structural performance of bolted joints. However, according to the analysis in Chapter 2, the contact pressure distribution affects the structural performance of bolted joints. Therefore, the contact pressure distribution on the faying surface was confirmed by measuring while scanning the ultrasonic probe on the steel plate surface. In addition, ultrasonic testing was conducted to specimens with different coating thicknesses. By analyzing the reflected ultrasonic waves and feeding them into machine learning, it was shown that it is possible to quantitatively evaluate the coating thickness of inorganic zinc-rich paint.

Chapter 5: Conclusion and Recommendations

The results of each chapter are summarized in this chapter. Based on the findings obtained in this study, recommendations are made for the slip coefficients evaluation of bolts in existing joints and for the quantitative structural performance evaluation of bolted joints.

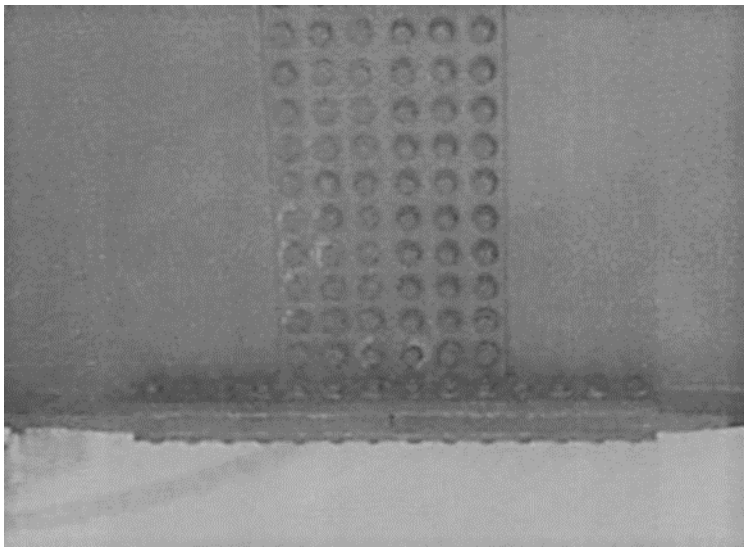

Figure 1.1 Steel bridge with occurred slip at bolted joint

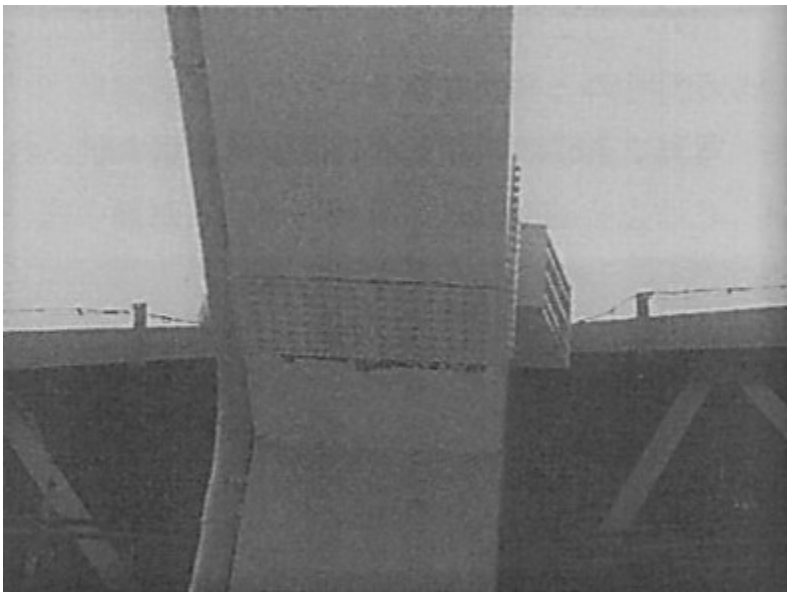

Figure 1.2 Steel bridge with peeling of coating at bolted joint

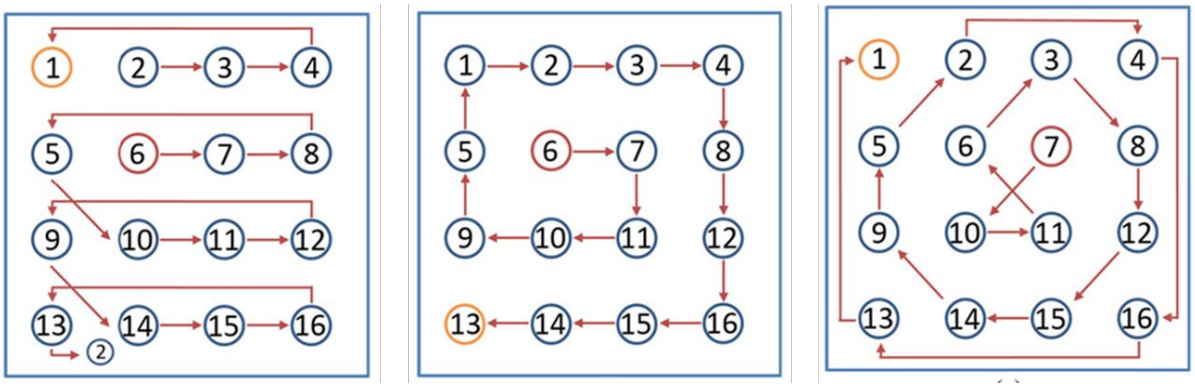

(a) European code (b) Chinese code (c) American code

Figure 1.3 Bolt tightening sequence for each country

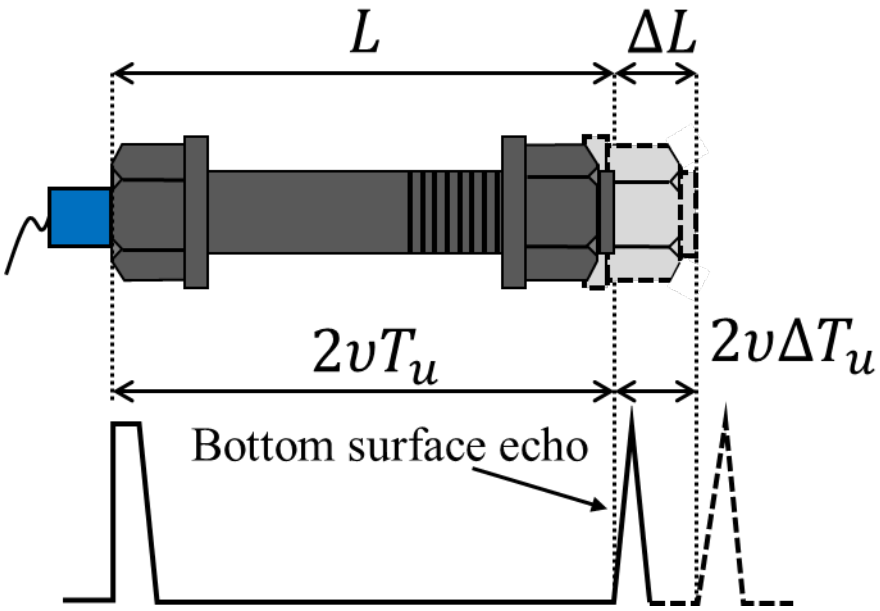

Figure 1.4 Propagation of an ultrasonic wave in a bolt and change of propagation time caused by axial load

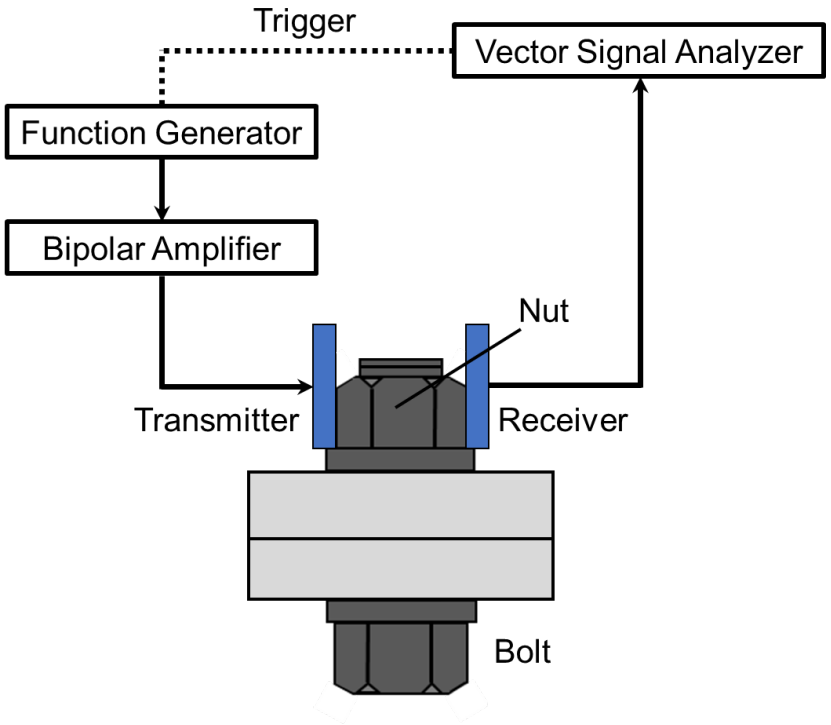

Figure 1.5 Measurement system for fastened condition of bolt-nut

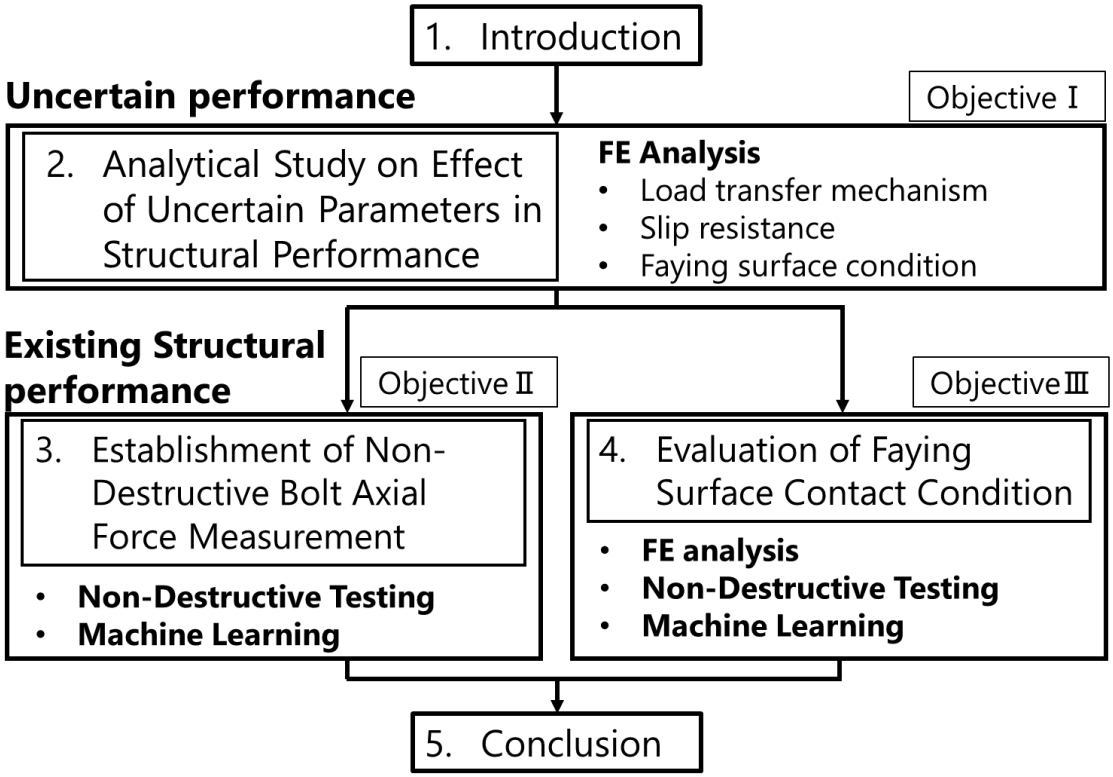

Figure 1.6 Flow of this dissertation

References (Chapter 1)

[1] JSSC: 鋼構造接合資料集成-リベット接合・高力ボルト接合-, 技報堂, 1977.

[2] Hanji, T., Sumi, S., Tateishi, K., Shimizu, M., Nagasaka, Y. and Takebuchi, T.: Mechanical Behavior and Strength Evaluation of Combination Joints Using Rivets and High-Strength Bolts, *Journal of the JSCE A1*, Vol.77, No. 3, pp.489-508, 2021.

[3] Ito, M.: 改訂 鋼構造学, 土木系大学講義シリーズ 11, コロナ社, 2005.

[4] Minami, K.: A Study on Influence of Bolt Axial Force on High Strength Bolted Joints Treated with Zinc-Rich Paint, *Journal of JSCE A1 (Structural Engineering & Earthquake Engineering)*, Vol.74, No.1, pp.58-63, 2018.

[5] Takahashi, S.: Surface Treatment II: Current Situation and Latest Trend of Heavy-Duty Coating, *Journal of the Society of Materials Science*, Vol.67, No.12, pp.1094-1099, 2018.12.

[6] 阪神高速道路公団: 大震災を乗り越えて-震災復旧工事誌-, 1997.9.

[7] Hirao, K., Sasaki, E., Tamura, H., Mitsugi, Y. and Kitane, Y.: 高力ボルト摩擦接合継手の圧縮荷重下の耐荷性能に与える鋼材強度の影響, *JSCE* 第 74 回年次学術講演会, I-421, 2019.9.

[8] Miki, C.: 鋼構造, テキストシリーズ土木工学 10, 共立出版, 2000.

[9] 日本道路協会: 道路橋示方書・同解説-II鋼橋・鋼部材編, 2017.11.

[10] Desplanques, Y.: Amontons-Coulomb Friction Laws, A Review of the Original Manuscript, *SAE International Journal of Materials and Manufacturing*, Vol.8, No.1, pp.98-103, 2015.1.

[11] Matsukawa, H., Otsuki, M. and Nakano, K.: Breakdown of Amontons' Law and the Appearance of New Friction Law due to Local Precursor Slip, *The Surface Science Society of Japan*, Vol.36, No.5, pp.222-229, 2015.

[12] Nishimura, A., Taido, Y., Sera, S., Hozumi, S. and Mitani, T.: On the Scattering of Clamping Forces of High-Strength Bolts in Actual Structural Joints, *Proceedings of the JSCE*, No.180, pp.1-9, 1970.8.

[13] Fukuoka, T. and Takai, T.: Mechanical Behaviors of Bolted Joint During Tightening Using Torque Control, *JSME International Journal Series A Solid Mechanics and Material Engineering*, Vol.41, No.2, pp.185-191, 1998.

[14] You, R., Ren, L. and Song, G.: A Novel Comparative Study of European, Chinese and American Codes on Bolt Tightening Sequence Using Smart Bolts, *International Journal of Steel Structures*, Vol.20, No.3, pp.910-918, 2020.

[15] Wang, Y.Q., Wu, J.K., Liu, H.B. and Xu, S.T.: Modeling and Numerical Analysis of Multi-Bolt Elastic Interaction with Bolt Stress Relaxation, *Proceedings of the Institution of Mechanical Engineers, Part C: Journal of Mechanical Engineering Science*, Vol.230, No.15, pp.2579-2587, 2015.

[16] Minami, K., Tamura, H., Uchida, D., Shirahata, H., Yoshioka, N., Tsutsui, K. and Fujino, D.: A Study on Initial Value Setting Method for Relaxation Tests in High Strength Bolted Joints, *Journal of JSCE A1 (Structural Engineering & Earthquake Engineering)*, Vol.76, No.3, pp.496-509, 2020.

[17] Abid, M., Khalil, M.S. and Wajid, H.A.: An Experimental Study on the Relaxation of Bolts, *IIUM Engineering Journal*, Vol.16, No.1, pp.43-52, 2015.

[18] Ishihara, Y., Kobayashi, G., Minada, O. and Nishimura, N.: Characteristic Investigation and Cyclic Slip Experiment of HSFG Bolted Joints Which were Damaged by Earthquake, *Journal of the JSCE A1*, No.745, I-65, pp.53-64, 2003.10.

[19] Wang, F., Ho, S.C.M. and Song, G.: Monitoring of Early Looseness of Multi-Bolt Connection: A New Entropy-Based Active Sensing Method Without Saturation, *Smart Materials and Structures*, Vol.28, No.10, pp.1-7, 2019.

[20] Marshall, M.B., Lewis, R., Howard, T. and Brunskill, H.: Ultrasonic Measurement of Self-Loosening in Bolted Joints, *Proceedings of the Institution of Mechanical Engineers, Part C: Journal of Mechanical Engineering Science*, 2011.

[21] Jiang, Y., Zhang, M. and Lee, C.H.: A Study of Early Stage Self-Loosening of Bolted Joints, *Journal of Mechanical Design, Transactions of the ASME*, Vol.125, pp.518-526, 2003.

[22] Tanihira, T., Kamei, M., Ishihara, Y. and Taido, Y.: Carrying Capacity Test for Friction Joint of High-Strength Bolt from a Removed Foot-Way Bridge Used Under 17 Years, *JSCE Journal of Structural Engineering*, Vol.36 A, pp.1087-1096, 1990.3.

[23] Kanou, M., Tanihira, T., Ishihara, Y., Kobayashi, G. and Nishio, H.: 高力ボルト軸力の経年変化に関する実験的研究, *JSCE* 第 56 回年次学術講演会, I-B162, pp.324-325, 2001.10.

[24] Ishihara, Y., Kobayashi, G., Kano, M., Kamei, M. and Tanihira, T.: The Influence of Reduction and Variation of Bolt Tensions by Aging on Limit States of HSFG Bolted Joint, *Journal of JSCE*, Vol.763, VI-63, pp.33-42, 2014.6.

[25] Temitope, S.J.: Condition Monitoring of Bolted Joints, Ph.D. *Thesis, University of Sheffield*, Sheffield, UK, 2015.6.

[26] Rafik, V., Combes, B., Daidié, A. and Chirol, C.: Experimental and Numerical Study of the Self-Loosening of a Bolted Assembly, *Advances on Mechanics, Design Engineering and Manufacturing II*, pp.85-94, 2019.

[27] Kikukawa, S., Murata, K. and Nishimura, A.: Secular Changes of Slip Resistance of Friction-Type Bolted Joints in Structural Members, *Kawasaki Steel Giho*, Vol.11, No.4, pp.127-135, 1979.

[28] Takai, T., Yamaguchi, T. and Yamashina, K.: Analytical Study on Influence of Irregularity on Slip Strength of High Strength Bolted Friction Type Joint, *JSCE Journal of Structural Engineering*, Vol.61 A, pp.605-613, 2015.3.

[29] Takai, T., Peng, X. and Yamaguchi, T.: An Analytical Study on Load Carrying Characteristic of High Strength Bolted Friction Type Joint with Thick Filler Plate, *Journal of JSCE A1 (Structural Engineering & Earthquake Engineering)*, Vol.71, No.1, pp.1-9, 2015.

[30] Tanaka, A., Masuda, H., Wakiyama, K., Tsujioka, S., Hirai, K. and Tateyama, E.: Experimental Study on High Strength Bolted Friction Joints with Oversized and Slotted Holes, *JSSC Steel Construction Engineering*, Vol.5, No.20, pp.35-44, 1998.12.

[31] Mori, T., Yamazaki, N. and Yamaguchi, J.: Slip and Yield Resistance of Friction Type of High Strength Bolted Connections with Over-Sized Holes, *Journal of the JSCE*, No.794, I-72, pp.157-169, 2005.7.

[32] Murakoshi, J., Sawada, M., Yamaguchi, T., Peng, X. and Ootake, A.: Slip Resistance Tests of Friction-Type High-Strength Multi Bolted Joints with Coated Contact Surfaces by Inorganic Zinc Rich Paint on Thick Plate, *Journal of JSCE A1 (Structural Engineering & Earthquake Engineering)*, Vol.70, No.1, pp.94-104, 2014.

[33] Peng, X., Yamaguchi, T., Takai, T., Murakoshi, J. and Sawada, M.: FEA Study on the Slip Behavior of High Strength Multi Bolted Friction Type Joints with Thick Plates by Structural

Dimensions, *Journal of JSCE A1 (Structural Engineering & Earthquake Engineering)*, Vol.69, No.3, pp.452-466, 2013.

[34] Kamei, Y., Matsuno, M. and Nishimura, N.: An Analytical Study on Slip Strength of Multi HSFG Bolted Joints in Tention, *Journal of JSCE*, No.640, I-50, pp.49-60, 2000.

[35] Geoffrey, L.K., John, W.F. and John, H.A.S.: Guide to Design Criteria for Bolted and Riveted Joints, Second Edition, *American Institute of Steel Construction, Inc.*, 1987.

[36] Tamura, H., Minami, K., Yoshioka, N., Uchida, D., Moro, M., Hama, T. and Hirao, K.: Applicability of Pretensioned Bolted Joints Including Different Contact Faces, *Journal of JSCE A1 (Structural Engineering & Earthquake Engineering)*, Vol.76, No.2, pp.255-274, 2020.4.

[37] Murakoshi, J., Sawada, M., Yamashina, K., Yamaguchi, T. and Ishihara, D.: Study of Influence on Slip Coefficient of High Strength Bolted Friction Type Joints by Painting Condition and Exposure Term, *Journal of JSCE A1 (Structural Engineering & Earthquake Engineering)*, Vol.73, No.1, pp.40-53, 2017.

[38] Minami, K., Mori, T. and Sugiya, T.: 摩擦面の状態が高力ボルト継手のすべり耐力に及ぼす影響, *JSCE* 第 59 回年次学術講演会, I-587, pp.1171-1172, 2004.9.

[39] Tajima, J.: 高力ボルト摩擦接合概説, 第 2 版, 技報堂, 1966.11.

[40] Miao, R., Shen, R., Zhang, S. and Xue, S.: A Review of Bolt Tightening Force Measurement and Loosening Detection, *sensors*, Vol.20, No.11, 3165, 2020.6.

[41] Jhang, K.Y., Quan, H.H., Ha, J. and Kim, N.Y.: Estimation of Clamping Force in High-Tension Bolts Through Ultrasonic Velocity Measurement, *Ultrasonics*, Vol.44, pp.e1339-e1342, 2006.12.

[42] Minakuchi, Y. and Nawa, T.: Ultrasonic Measurement of the Bolt Axial Force of a Bolted Joint after Tightening, *Journal of the Japanese Society for Non-Destructive Inspection*, Vol.54, No.7, pp.365-371, 2005.7.

[43] Joshi, S.G. and Pathare, R.G.: Ultrasonic Instrument for Measuring Bolt Stress, *Ultrasonics*, Vol.22, pp.261-269, 1984.11.

[44] Sakai, T., Makino, T. and Toriyama, H.: 超音波を利用したボルト軸力の測定, *Journal of JSME*, Vol.43, No.366, pp.723-729, 1977.2.

[45] Takahashi, M., Fukuda, M. and Imano, K.: A Method for Evaluation of Fastened Condition of Bolt – Nut Using Ultrasonic Waves, *SICE Tohoku Chapter* 第 285 回研究集会, No.285-9, pp.1-5, 2013.12.

[46] Argatov, I. and Sevostianov, I.: Health Monitoring of Bolted Joints Via Electrical Conductivity Measurements, *Int. J. Eng. Sci.*, Vol.48, pp.874-887, 2010.

[47] Ritdumrongkul, S., Abe, M., Fujino, Y. and Miyashita, T.: Quantitative Health Monitoring of Bolted Joints Using a Piezoceramic Actuator–Sensor, *Smart Materials and Structures*, Vol.13, pp.20-29, 2004.

[48] Daniel, M.P., Park, G. and Daniel, J.I.: Improving Accessibility of the Impedance-Based Structural Health Monitoring Method, *J. Intelligent Material Systems and Structures*, Vol.15, pp.129-139, 2004.2.

[49] Tao, W., Shaopeng, L., Junhua, S. and Yourong, L.: Health Monitoring of Bolted Joints Using the Time Reversal Method and Piezoelectric Transducers, *Smart Materials and Structures*, Vol.25, No.2, 025010, 2016.1.

[50] Hosoya, N., Niikura, T., Hashimura, S., Kajiwara, I. and Giorgio-Serchi, F.: Axial Force Measurement of the Bolt/Nut Assemblies Based on the Bending Mode Shape Frequency of the Protruding Thread Part Using Ultrasonic Modal Analysis, *Measurement: Journal of the International Measurement Confederation*, Vol.162, pp.1-10, 2020.10.

[51] Hosoya, N., Hosokawa, T., Kajiwara, I., Hashimura, S. and Huda, F.: Evaluation of the Clamping Force of Bolted Joints Using Local Mode Characteristics of a Bolt Head, *Journal of Nondestructive Evaluation*, Vol.37, No.4, 2018.

[52] Park, S., Yun, C.B. and Roh, Y.: Active Sensing-Based Real-Time Nondestructive Evaluations for Steel Bridge Members, *KSCE J. Civ. Eng.*, Vol.10, pp.33-39, 2006.

[53] Marshall, M.B., Zainal, I. and Lewis, R.: Influence of the Interfacial Pressure Distribution on Loosening of Bolted Joints, *An International Journal for Experimental Mechanics, Strain*, Vol.47, I-s2, pp.65-78, 2011.12.

[54] Akutsu, A., Bajracharya, S., Sasaki, E., Shimozato, T. and Tai, M.: Eddy Current Based Evaluation of Axial Force of High-Strength Bolts, *IABSE Congress: Resilient technologies for sustainable infrastructure*, pp.1-9, Christchurch, New Zealand, 2020.9.

[55] Kong, Q., Zhu, J., Ho, S.C.M. and Song, G.: Tapping and Listening: A New Approach to Bolt Looseness Monitoring, *Smart Materials and Structures*, Vol.27, No.7, 07LT02, 2018.6.

[56] Wang, F. and Song, G.: Monitoring of Multi-Bolt Connection Looseness Using a Novel Vibro-Acoustic Method, *Nonlinear Dynamics*, Vol.100, No.10, pp.243-254, 2020.2.

[57] Yuan, C., Wang, S., Qi, Y. and Kong, Q.: Automated Structural Bolt Looseness Detection Using Deep Learning-Based Prediction Model, *Structural Control Health Monitoring*, e2899, 2021.

[58] Zhao, X., Zhang, Y. and Wang, N.: Bolt Loosening Angle Detection Technology Using Deep Learning, *Structural Control Health Monitoring*, Vol.26, No.1, e2292, 2019.1.

[59] Mikami, I., Tanaka, S., Hiwatashi, T. and Yamaura, T.: A System for Inferring Axial Force of High-Strength Bolts on Steel Bridges, *Journal of JSCE*, No.549, I-37, pp. 77-90, 1996.10.

[60] Huynh, T.C., Park, J.H., Jung, H.J. and Kim, J.T.: Quasi-Autonomous Bolt-Loosening Detection Method Using Vision-Based Deep Learning and Image Processing, *Autom. Constr.*, Vol.105, 102844, 2019.9.

[61] Zhang, Y., Sun, X., Loh, K.J., Su, W., Xue, Z. and Zhao, X.: Autonomous Bolt Loosening Detection Using Deep Learning, *Struct. Health Monit.*, Vol.19, No.1, pp.105-122, 2020.

[62] Tsuji, Y., Hirokane, M., Hayashi, I. and Konishi, H.: Analysis of Characteristics for Diagnosing Axial Force of High-Strength Bolts, *Journal of JSCE F6 (Safety Problem)*, Vol.72, No.2, pp. I_177-I_182, 2016.

[63] Kuramoto, N. and Chun, P.J.: Detection of Pavement Crack from Image by Decision Tree Learning, *Journal of JSCE A2 (Applied Mechanics)*, Vol.71, No.2, pp.I_823-I_830, 2015.

[64] Chun, P.J. and Igo, A.: Crack Detection from Image Using Random Forest, *Journal of JSCE F3 (Civil Engineering Informatics)*, Vol.71, No.2, pp. I_1-I_8, 2015.

[65] Chun, P.J., Igo, A., Namera, Y., Kuroki, K. and Okubo, K.: Deep Learning Based Crack Ratio Evaluation on Asphalt Pavement from Image Taken by Car-Mounted Camera, *Journal of JSCE E1 (Pavement Engineering)*, Vol.73, No.3, pp. I_97-I_105, 2017.

[66] Tran, D.Q., Kim, J.W., Tola, K.D., Kim, W. and Park, S.: Artificial Intelligence-Based Bolt Loosening Diagnosis Using Deep Learning Algorithms for Laser Ultrasonic Wave Propagation Data, *Sensors*, Vol.20, No.18, 5329, 2020.9.

[67] Cha, Y.J., Choi, W., Suh, G. and Mahmoudkhani, S.: Autonomous Structural Visual Inspection Using Region-Based Deep Learning for Detecting Multiple Damage Types, *Comput.-Aided Civ. Infrastruct. Eng., Special Issue:Health Monitoring of Structures*, Vol.33, No.9, pp.731-747, 2018.9.

[68] Cha, Y.J., Choi, W. and Büyüköztürk, O.: Deep Learning-Based Crack Damage Detection Using Convolutional Neural Networks, *Comput.-Aided Civ. Infrastruct. Eng.*, Vol.32, No.5, pp.361-378, 2017.5.

[69] Kiranyaz, S., Ince, T., Abdeljaber, O., Avci, O. and Gab-bouj, M.: 1-D Convolutional Neural Networks for Signal Processing Applications, *ICASSP 2019 IEEE*, pp.8360-8364, 2019.

[70] Tsuji, H., Suzuki, K. and Hirata, H.: 機械学習を援用したコンクリート内鉄筋の腐食判別の試み, *JSCE* 第 75 回年次学術講演会, 2020.

[71] Cha, Y.J., You, K. and Choi, W.: Vision-Based Detection of Loosened Bolts Using the Hough Transform and Support Vector Machines, *Autom. Constr.*, Vol.71, pp.181-188, 2016.11.

[72] JSCE 鋼構造委員会, 高力ボルト摩擦接合継手の設計・施工・維持管理指針(案), 鋼構造シリーズ 15, 2006.12.

[73] Zhang, Z., Ikeuchi, H., Saiki, N., Imamura, T., Ishii, H., Toda, H. and Miyake, T.: Parasitic Discrete Wavelet Transform and its Application on Abnormal Signal Detection, *Transactions of the JSME (Series C)*, Vol.75, No.757, pp. 163-170, 2009.9.

[74] Tsunoda, T. and Suzuki, K.: Image Sharppening of Linearized Inverse Scattering Method for Concrete Voids, *Journal of JSCE A2 (Applied Mechanics)*, Vol.75, No.1, pp. 23-36, 2019.

[75] Tsunoda, T. and Suzuki, K.: Image Sharppening of Concrete Voids with the Application of Parasitic Discrete Wavelet Transform, *Journal of JSCE A2 (Applied Mechanics)*, Vol.73, No.2, pp. I_691-I_698, 2017.

[76] Hirao, K., Suzuki, K., Kimura, S., Kita, R. and Moriyama, M.: Detection of Horizontal Crack in RC Deck by Ultrasonic Testing from the Surface of Asphalt Pavement, *Journal of JSCE A2 (Applied Mechanics)*, Vol.73, No.2, pp. I_739-I_746, 2017.

[77] McCarthy, J., Minsky, M.L., Rochester, N. and Shannon, C.E.: A Proposal for the Dartmouth Summer Research Project on Artificial Intelligence, *Proposal documents to the Rockefeller Foundation*, 1955.8.

[78] Moor, J.: The Dartmouth College Artificial Intelligence Conference: The Next Fifty Years, *AI Magazine*, Vol.27, No.4, pp.87-91, 2006.7.

[79] Chun, P.J.: A.I. in Civil Engineering: A Roadmap for Research and Development, *JSCE Intelligence, Informatics and Infrastructure*, Vol.1, I-J1, pp.9-15, 2020.

Chapter 2

Analytical Study on Effect of Uncertain Parameters in Structural Performance of Bolted Joints

2.1. Overview

In the field of civil engineering, the maintenance and management of bridges has received much attention. However, for bolted joints, a method for quantitatively evaluating the structural performance of bolts in existing joints has not been established, and currently a method of checking the looseness of bolts by impacting them with a hammer is used in the field. In other words, if the bolts do not loosen sufficiently, it is not possible to notice that the structural performance has deteriorated. In order to maintain steel structures more safely, quantitative evaluation of the structural performance of bolts in existing joints is required.

Slip resistance evaluation is used as an index for inspecting bolted joints. Currently, the slip resistance is evaluated by the bolt axial force and the slip coefficient, as shown in

$$R_s = N_0 \cdot \mu_0 \cdot m \cdot n \tag{2-1}$$

which is also described in the background of Chapter 1. However, because bolted joints contain uncertain influence parameters, the actual bolt axial forces and slip coefficients could differ from the design values and those of the new construction. It is possible that the actual bolt axial force and slip coefficient could differ due to uncertain influential parameters. Hence, the effects of bolt axial forces, misalignment between washers and bolts and bolted joint faying surface contact conditions on the bolted joints structural performance are identified in this chapter. As it is difficult to visually confirm these effects experimentally, a numerical analysis was conducted. Therefore, in this chapter, structural performance and boundary conditions for numerical analysis are described in detail. For each analysis result, the parameters that have a critical influence on the structural performance of the bolted joint were discussed.

2.2. Design Standards for High Strength Bolted Friction Joints

For basic knowledge of bolted joints, the design standards for bolted joints in the most commonly dealt with road bridge specifications in Japan are explained. Based on these design standards, the structural performance and setting conditions for the analysis are determined in this dissertation. There are three types of bolted joints: friction, bearing, and tension. In this study, the focus is on high strength bolted friction joints, which will be referred to as "bolted joints.

The bolt hole of the bolt joint is designed to be slightly larger than the diameter of the bolt. Since the F10T M22 bolts used in this study have a diameter of 22 mm, the diameter of the bolt holes is generally designed to be 24.5 mm. Hence, when the bolted joint is subjected to a large load that exceeds the slip resistance, slipping occurs and the bolt contacts the bolt hole wall. This condition is called the bearing condition. After the bolt contacts the bolt wall due to slip, the plastic deformation of the bolt hole wall increases and finally leads to the fracture of the bolt or base metal [1-6]. As replacing the steel is costly in terms of managing bolted joints, the steel is designed with the occurrence of slip as the ultimate limit state, so that the steel is not plasticised. In addition, if steel strength of the splice plate is low, the yielding of the steel will precede the slip, so the design of the bolted joint should be such that the splice plate has higher strength than the base plate. This design causes the bolted joint to slip before yielding, and the bolted joint is generally designed to slip before yielding. The yield strength, R_y is described by

$$R_y = (W - d_h) \cdot t \cdot \sigma_y \tag{2-2}$$

where, W is the steel width, d_h is the bolt hole diameter, t is the steel thickness, and σ_y is the yield stress. The smaller of the thickness of one base plate and the total thickness of the two splice plates is applied for t. For the design of slip precedence type, bolted joints are designed so that the ratio of design slip resistance to design yield resistance β, which is the ratio of the slip resistance R_s to the yield resistance R_y, does not exceed 1. β is described by the following:

$$\beta = \frac{R_s}{R_y} \tag{2-3}$$

Based on the above, bolted joints are designed to be slip precedence type in the current Japanese design standards [7]. Furthermore, since the occurrence of slipping is assumed to be the ultimate limit state, the design is such that the assumed load does not exceed the slip resistance R_s.

Therefore, the numerical analyses conducted in this study were considered with a focus on the phenomena leading up to the occurrence of the slip. In recent years, there have been cases where the occurrence of slip is determined by the load value when the relative displacement between the base plate and the splice plate reaches 0.2 mm. This is the recommended method of determination in the field of architecture [8]. the occurrence of slip in this study was defined as “the occurrence of slip is judged when the relative displacement between the base plate and the splice plate reaches 0.2mm.”

2.3. Validity of Analytical Models in this Study

In this chapter, the discussion proceeds with numerical analysis. Therefore, the validity of the analytical model developed and used for this study will be explained. The results of the compressive loading tests conducted by the author during the master's course are compared with the results of the analysis conducted in this study. It is necessary that the behaviour confirmed by experiment and analysis is similar in order to confirm the validity of the analytical model. In the tensile loading tests, the simple slip behaviour is that the bolt slips from the side to which the tensile force is applied. On the other hand, in compressive loading tests, the slip behaviour is different and more complex than in tension due to the Poisson effect. If the analysis can reproduce the slip behaviour in compressive loading tests, it can be confirmed that the analytical model also reflects the effect of the Poisson effect, which changes the thickness of the steel plate.

2.3.1. Compressive Loading Experiment for Bolted Joint Models

In order to confirm the occurrence of slip in the compressive loading experiment, a bolted joint specimen was modeled with a slip precedence such that the slip resistance was less than 1,000kN of the load capacity. The specimen is a basic 1 by 2 friction joint modelled on the dashed line portion of the bolted joints as shown in **Figure 2.1**. The dimensions and shape of the specimen are shown in **Figure 2.2**. In addition, the material properties of steel plates were determined based on the results of material tests using standard tensile specimens fabricated from the same lot as the specimens. The specifications and mechanical properties of the materials used are given in **Table 2.1**. The bolt axial force F is described by

$$F = \frac{T}{k \cdot d} \tag{2-4}$$

where, T is the tightening torque, k is the torque coefficient, and d is the diameter of the bolt. In this experiment, the bolt axial force was introduced by controlling the tightening torque with a torque wrench (**Figure 2.3**). The bolts were tightened by 10% more than the design bolt axial force, referring to the bolt axial force introduction standard for bolted joints [9]. This means that the axial force of the tightening bolt is 226kN. Since the bolt axial force decreases with time, the bolt axial force during the compressive loading experiment is assumed to be 208kN, based on the results of the relaxation test [10]. In addition, when the faying surface is an inorganic zinc-rich paint,

literature [11] gives a suggested value of 0.55 for the slip coefficient. Based on the above, the design slip resistance of the specimen used is approximately 457.6 kN from Equation (2-1). When subjected to compressive loads, the actual slip resistance can be assumed to be much higher due to the influence of the Poisson effect.

To confirm the occurrence of slipping, clip gauges (clip-type displacement gauges) C1 and C2 were installed at the locations shown in **Figure 2.4**. In the compressive loading experiment, the lower part of the splice plate was fixed and the ball seat head was pressed against the upper part of the base plate to apply the compressive load. The upper part of the base plate was pushed in at a rate of 1 to 2 [kN/s]. In the case of compression, the specimen was covered with the acrylic pipe to prevent the bolts from breaking (**Figure 2.5**). The point of focus in this study is slip. However, this experiment was continued after the bearing pressure was applied, and the load was applied up to 1,000kN, which is the capacity of the compression machine.

The relationship between the compressive load and the relative displacement of the base plate and the splice plate, generated from the data of the clip gauges C1 and C2, is shown in **Figure 2.6**. **Figure 2.6** shows that the slip started gradually at C1 first, and then a rapid slip was observed at C2 when the compressive load was about 500 kN. Applying a compressive load from the top of the base plate increases the plate thickness at Bolt 2. On the other hand, the plate thickness at Bolt 1 does not increase as much as at Bolt 2, which suggests that C1 starts to slip first and that rapid slip occurs at C2 after the slip resistance is reached. In addition, considering the phenomenon of increased plate thickness, the actual slip resistance may be greater than in a tensile test. This phenomenon is thought to be due to the Poisson effect of compressive load. When the steel plate is pulled in the longitudinal direction, the thickness of the plate decreases and the bolt axial force decreases. On the other hand, when a longitudinal compressive load is applied to the steel plate, the thickness of the steel plate increases and the bolt axial force increases. This is the effect of the Poisson effect. **Figure 2.7** shows the relationship between the compressive load and the displacement of the compression machine. It can be seen that the slip resistance is in close agreement with the slip resistance evaluated from the relative displacements of the base plate and splice plate.

As the experimentally confirmed slip resistance is approximately 500 kN, the slip coefficient is estimated to be approximately 0.57 from Equation 2-1. The actual bolt axial forces immediately

prior to the compressive loading tests and the slip coefficient of 0.57 estimated from the experiments are applied to the analysis and compared with the experimental results.

2.3.2. Reproduction of Compressive Loading Experiment by Analysis

In order to demonstrate the effectiveness of the analytical model used in this study, a numerical analysis reproducing a compressive loading experiment was conducted. The modeled analytical model will be described. Abaqus 6.14, a finite element analysis software, was used in this study [12]. **Figure 2.8** shows the analytical model. Since the target specimen is symmetrical, the symmetry condition was set and the model was designed as a 1/2 symmetric model. The peaks and valleys of the bolt threads were not reproduced, as the slip test analysis generally has little effect on the slip resistance without reproducing the threads. The shape of the analytical model faithfully reproduced the specimen. For the material properties of the steel and bolts, the values shown in **Table 2.1** were used. The bolt axial force was introduced as shown in **Figure 2.9**. First, the bolt shank was divided at the center of bolt shank length, and a load equivalent to the bolt axial force was applied to the cut surface. Then, after the load was introduced, the bolt length was fixed to model the bolt after fastening [13-17]. For the contact conditions, a slip coefficient of 0.57 was set as the static friction coefficient, which was estimated from the experimental results. The entire surface of the upper part of the base plate was slaved, with the bottom of the splice plate as the fixed side, to introduce a forced displacement in the compression direction in the upper surface of the base plate. The mesh size was set to 4 mm in this verification.

The behaviour of C1 and C2 is shown in **Figure 2.10**, where it is observed that C1 slips gradually first and C2 slips rapidly when the load reaches approximately 500 kN. This behaviour is similar to the experimental results shown in **Figure 2.6**, which confirms that this analytical model can also reproduce the influence of the Poisson effect. Thus, it can be said that this analytical model is valid up to the occurrence of slip. Therefore, this analytical model will be used as the basis for various numerical analyses in this study.

2.4. Effect of Each Influential Parameter on Structural Performance of Bolted Joints

Many studies [18-44] have investigated bolted joints under the influence of erection conditions, age, and earthquakes, and have shown that the strength of bolted joints has actually decreased. These are often considered for parameters that degrade the function of the bolted joint. The purpose of this study is to quantitatively evaluate the uncertain parameters that affect the structural performance of bolted joints. Then, numerical analysis is conducted for the cases under consideration with varying considered parameter. In these analyses, tensile load is considered, the load transfer mechanism of bolted joints, the slip resistance, and the faying surface contact condition are focused on and discussed. The uncertain influence parameters considered in the following are the distribution of the bolt axial force and the faying surface contact condition, misalignment of bolts and washers, and the slip coefficient.

2.4.1. Effect of Bolt Axial Force on Structural Performance

To clarify the effect of bolt axial force distribution on the structural performance of bolted joints. First, the analytical model used is described. The analytical model in this study is shown in **Figure 2.11**. The mesh size is 4 mm. To represent the distribution of the bolt axial force, a basic 1 by 3 two-sided friction bolted joint was modeled. In addition, a 1/2 model was designed to specify the symmetric part. The steel type (SS400), plate thickness (22mm for base plate, 12mm for splice plate) and bolt type (F10T M22) used are the same as in **Table 2.1**. The slip coefficients were set assuming that the steel surfaces were coated with inorganic zinc-rich paint, which is commonly used in bolted joints. In these analyses, the slip coefficient was set as 0.5, referring to the proposed value of slip coefficient when the faying surface is inorganic zinc-rich paint by Nishimura et al. [11]. Four cases of bolt axial force distributions were studied, and the cases are shown in **Table 2.2**. The basic bolt axial force is considered, and the base is set to 205kN, which is the design bolt axial force. The axial force of the loosened bolts is reported in the literature [45], where the bolt axial force is reduced by about 20% based on the results of a survey of actual structures. Hence, the axial force of the loosened bolt was 164kN, a 20% reduction from the design bolt axial force. The case of one of the three bolts being loose was considered. More complex variations in bolt

axial forces will be considered in the future. The tensile load on the bolted joint was reproduced by introducing a forced displacement to the base plate. The relative displacements and slip resistance were calculated at each bolt position targeting up to slip. In addition, the stress distribution on the faying surface at post-slip was investigated.

Figure 2.12 shows the relative displacement of the base plate and the splice plate at each bolt position. In this study, the slip of bolted joints is considered to be when the relative displacement first reaches 0.2mm at the bolt position. This study was conducted to investigate the effect of each bolt axial force on the bolted joints, and all bolts were confirmed up to slip. In this study, the Bolt 3 side is referred to as the "outer bolt" and the Bolt 1 side as the "inner bolt". The order of slip occurrence was confirmed to be that Bolt 3 slipped first in all cases except for Case 4. The outer bolt axial force is considered to be important. However, even though the outer bolts are loose in Case 2, the slip resistance is almost the same compared to the cases where the outer bolts are sufficiently tight (Case 3 and Case 4). Therefore, it can be said that the slip resistance is determined by the sum of the bolt axial forces.

On the other hand, the stress distribution on the faying surface of the steel is considered to differ according to the distribution of bolt axial forces. In order to investigate the stress distribution of steel, the stress distribution on the faying surface at post-slip is shown in **Figure 2.13**. According to the faying surface of the base plate, the stresses are concentrated on the side on which the tensile load is acting. According to the faying surface of the splice plate, it can be seen that the stresses are concentrated in the bolt holes opposite to the base plate. Stresses were confirmed to be concentrated on both sides. In this consideration, the stresses borne by the area around the central bolt were investigated in detail. In **Figure 2.14**, the central bolt (Bolt 2) is focused on, and the faying surface stress distribution of the splice plate at post-slip is shown. In the splice plate, the stresses decrease from the inside to the outside in all cases except Case 4, the stresses around the outer bolt are small, and it can be considered that they slip in the same order from the outside to the inside as the results in **Figure 2.12**. Only in Case 4, the central bolt (Bolt 2) is loose, so the stresses in Bolt 2 and Bolt 3 are small. The stresses on Bolt 2 and Bolt 3 are small. As the outer bolt is tightened at 205 kN, the central bolt slips first, which is considered to have caused the behaviour of the inner bolt to slip almost simultaneously with the central bolt. This result indicates that if the bolts on the load-bearing side are sufficiently tightened and the central bolt is loose, the bolts on the non-load-bearing side could slip.

2.4.2. Effect of Misalignment of Bolts and Washers on Structural Performance

The bolt hole of the bolt joint is designed to be larger than the bolt diameter. In the case of the F10T M22 bolts with a diameter of 22 mm used in this study, the bolt holes are designed to be 24.5 mm. The clearance is 2.5 mm. It is desirable that the bolts be placed in the center of the bolt holes, but this is difficult to achieve in actual construction sites. In many cases, bolts and washers are placed close to the bolt hole walls. However, the effect of these misalignments is not considered in the current structural performance evaluation of bolted joints. In addition, although there have been some studies on bolt misalignment [46], there have been few investigations on models with washers that assume actual bolted joints. Therefore, the effect of the misalignment of bolts and washers on the structural performance of bolted joints was investigated.

The analytical model used is shown in **Figure 2.15**. The mesh size is 4 mm. A basic 1 by 2 two-sided friction bolted joint is considered using a 1/2 model with the symmetric part specified. The steel type (SS400), plate thickness (22mm for base plate, 12mm for splice plate) and bolt type (F10T M22) used are the same as in (2.3) above. The slip coefficient was set to 0.5 as in 2.4.1, assuming that the steel was coated with inorganic zinc-rich paint. The bolt axial force was set to 205kN, the design bolt axial force, in all cases. The items to be examined are divided into two major categories, A and B. In A, the bolt is in the center of the bolt hole and only the washer is considered to be misaligned. For B, misalignment of both bolts and washers is considered. There are four more cases to consider for A and B. Case 1 is the case with the two bolts in the center as shown in **Figure 2.15**. Case A/B-2 are the case where only Bolt 1 is misaligned. Case A/B-3 are the case where only Bolt 2 is misaligned. Case A/B-4 are a case where both bolts are misaligned. Considered cases A and B are shown in **Table 2.3** and **Table 2.4**, respectively. When bolts and washers are installed at a construction site, the direction of displacement of the bolts and washers was designed as shown in **Figure 2.16**, because it is considered that the bolts and washers will be misaligned in the vertical direction of the load in most cases due to gravity. The tensile load was expressed by introducing a forced displacement at the upper surface of the base plate. The slip resistance and the stress concentration in the bolt hole wall were investigated for each case.

The results of the investigation of the slip resistance for each case are shown in **Figure 2.17**. According to the results, when the direction of misalignment is **Figure 2.16**, it is confirmed that the slip resistance increases when both the bolt and the washer are misaligned. Furthermore, the lowest slip resistance was observed in the normal case where the bolt and washer were located in

the center of the bolt hole. After the relative displacement of 0.2 mm, the difference in strength widens further. The misalignment of the bolts is similar to the bearing pressure condition. Therefore, when the bolt shank was in contact with the bolt hole wall due to misalignment, both frictional force and bearing force acted, and the slip resistance was considered to have increased. The stress concentrations in the bolt hole walls were investigated and are shown in **Figure 2.18**. These are the stress distributions on the faying surface at post-slip. The areas where stress is particularly concentrated are shown as color maps, and the areas with low stress are shown in black. These confirmed that the stress was concentrated in the surrounding area including the bolt hole wall of the splice plate. In particular, the stress was concentrated in Bolt 1 of the splice plate, and **Figure 2.19**, which focuses on the splice plate, further confirms the area where the stress is concentrated. In Case 0, where the bolt and washer are at the center of the bolt hole, the stress is uniform on both sides and decreases as it moves away from the bolt center. In Case A-3 and Case B-3, where the bolts and washers are misaligned, the stresses are distributed asymmetrically. It was confirmed by these results that the misalignment of the bolt and washer has some effect on the structural performance of the 1 by 2 bolted joints considered. In the case of multi-row bolted joints with a large number of bolts, the effect might be significant, and further research is expected.

2.4.3. Effect of Faying Surface Condition on Structural Performance

The bolted joint contains many uncertain influence parameters, among which the most complicated parameter is considered to be the slip coefficient. The slip coefficient is considered to be a particularly complex parameter because bolted joints contain many uncertain influential parameters and the condition of the faying surface is not always constant. Hence, many researchers [47-58] have studied slip coefficients since the 1970s, when bolted joints came into common use, but even in 2022 there are still many uncertain parameters. Nowadays, the slip coefficients for each faying surface treatment can be determined by the many experiments and analyses they have conducted. However, despite the differences between the allowable stress design method and the limit state design method, the Japanese standards [59-62] have provisions with sufficient bearing capacity compared to the standards of other countries [63-66]. In the Japanese standard, all uncertain influence parameters of faying surface contact condition are considered for safe design. On the other hand, in other countries, standard values are often set for each uncertain influence

parameter. In order to determine the slip coefficient for each faying surface, the faying surface contact condition must first be clarified.

It has been observed that the contact conditions between steel plates change depending on the order of bolt tightening, with the bolt axial force decreasing from the bolt tightened first [19]. This effect makes the faying surface contact condition unclear. Hence, the change in the faying surface contact condition due to the tightening of the bolt was focused on. When bolts are tightened on a bolt joint at a construction site, they are tightened in sequence from the center to the outside [67]. The effect of tightening the bolts in sequence on the faying surface contact condition was considered. **Figure 2.20** was used as the analytical model. No load was introduced, and the bolt axial force was tightened in the order of Bolt 1 and Bolt 2. The slip coefficient was set at 0.5. Since the distribution of contact pressure due to bolt tightening is assumed to spread in concentric circles, the mesh was created in concentric circles around the bolts. The distribution of contact pressure on the faying surface between the base plate and the splice plate is shown in **Figure 2.21**. It was confirmed that the contact pressure was distributed in concentric circles around the bolt. The contact pressure was very low except around the bolts, suggesting that the splice plate may have been deformed in the out-of-plane direction. Thus, the deformation shapes of bolted joints was confirmed. The bolt axial force was introduced according to the bolt tightening sequence of the bolt joint. The out-of-plane displacement of the splice plate due to bolt tightening was confirmed as shown in **Figure 2.22**, which is a deformation diagram for each stage. In this figure, the deformation factor is shown by a factor of 200. From the above, it is clear that the contact area that is considered to have actual frictional force is around the washer. In addition, You et al [68] pointed out that when bolts are tightened in sequence, the bolt loosens due to the cross talk effect which is caused by the inclination of the steel plate when tightening diagonal or opposite positions. However, the splice plates are thin and the bolt axial forces are considered to be smaller than the design bolt axial force. There are other reports that bolts loosen due to the effect of elastic interaction [69], but the target joints are different. In the future, the mechanism of bolt loosening in multi-row bolted joints when tightening with the design bolt axial force will be clarified. It is also necessary to clarify the effect of the splice plate thickness.

To further determine this result, an analysis was conducted to identify the areas where frictional forces were acting on the faying surface. In the above study, a large contact pressure was observed around the washers, and four cases were investigated as shown in **Figure 2.23**. These cases show

faying surfaces, and the reason why washers are included in the figures is to help understand the scale of the contact area under consideration. By setting the slip coefficient μ of the contact surface to 0.5 and the slip coefficient μ of the non-contact surface to 0, the faying surface contact condition was reproduced. In each study case, the slip coefficient of only the faying surface was varied, and all other surfaces were set to 0.5 for all surfaces on the bolt head and nut sides of bolted joints. Case 0 and Case 1 were compared to confirm that all areas other than around the washer were non-contact areas. In addition, Case 2 and Case 3 were examined to investigate the effect of the contact condition between bolts on the structural performance of bolted joints. A tensile load was then introduced at the upper surface of the base plate, and the effect on the slip resistance of each case was investigated.

Figure 2.24 shows the evaluation of slip resistance by relative displacement for each case. As a result, it was confirmed that the slip resistance decreased only in Case 3. The slip resistance of Case 3 was found to be 3% lower than that of the other cases. Therefore, the contact pressure is acting in a certain area in concentric circles from just below the washer. Besides, since the area set as non-contact in Case 1 is almost unaffected, it is possible that the outside of the bolted joint is non-contact. As a result of these considerations, it was found that the structural performance of the bolted joint was affected in a certain area spreading concentrically from the bolt. Based on these results, an evaluation method for uncertain influential parameters is proposed in Chapter 4 of this dissertation.

From the above considerations, a question arose as to the cause of the distribution of contact pressure only around the bolt hole in bolt tightening. Since the contact pressure could be distributed around the bolt hole due to the slip coefficient of the faying surface, only the slip coefficient of the faying surface was set to 0 and an analysis was conducted for bolt tightening only. The boundary conditions of the analysis were the same as in **Figure 2.20** and the results are shown in **Figure 2.25**. The contact pressure distribution is almost the same as in **Figure 2.21**, and it is clear that the slip coefficient of the faying surface is not the cause of the contact pressure concentration around the bolt holes. Incidentally, although the contact pressure is distributed around the bolted holes, the slip coefficient is 0. Thus, when tensile or compressive forces are applied to bolted joints, slip will of course easily occur.

2.5. Summary

In this chapter, the analysis was conducted by varying various parameters. The uncertain parameters considered were the bolt axial force, the position of bolts and washers in the bolt hole, and the slip coefficient. Numerical analysis confirmed the effects of these uncertainties on the load transfer mechanism and slip resistance of the bolted joints. The structural performance, boundary conditions, and definitions adopted in this dissertation were described. The results of the analysis were explained using distribution diagrams, deformation diagrams and graphs. For each analysis result, the factors that have a critical influence on the structural performance of the bolted joint were discussed.

In the analysis that examined the distribution of bolt axial forces, it was confirmed that slipping occurred in sequence from the outer bolts. However, it was found that the effect of the distribution of the bolt axial force may differ from that phenomenon. Assuming a single group of bolted joints, if the inner bolt axial force is large, the stress distributed to the central bolt is small. However, when sufficient bolt axial force was introduced in the inner bolt, but the central bolt was loose, the stress borne by the inner bolt was observed to be larger.

In the consideration on the misalignment of bolts and washers, the case where the bolts and washers are misaligned in the vertical direction of the loading direction was examined. When the bolt shank is in contact with the bolt hole wall due to the misalignment of the bolts and washers, both the frictional force and the bearing pressure will act, and the slip resistance will increase. On the other hand, there is a possibility that the stress may be concentrated in the bolt hole walls, resulting in the localized stress exceeding the yield stress.

In the consideration of the faying surface contact condition, the effect of the tightening sequence of the bolts on the faying surface was clarified. It was confirmed that the contact pressure between the base plate and the splice plate of bolted joints was distributed in a uniform concentric circle around the washer. The contact pressure is low except around the washer, indicating the possibility that there was no contact outside the bolted joint.

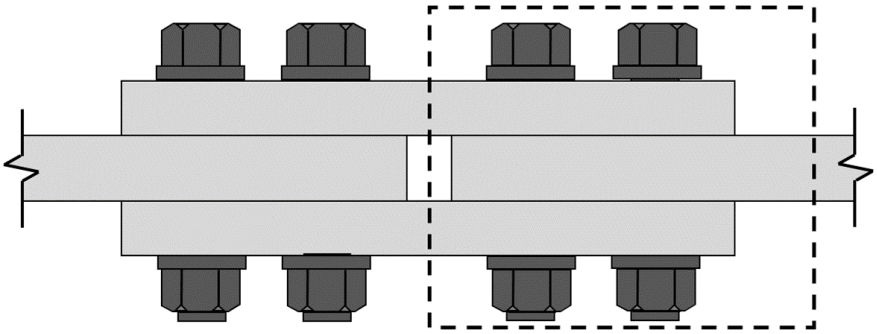

Figure 2.1 Modelling range of bolted joints

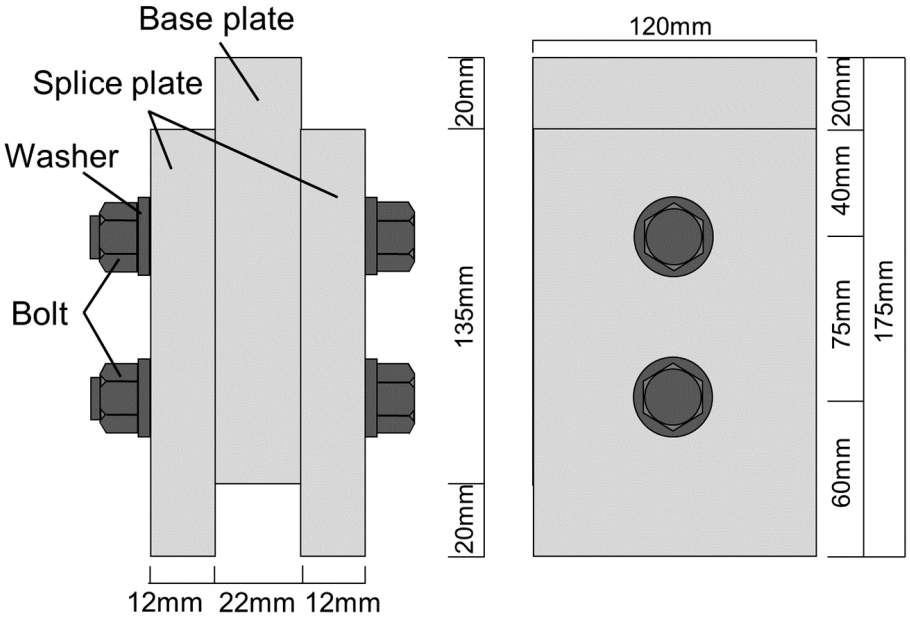

Figure 2.2 Dimensions and shape of specimens

Table 2.1 Specifications and mechanical properties of materials used

Material	Specification	Surface treatment	Yield stress [N/mm^2]	Tensile strength [N/mm^2]	Elongation [%]	Torque coefficient
Base plate	SS400	Inorganic zinc-rich paint (Thickness: 75μm)	273	427	31	
Splice plate			282	438	33	
Bolt	High strength hexagonal bolt	Mill scale	1061	1114	21	0.131

Figure 2.3 Torque wrench used to tighten bolts

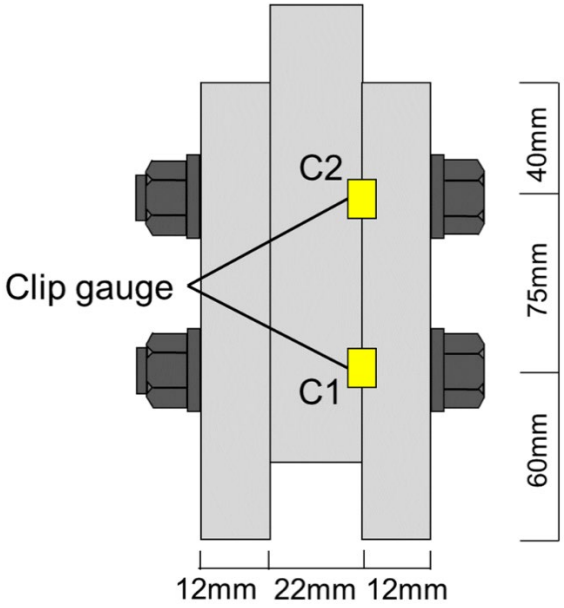

Figure 2.4 Installation position of clip gauges

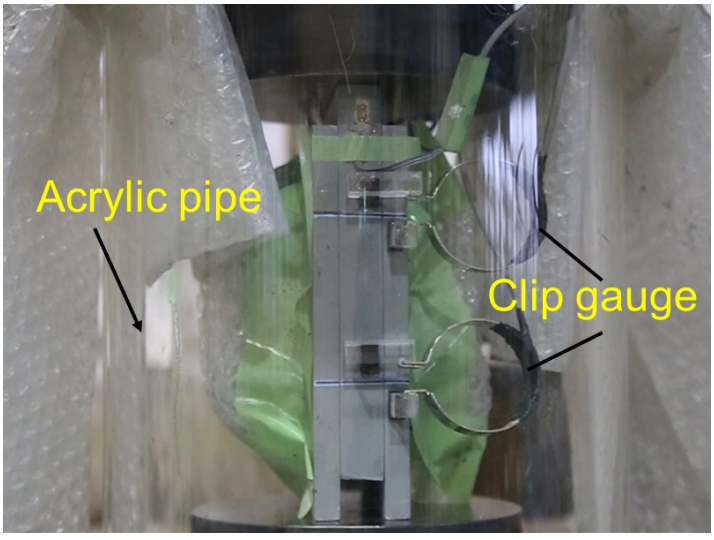

Figure 2.5 Experiment using an acrylic pipe

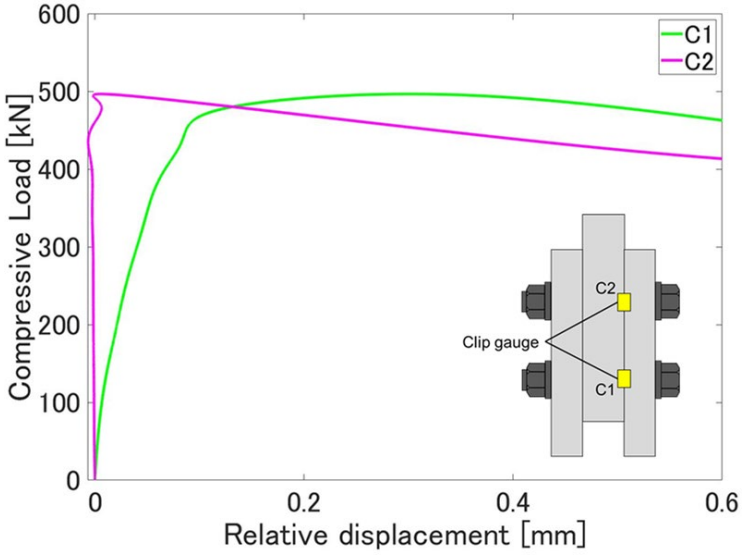

Figure 2.6 Relationship between load and relative displacement of base plate and splice plate

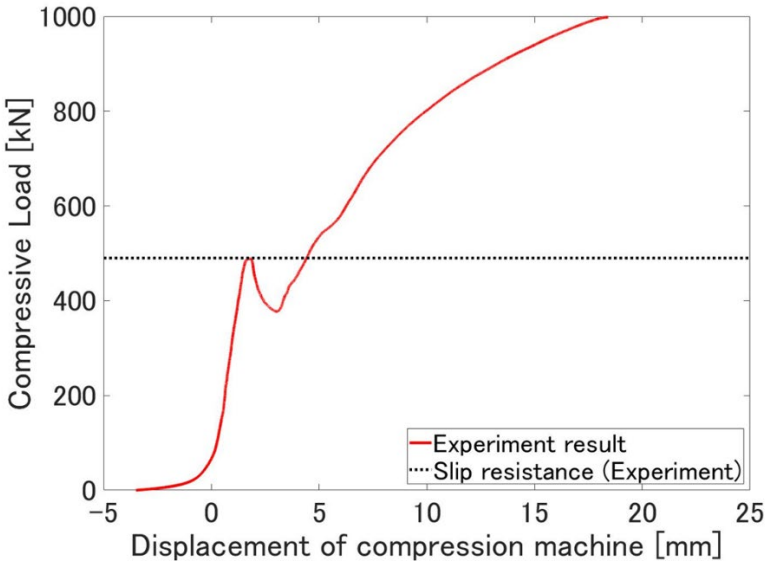

Figure 2.7 Relationship between load and displacement of compression machine

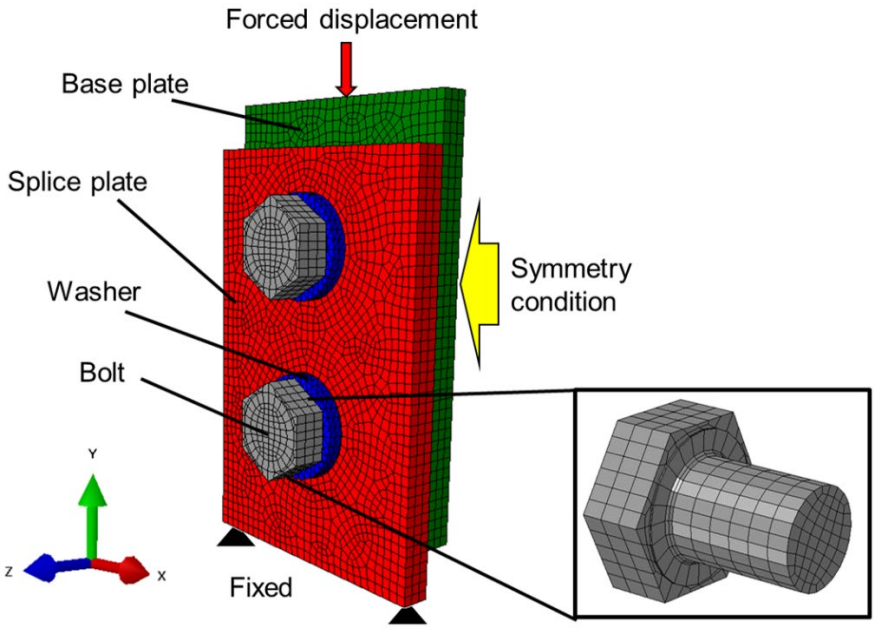

Figure 2.8 Analytical model

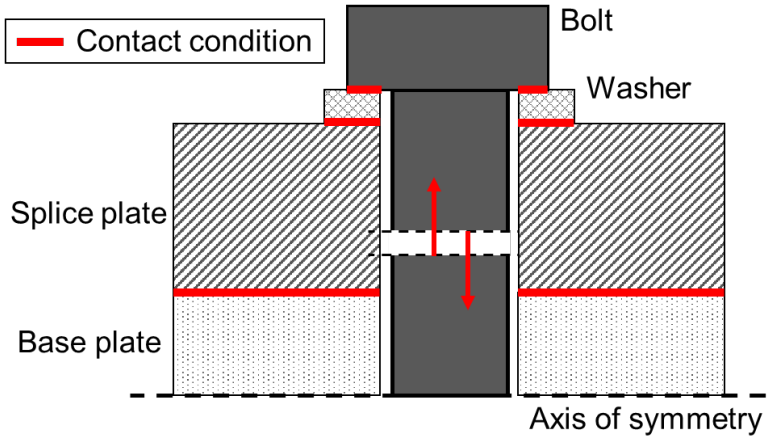

Figure 2.9 Analytical model for the introduction of the bolt axial force

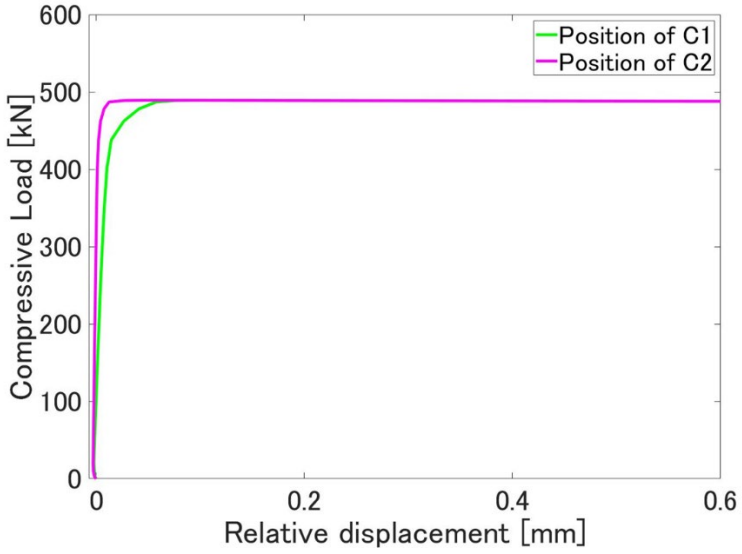

Figure 2.10 Relationship between load and relative displacement by analysis

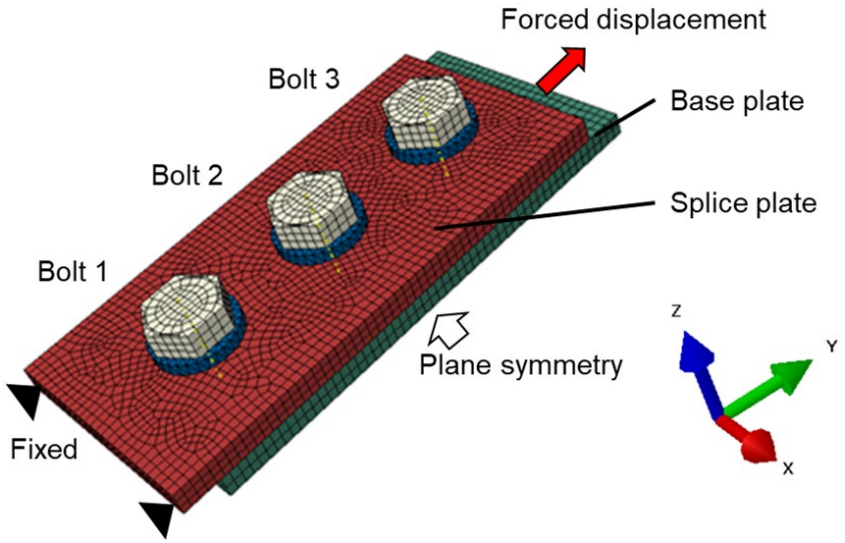

Figure 2.11 Analytical model for investigating the effects of variations in bolt axial force

Table 2.2 Consideration cases for investigating the effects of variations in the bolt axial force

Case	Bolt axial force [kN]		
	Bolt 1	Bolt 2	Bolt 3
1	205	205	205
2	205	205	164
3	164	205	205
4	205	164	205

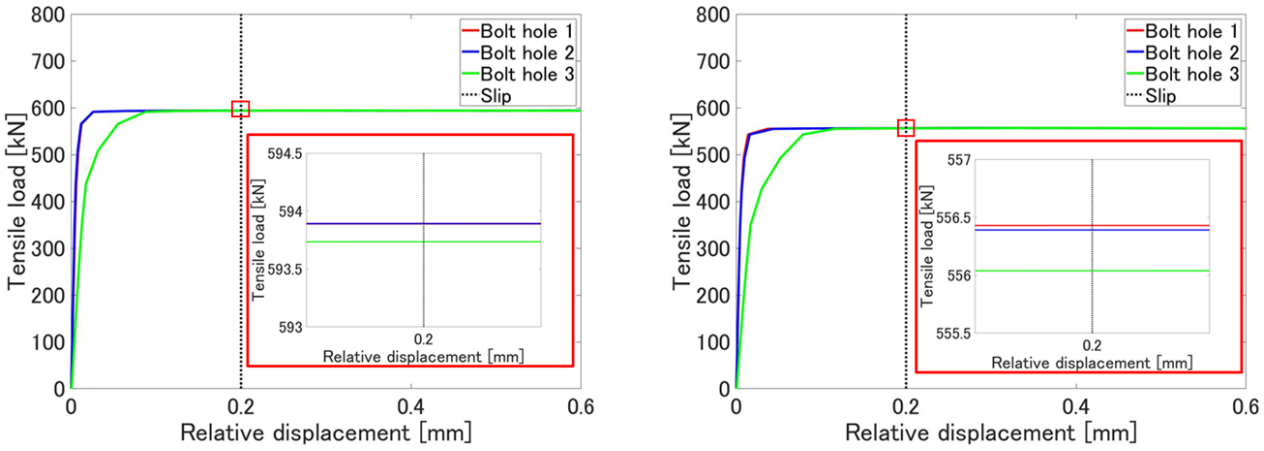

(a) Case 1

(b) Case 2

(c) Case 3

(d) Case 4

Figure 2.12 Relative displacement of the base plate and the splice plate at each bolt position

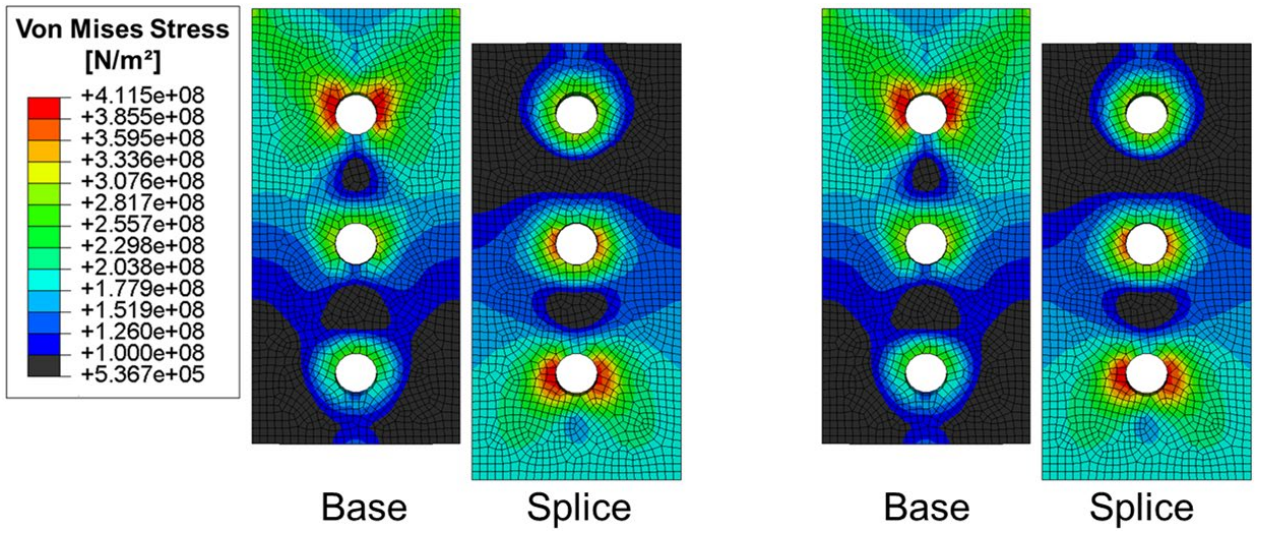

(a) Case 1 (b) Case 2

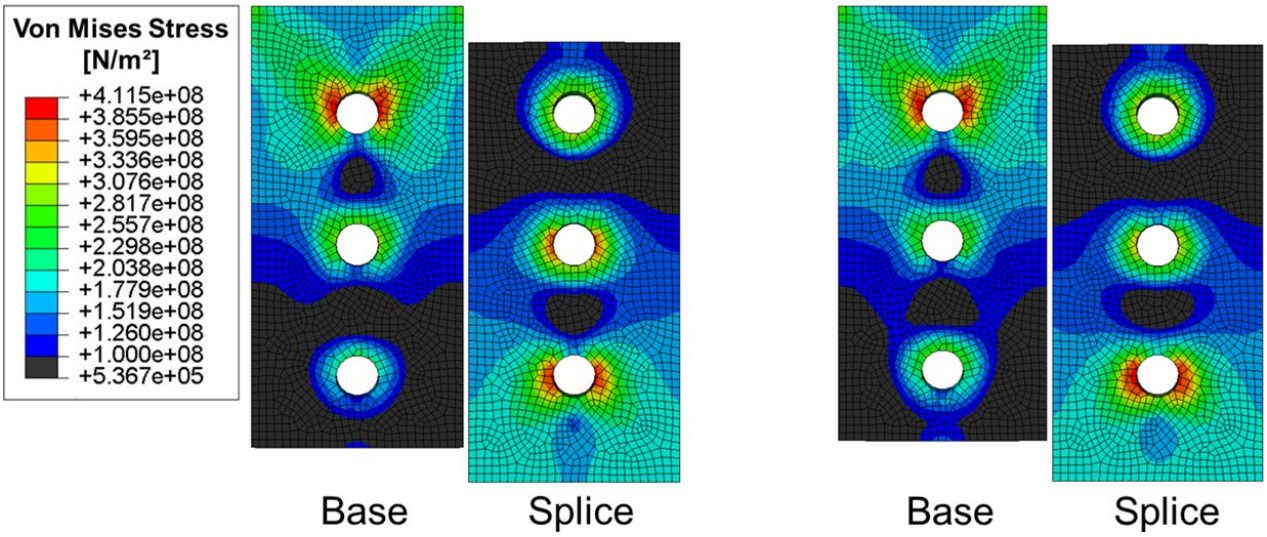

(c) Case 3 (d) Case 4

Figure 2.13 Stress distribution on faying surface in post-slip

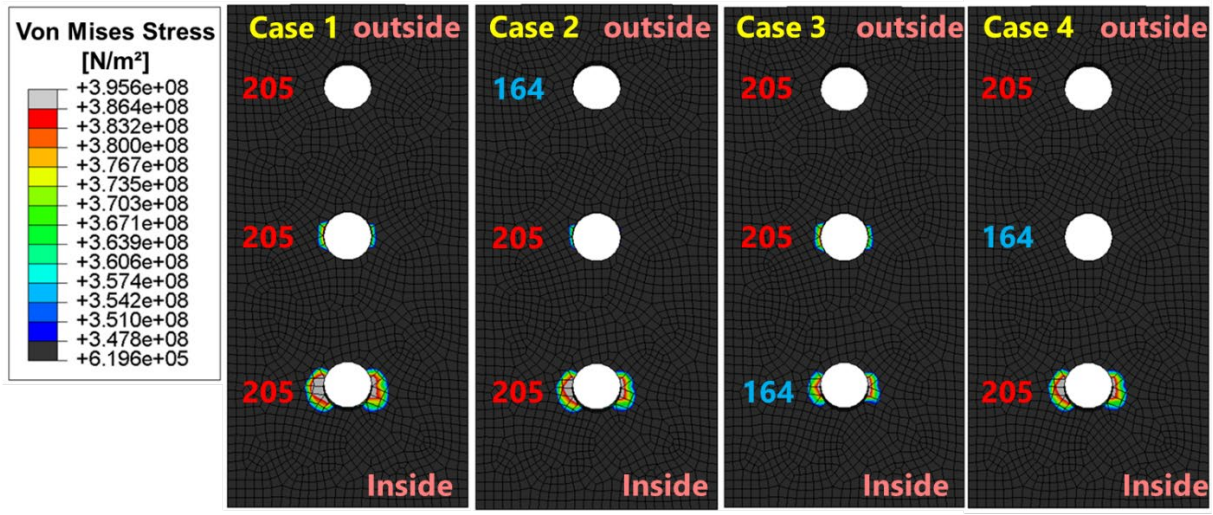

(a) Case 1 (b) Case 2 (c) Case 3 (d) Case 4

Figure 2.14 Stress distribution on the faying surface of the splice plate in post-slip, focusing on the bolt in the center (Bolt 2)

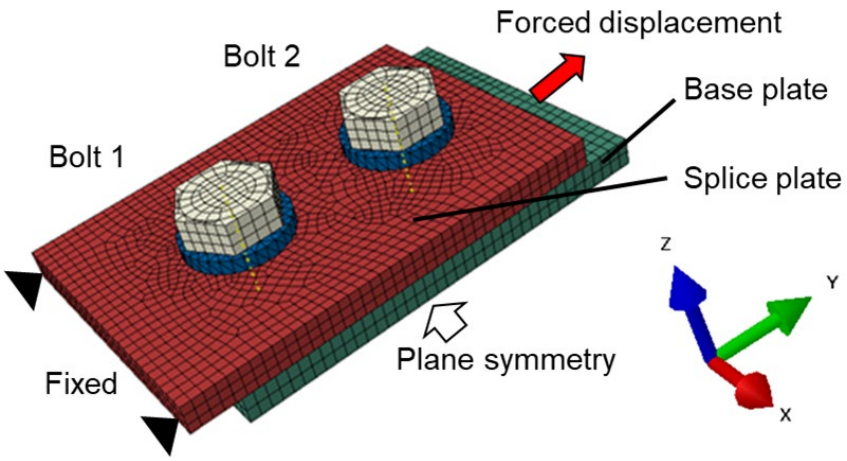

Figure 2.15 Analytical model for investigating the effects of eccentricity of bolt and washer

Table 2.3 Consideration cases for investigating the effect of washers eccentricity

Case	Position of washers	
	Bolt 1	Bolt 2
0	Center	Center
A-1	Side	Center
A-2	Center	Side
A-3	Side	Side

Table 2.4 Consideration cases for investigating the effect of bolts and washers eccentricity

Case	Position of bolts and washers	
	Bolt 1	Bolt 2
0	Center	Center
B-1	Side	Center
B-2	Center	Side
B-3	Side	Side

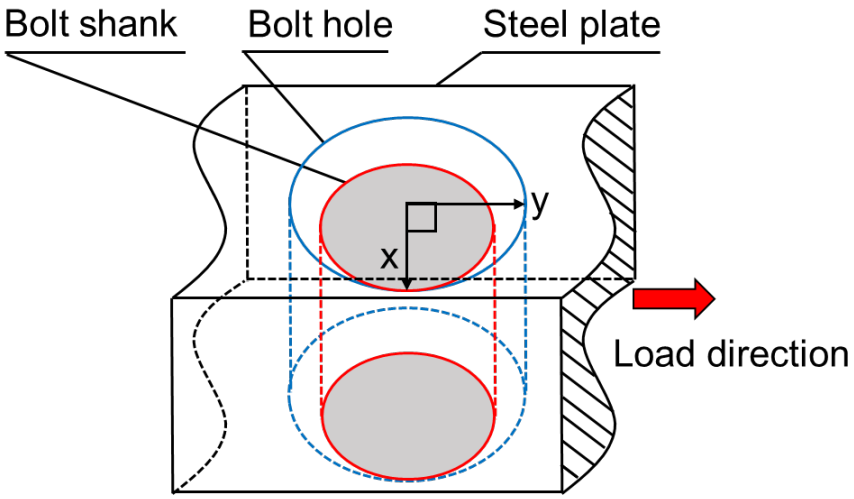

Figure 2.16 Misalignment direction of bolt shank to bolt hole

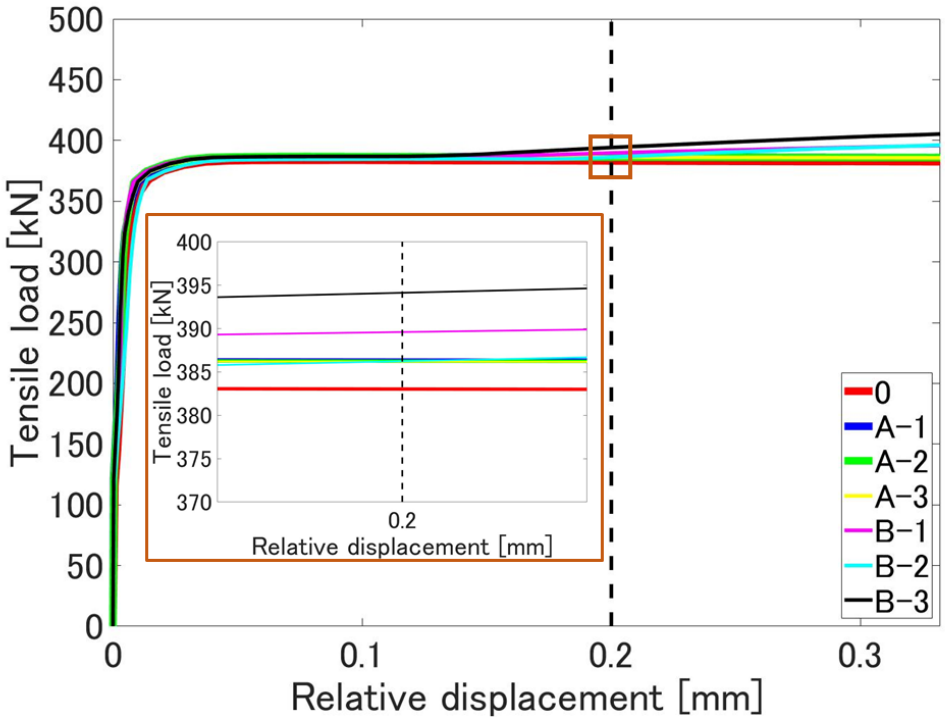

Figure 2.17 Relative displacement of the base plate and the splice plate in each case

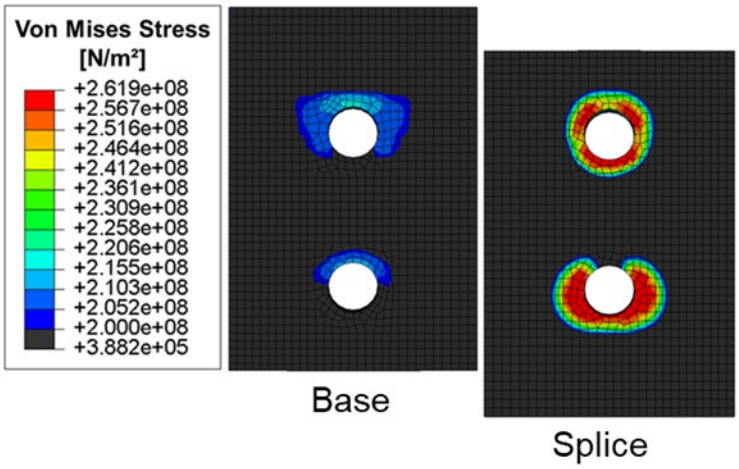

(a) Case 0

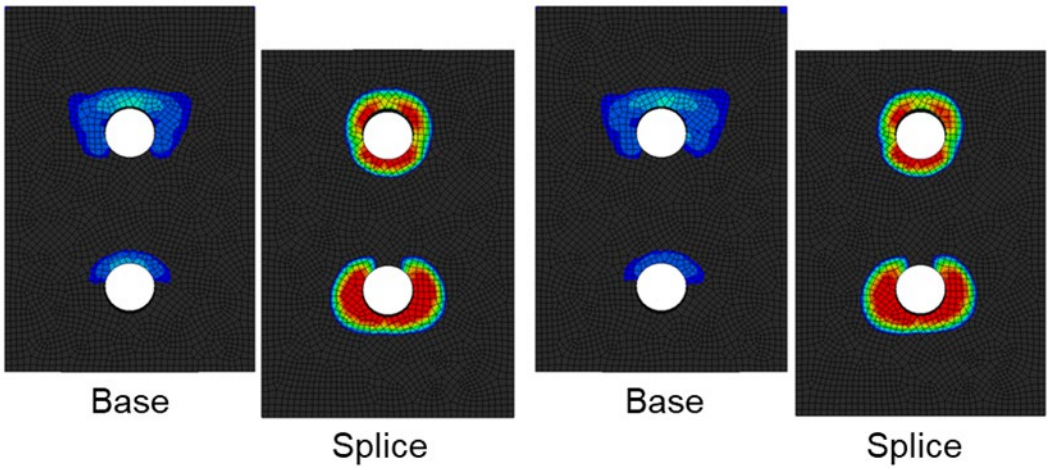

(b) Case A-3 (c) Case B-3

Figure 2.18 Stress concentration on faying surface in post-slip

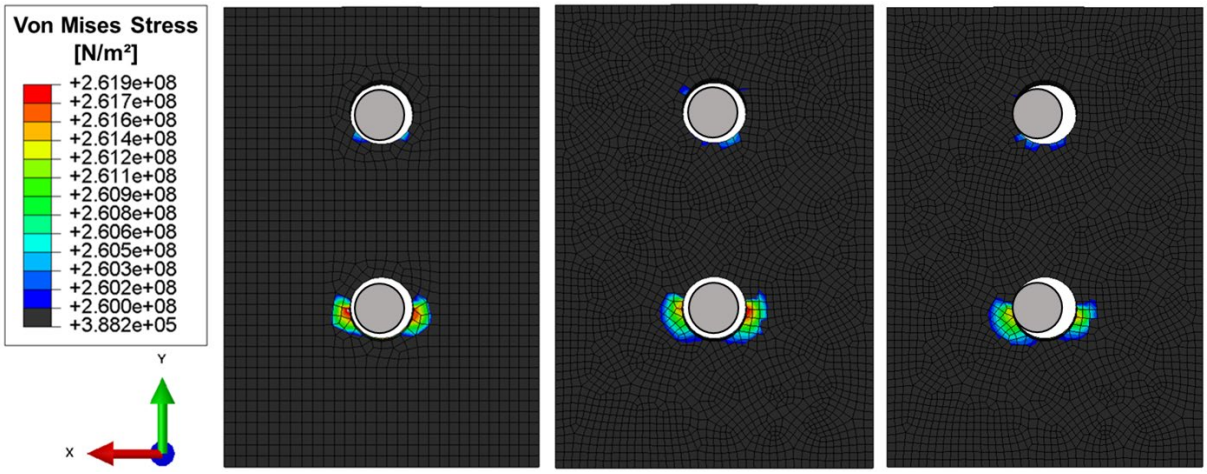

Figure 2.19 Local stress concentration on faying surface of splice plate in post-slip

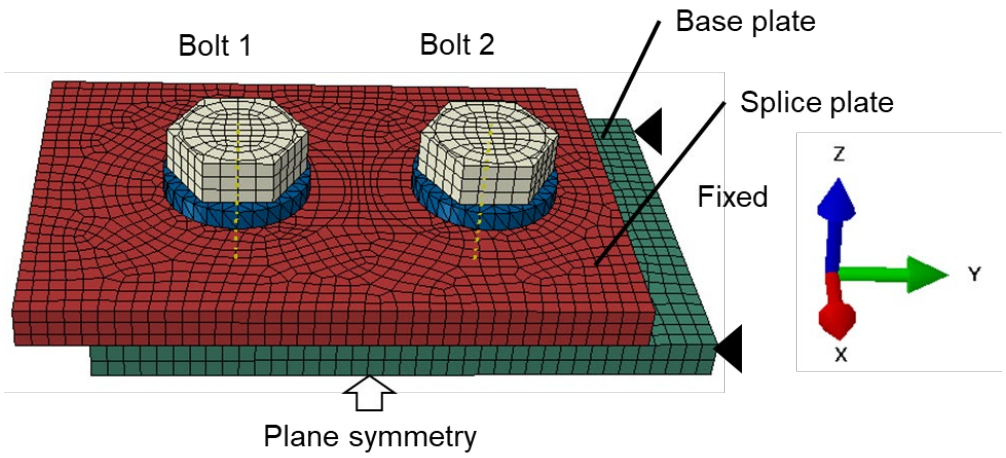

Figure 2.20 Analytical model to reproduce bolts tightening

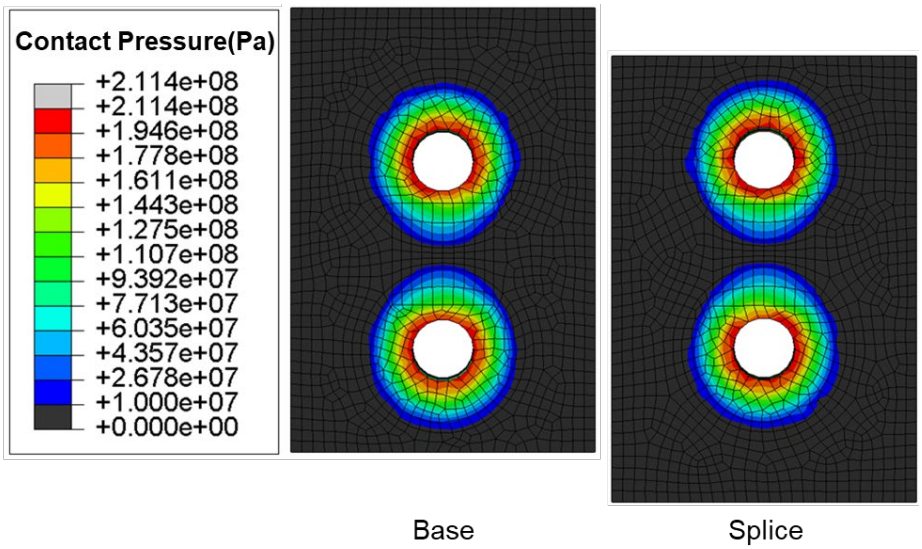

Figure 2.21 Contact pressure distribution of faying surface by bolts tightening

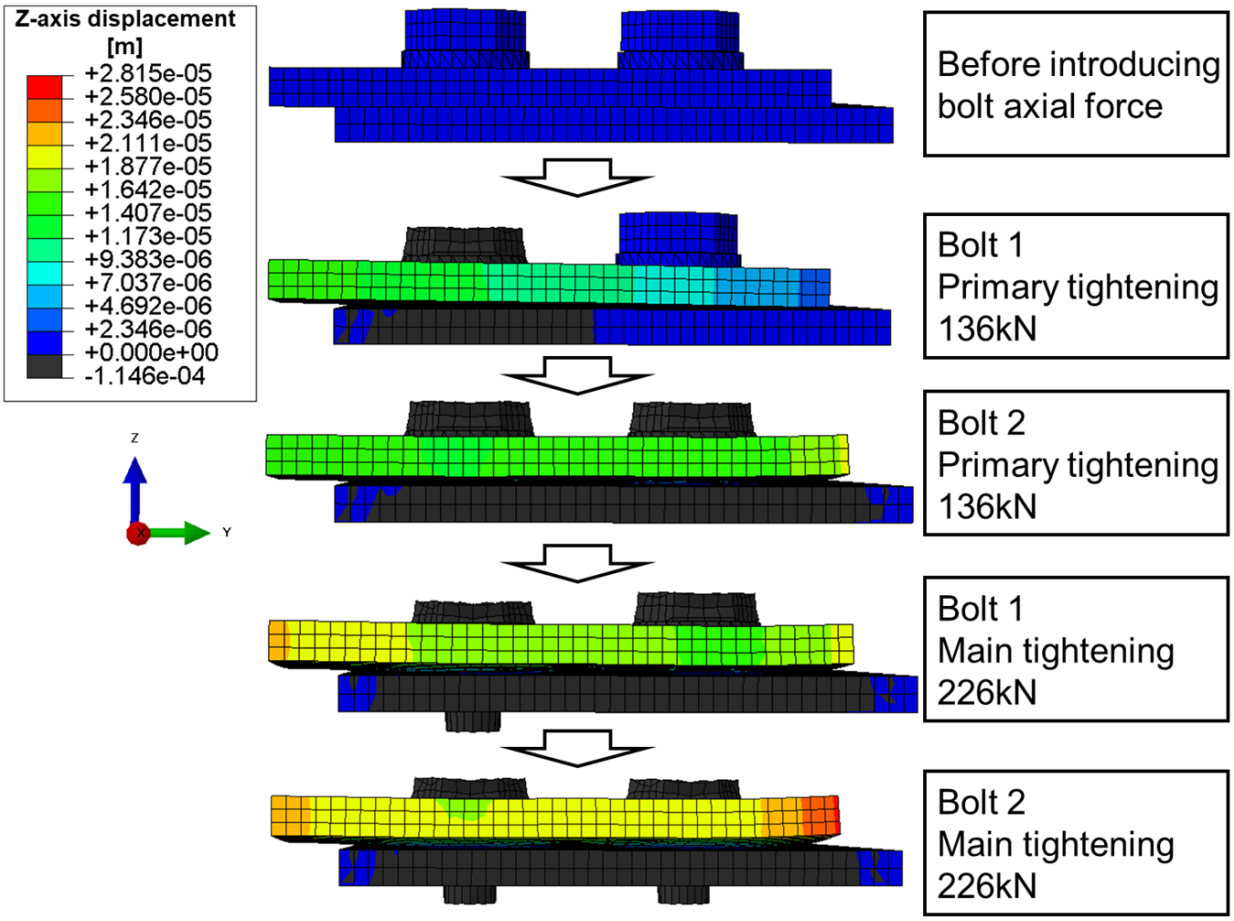

Figure 2.22 Deformation by bolt tightening order (Deformation magnification ×200)

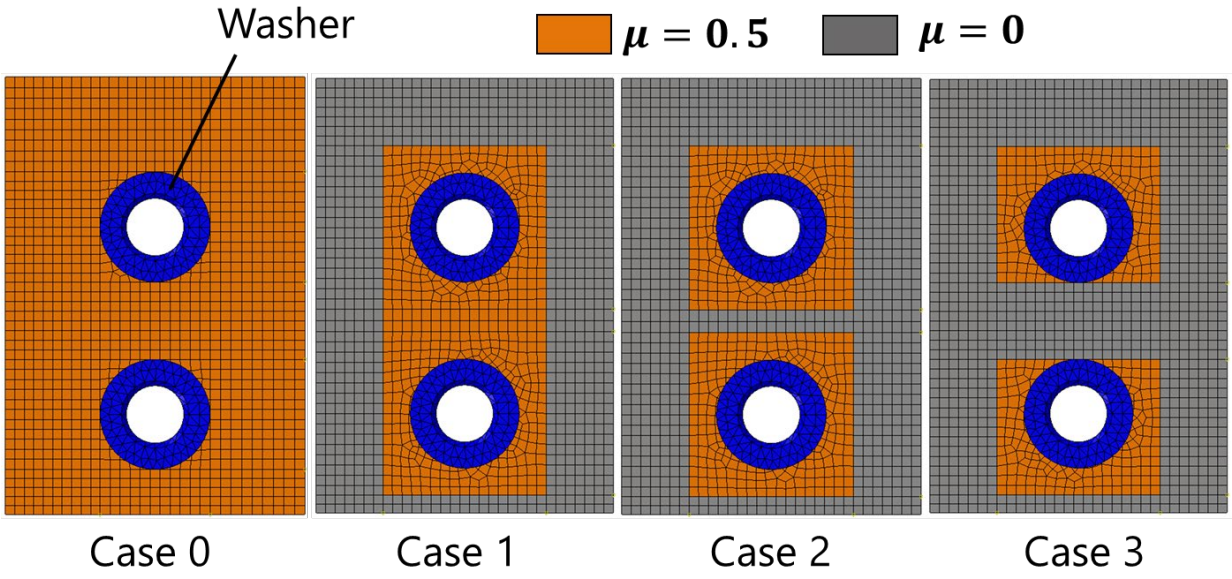

Figure 2.23 Consideration case for investigating the faying surface contact condition

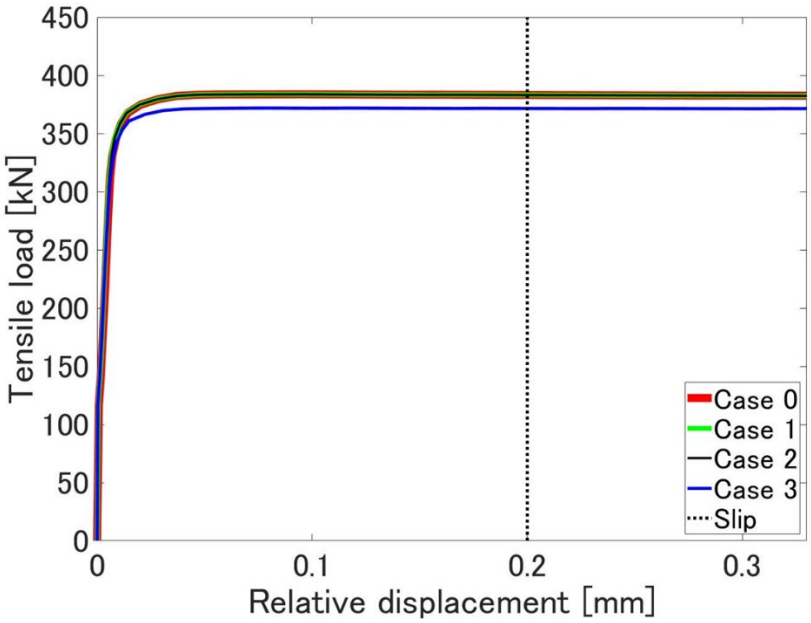

Figure 2.24 Comparison of slip resistance by contact pressure distribution

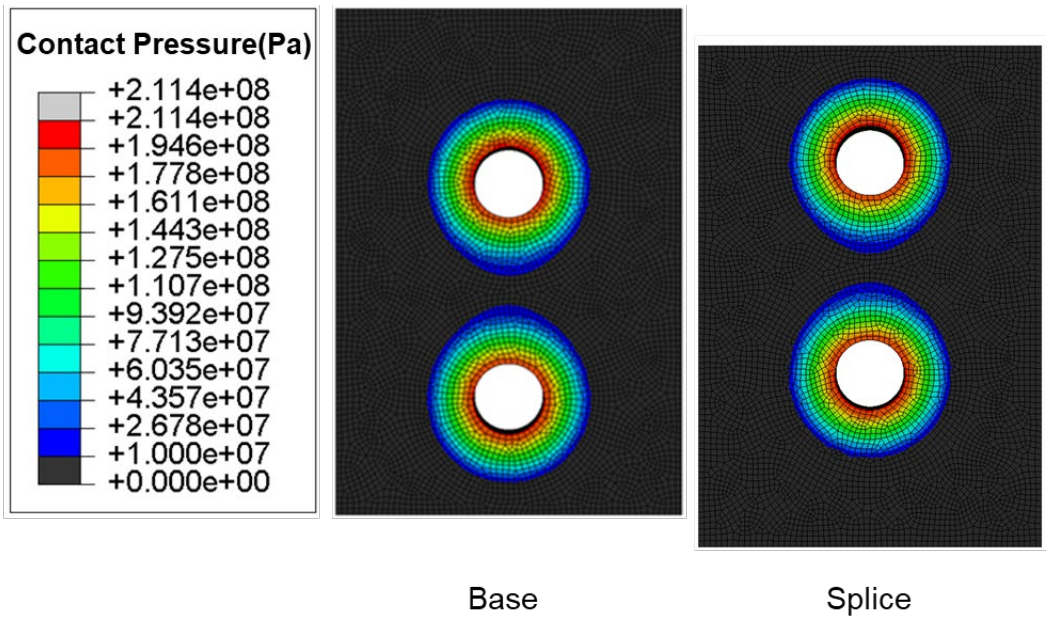

Figure 2.25 Contact pressure distribution on faying surfaces due to bolt tightening when the slip coefficient of the faying surfaces is set to 0

References (Chapter 2)

[1] Moriyama, H., Takai, T., Yamaguchi, T. and Lan, Y.: Effect of Cross-Sectional Dimensions and Bolt Arrangement on Deformed Bearing Limit Resistance of High-Strength Frictional Bolted Joints after Major Slip, *JSCE Journal of Structural Engineering*, Vol.66 A, pp.507-520, 2020.3.

[2] Moriyama, H., Sugiyama, H., Yamaguchi, T. and Lang, Y.: The Influence of Width and Thickness on Bearing Limit State of High Strength Frictional Bolted Joints, *Journal of JSCE A1 (Structural Engineering & Earthquake Engineering)*, Vol.74, No.1, pp.28-43, 2018.

[3] Toda, Y., Yamaguchi, T., Mineyama, Y. and Naoe, Y.: Experimental Study of Bearing Strength of Frictional Bolted Connection Based on Bolt Hole Deformation, *Journal of JSCE A1 (Structural Engineering & Earthquake Engineering)*, Vol.70, No.3, pp.333-345, 2014.

[4] Toda, Y., Yamaguchi, T., Matsumura, M., Naoe, Y. and Mineyama, Y.: 高力ボルト摩擦接合継手のすべり以後の支圧変形量と残存摩擦力の定量的評価, *JSCE* 第 67 回年次学術講演会, I-336, pp.671-672, 2012.9.

[5] Vangrimde, B. and Boukhili, R.: Descriptive Relationships Between Bearing Response and Macroscopic Damage in GRP Bolted Joints, *Composites Part B, Engineering*, Vol.34, I-7, pp.593-605, 2003.10.

[6] Fujimoto, M. and Satoh, N.: Study on Bearing Strength and Allowable Bearing Stress in Bolted Connection (Part 3) Synthesis, Transactions of AIJ, Vol.218, pp.27-36, 1974.4.

[7] JSCE 鋼構造委員会: 高力ボルト摩擦接合継手の設計・施工・維持管理指針(案), 鋼構造シリーズ 15, 2006.12.

[8] 日本建築学会: 鋼構造接合部設計指針, 2012.3.

[9] 日本道路協会: 道路橋示方書・同解説-II鋼橋・鋼部材編, 2017.11.

[10] Hirao, K.: Influence of Steel Strength on Load Carrying Capacity of High-Strength Bolted Frictional Joints Under Compression, *Bulletin of Master's Thesis, Department of Civil and Environmental Engineering, Tokyo Institute of Technology*, pp.283-292, 2019.3.

[11] Nishimura, N., Akiyama, H. and Kamei, Y.: Trend of Studies on High-Strength Friction Grip Bolt Joint, *Journal of the JSCE*, No.675, I-55, pp.1-14, 2001.4.

[12] Dassault Systemes SIMULIA User Assistance 2017: Abaqus/CAE User's Guide Online Documentation, 2017.

[13] Krolo, P., Grandić, D. and Bulic, M.: The Guidelines for Modelling the Preloading Bolts in the Structural Connection Using Finite Element Methods, *Journal of Computational Engineering*, Vol.2016, pp.1-8, 2016.1.

[14] Fukuoka, T.: Theory and Practice of Bolt Tightening Process (1), *Journal of the JIME*, Vol.46, No.3, pp.119-125, 2011.

[15] Fukuoka, T.: Theory and Practice of Bolt Tightening Process (2), *Journal of the JIME*, Vol.46, No.3, pp.126-131, 2011.

[16] Takaki, T. and Fukuoka, T.: Elasto-Plastic Analysis of the Tightening Process of Bolted Joint, Transactions of the JSME, Vol.67, No.660, pp.1269-1275, 2001.8.

[17] Tamakoshi, T., Ishio, M., Yokoi, Y., Yamasaki, K. and Mizuguchi, T.: Study on the Analytical Model Considered Introducing the Axial Force to Bolts of High Strength Bolted Friction Joints, *Journal of the JSSC*, Vol.21, No.84, pp.95-110, 2014.12.

[18] Nishimura, A., Taido, Y., Sera, S., Hozumi, S. and Mitani, T.: On the Scattering of Clamping Forces of High-Strength Bolts in Actual Structural Joints, *Proceedings of the JSCE*, No.180, pp.1-9, 1970.8.

[19] Fukuoka, T. and Takai, T.: Mechanical Behaviors of Bolted Joint During Tightening Using Torque Control, *JSME International Journal Series A Solid Mechanics and Material Engineering*, Vol.41, No.2, pp.185-191, 1998.

[20] You, R., Ren, L. and Song, G.: A Novel Comparative Study of European, Chinese and American Codes on Bolt Tightening Sequence Using Smart Bolts, *International Journal of Steel Structures*, Vol.20, No.3, pp.910-918, 2020.

[21] Wang, Y.Q., Wu, J.K., Liu, H.B. and Xu, S.T.: Modeling and Numerical Analysis of Multi-Bolt Elastic Interaction with Bolt Stress Relaxation, *Proceedings of the Institution of Mechanical Engineers, Part C: Journal of Mechanical Engineering Science*, Vol.230, No.15, pp.2579-2587, 2015.

[22] Minami, K., Tamura, H., Uchida, D., Shirahata, H., Yoshioka, N., Tsutsui, K. and Fujino, D.: A Study on Initial Value Setting Method for Relaxation Tests in High Strength Bolted Joints,

Journal of JSCE A1 (Structural Engineering & Earthquake Engineering), Vol.76, No.3, pp.496-509, 2020.

[23] Abid, M., Khalil, M.S. and Wajid, H.A.: An Experimental Study on the Relaxation of Bolts, *IIUM Engineering Journal*, Vol.16, No.1, pp.43-52, 2015.

[24] Ishihara, Y., Kobayashi, G., Minada, O. and Nishimura, N.: Characteristic Investigation and Cyclic Slip Experiment of HSFG Bolted Joints Which were Damaged by Earthquake, *Journal of the JSCE A1*, No.745, I-65, pp.53-64, 2003.10.

[25] Wang, F., Ho, S.C.M. and Song, G.: Monitoring of Early Looseness of Multi-Bolt Connection: A New Entropy-Based Active Sensing Method Without Saturation, *Smart Materials and Structures*, Vol.28, No.10, pp.1-7, 2019.

[26] Marshall, M.B., Lewis, R., Howard, T. and Brunskill, H.: Ultrasonic Measurement of Self-Loosening in Bolted Joints, *Proceedings of the Institution of Mechanical Engineers, Part C: Journal of Mechanical Engineering Science*, 2011.

[27] Jiang, Y., Zhang, M. and Lee, C.H.: A Study of Early Stage Self-Loosening of Bolted Joints, *Journal of Mechanical Design, Transactions of the ASME*, Vol.125, pp.518-526, 2003.

[28] Tanihira, T., Kamei, M., Ishihara, Y. and Taido, Y.: Carrying Capacity Test for Friction Joint of High-Strength Bolt from a Removed Foot-Way Bridge Used Under 17 Years, *JSCE Journal of Structural Engineering*, Vol.36 A, pp.1087-1096, 1990.3.

[29] Kanou, M., Tanihira, T., Ishihara, Y., Kobayashi, G. and Nishio, H.: 高力ボルト軸力の経年変化に関する実験的研究, *JSCE* 第 56 回年次学術講演会, I-B162, pp.324-325, 2001.10.

[30] Ishihara, Y., Kobayashi, G., Kano, M., Kamei, M. and Tanihira, T.: The Influence of Reduction and Variation of Bolt Tensions by Aging on Limit States of HSFG Bolted Joint, *Journal of JSCE*, Vol.763, VI-63, pp.33-42, 2014.6.

[31] Temitope, S.J.: Condition Monitoring of Bolted Joints, Ph.D. *Thesis, University of Sheffield*, Sheffield, UK, 2015.6.

[32] Rafik, V., Combes, B., Daidié, A. and Chirol, C.: Experimental and Numerical Study of the Self-Loosening of a Bolted Assembly, *Advances on Mechanics, Design Engineering and Manufacturing II*, pp.85-94, 2019.

[33] Kikukawa, S., Murata, K. and Nishimura, A.: Secular Changes of Slip Resistance of Friction-Type Bolted Joints in Structural Members, *Kawasaki Steel Giho*, Vol.11, No.4, pp.127-135, 1979.

[34] Takai, T., Yamaguchi, T. and Yamashina, K.: Analytical Study on Influence of Irregularity on Slip Strength of High Strength Bolted Friction Type Joint, *JSCE Journal of Structural Engineering*, Vol.61 A, pp.605-613, 2015.3.

[35] Takai, T., Peng, X. and Yamaguchi, T.: An Analytical Study on Load Carrying Characteristic of High Strength Bolted Friction Type Joint with Thick Filler Plate, *Journal of JSCE A1 (Structural Engineering & Earthquake Engineering)*, Vol.71, No.1, pp.1-9, 2015.

[36] Tanaka, A., Masuda, H., Wakiyama, K., Tsujioka, S., Hirai, K. and Tateyama, E.: Experimental Study on High Strength Bolted Friction Joints with Oversized and Slotted Holes, *JSSC Steel Construction Engineering*, Vol.5, No.20, pp.35-44, 1998.12.

[37] Mori, T., Yamazaki, N. and Yamaguchi, J.: Slip and Yield Resistance of Friction Type of High Strength Bolted Connections with Over-Sized Holes, *Journal of the JSCE*, No.794, I-72, pp.157-169, 2005.7.

[38] Murakoshi, J., Sawada, M., Yamaguchi, T., Peng, X. and Ootake, A.: Slip Resistance Tests of Friction-Type High-Strength Multi Bolted Joints with Coated Contact Surfaces by Inorganic Zinc Rich Paint on Thick Plate, *Journal of JSCE A1 (Structural Engineering & Earthquake Engineering)*, Vol.70, No.1, pp.94-104, 2014.

[39] Peng, X., Yamaguchi, T., Takai, T., Murakoshi, J. and Sawada, M.: FEA Study on the Slip Behavior of High Strength Multi Bolted Friction Type Joints with Thick Plates by Structural Dimensions, *Journal of JSCE A1 (Structural Engineering & Earthquake Engineering)*, Vol.69, No.3, pp.452-466, 2013.

[40] Kamei, Y., Matsuno, M. and Nishimura, N.: An Analytical Study on Slip Strength of Multi HSFG Bolted Joints in Tention, *Journal of JSCE*, No.640, I-50, pp.49-60, 2000.

[41] Geoffrey, L.K., John, W.F. and John, H.A.S.: Guide to Design Criteria for Bolted and Riveted Joints, Second Edition, *American Institute of Steel Construction, Inc.*, 1987.

[42] Tamura, H., Minami, K., Yoshioka, N., Uchida, D., Moro, M., Hama, T. and Hirao, K.: Applicability of Pretensioned Bolted Joints Including Different Contact Faces, *Journal of*

JSCE A1 (Structural Engineering & Earthquake Engineering), Vol.76, No.2, pp.255-274, 2020.4.

[43] Murakoshi, J., Sawada, M., Yamashina, K., Yamaguchi, T. and Ishihara, D.: Study of Influence on Slip Coefficient of High Strength Bolted Friction Type Joints by Painting Condition and Exposure Term, *Journal of JSCE A1 (Structural Engineering & Earthquake Engineering)*, Vol.73, No.1, pp.40-53, 2017.

[44] Minami, K., Mori, T. and Sugiya, T.: 摩擦面の状態が高力ボルト継手のすべり耐力に及ぼす影響, *JSCE* 第 59 回年次学術講演会, I-587, pp.1171-1172, 2004.9.

[45] Tajima, J.: 高力ボルト摩擦接合概説, 第 2 版, 技報堂, 1966.11.

[46] Nishimura, A., Tajima, J. and Yamasaki, T.: Aging of High Strength Bolted Joints in Long Service, *IABSE Reports*, Vol.39, pp.149-154, 1982.

[47] Liu, W. and Lin, W.: Effects of Bolt Misalignment on Stress Around Plate Hole, *Advances in Mechanical Design*, pp.1511-1524, 2017.

[48] Tamura, H., Minami, K., Yoshioka, N., Uchida, D., Moro, M., Hama, T. and Hirao, K.: Applicability of Pretensioned Bolted Joints Including Different Contact Faces, *Journal of JSCE A1 (Structural Engineering & Earthquake Engineering)*, Vol.76, No.2, pp.255-274, 2020.4.

[49] Murakoshi, J., Sawada, M., Yamashina, K., Yamaguchi, T. and Ishihara, D.: Study of Influence on Slip Coefficient of High Strength Bolted Friction Type Joints by Painting Condition and Exposure Term, *Journal of JSCE A1 (Structural Engineering & Earthquake Engineering)*, Vol.73, No.1, pp.40-53, 2017.

[50] Minami, K., Mori, T. and Sugiya, T.: 摩擦面の状態が高力ボルト継手のすべり耐力に及ぼす影響, *JSCE* 第 59 回年次学術講演会, I-587, pp.1171-1172, 2004.9.

[51] Tajima, J.: 高力ボルト摩擦接合概説, 第 2 版, 技報堂, 1966.11.

[52] Mori, T., Amitani, T. and Uchida, D.: Influence of Bolt Tightening Force on Slip Coefficient of High-Strength Bolted Friction Type Joints, *Journal of JSCE A1 (Structural Engineering & Earthquake Engineering)*, Vol.75, No.1, pp.58-66, 2019.

[53] Maiorana, E., Zampieri, P. and Pellegrino, C.: Experimental Tests on Slip Factor in Friction Joints: Comparison Between European and American Standards, *Frattura ed Integrità Strutturale*, Vol.43, pp.205-217, 2018.

[54] Cruz, A., Simões, R. and Alves, R.: Slip Factor in Slip Resistant Joints with High Strength Steel, *Journal of Constructional Steel Research*, Vol.70, pp.280-288, 2012.

[55] Koike, Y., Kasugai, T. and Ichimiya, M.: Developmental Study on Inorganic and Organic Zinc-Rich Paint with High Slip Factor for High Strength Friction Grip Bolted Joints, *Journal of JSSC*, Vol.16, No.62, pp.75-84, 2009.6.

[56] Nah, H.S., Lee, H.J. and Kim, K.S.: Evaluation of Slip Coefficient of Slip Critical Joints with High Strength Bolts, *Structural Engineering and Mechanics*, Vol.32, No.4, pp.477-488, 2009.

[57] Uno, N., Inoue, K., Takeuchi, I., Azuma, S. and Kita, T.: Experimental Study on High Strength Bolted Friction Joints with HF-Splice-Plates, *AIJ Journal of Structural and Construction Engineering*, No.502, pp.127-133, 1997.12.

[58] Kamura, T. and Hokugo, H.: The Effect of Surface Roughness of High Strength Bolt Frictional Joints on Slip Resistance, *AIJ Journal of Structural and Construction Engineering*, No.485, pp.127-134, 1996.7.

[59] Mori, T., Minami, K., Inokuchi, S. and Yamaguchi, T.: Slip Coefficient and Contact Surface Condition of Friction Type of High Strength Bolted Connections, *Journal of JSCE A*, Vol.64, No.1, pp.48-59, 2008.1.

[60] Railway Technical Research Institute: 鉄道構造物等設計基準・同解説「鋼・合成構造物」, 2000.7.

[61] Architectural Institute of Japan: 鋼構造許容応力度設計規準, 2019.10.

[62] Architectural Institute of Japan: 鋼構造接合部設計指針, 2021.2.

[63] ISO: *ISO 10721-1, Steel structures-Part 1, Materials and design*, 1997.2.

[64] AASHTO: *Standard Specifications for Highway Bridges*, 2002.

[65] Eurocode: *Eurocode 3 Part 2, Steel bridges and plated structures*, 1995.6.

[66] BSI: *BS 5400, Part 3, Code of practice for design of steel bridges*, 1982.

[67] Architectural Institute of Japan: 建築工事標準仕様書 JASS6 鉄骨工事, 2018.1.

[68] You, R., Ren, L. and Song, G.: A Novel Comparative Study of European, Chinese and American Codes on Bolt Tightening Sequence Using Smart Bolts, *International Journal of Steel Structures*, Vol.20, No.3, pp.910-918, 2020.

[69] Zhu, L., Bouzid, A. H. and Hong, J.: Numerical and Experimental Study of Elastic Interaction in Bolted Flange Joints, *Journal of Pressure Vessel Technology*, Vol. 139, pp. 021211-1-021211-7, 2017.4.

Chapter 3

Establishment of Non-Destructive Bolt Axial Force Measurement

3.1. Overview

It has been reported that the bolt axial force of high strength bolted joints used in many structures may decrease even after operation due to the effects of vibration and earthquakes, as well as relaxation due to initial loosening [1-28]. Therefore, as a maintenance technology to ensure the safety of structures, it is required to establish a method for accurately and quantitatively evaluating the axial force of existing bolts. Currently, there are many reports that propose a method for evaluating the bolt axial force non-destructive [29-43]. Among them, there is a method using ultrasonic waves that uses changes in propagation time. The method evaluates the bolt axial force by using the change in the propagation time until the ultrasonic wave transmitted from the bolt head is reflected from the bottom surface and returned. In the method using the change of propagation time, there is a high correlation between bolt elongation and bolt axial force, and, the bolt axial force is evaluated by the difference in ultrasonic propagation time between when the bolt axial force is not introduced and when the bolt axial force is introduced. However, the bolt length varies due to manufacturing errors, in applying this method, it is necessary to separately measure the ultrasonic propagation time before the introduction of axial force for each bolt to be measured. In addition, consideration must be given to smoothing the tip of the bolt shank [44], making it difficult to use for evaluating the axial force of existing bolts.

In this way, conventional research that attempts to evaluate bolt axial force has problems in terms of quantification and applicability of existing bolt axial force evaluation, and there is room for improvement. On the other hand, in recent years, in the field of civil engineering, many studies have been conducted in combination with machine learning [45-61]. However, the bolt axial force evaluation method that combines ultrasonic waves and machine learning has not been established so far. Therefore, in this research, it is proposed a method with sufficient evaluation accuracy by combining ultrasonic waves, signal processing, and machine learning. Furthermore, it is proposed to build a quantitative bolt axial force evaluation method for existing bolts that are easy to apply in practice. Since the purpose is to apply to existing bolts, the information on bolt length is not used, and attention is paid to changes in the shape of the bolt head due to the introduction of bolt axial force. First, FE analysis clarified the change in the shape of the bolt head when the bolt axial force was introduced. Next, frequency analysis was applied to the data in the initial time zone obtained by ultrasonic measurement from the bolt head and then a random forest was used to select

signals containing information on the bolt head deformation. The characteristic signal related to the bolt axial force was extracted from the raw waveform in the initial time zone by frequency analysis and machine learning. Signal processing by the parasitic discrete wavelet transform (P-DWT) [62-63] was added to the characteristic signal, and finally, machine learning using linear regression [64-65] was applied to the waveform after signal processing. As a result, the attempt is to improve the accuracy of bolt axial force evaluation.

3.2. Ultrasonic Measurement

The purpose of this study is to quantitatively evaluate the uncertain influential parameters contained in bolted joints for bolted joints coated with inorganic zinc-rich paint. Many non-destructive evaluation methods are being studied to evaluate bolt axial forces. In particular, there are many studies on bolt axial force evaluation using ultrasonic waves. However, due to the problem of bolt length manufacturing error, cause of the drawing of the bolt shank at the bolt manufacturing stage, it is difficult for most of the proposed methods to deal with bolts in existing joints. Therefore, in this chapter, a new measurement method using ultrasonic waves that does not use bolt length information is proposed. The basic characteristics of ultrasonic waves are described below. In addition, after introducing the conventional ultrasonic measurement methods and understanding the problems they have, consideration was given to improve the current shortcomings.

3.2.1. Ultrasonic Measurement Devices Used in this Study

First, the understanding of the generation, transmission, and reception of ultrasonic waves can be deepened. Ultrasound measurement generally follows the procedure shown in **Figure 3.1** [66]. In this study, a unique method has been developed at the stage of feature extraction and evaluation. However, the general procedure is as shown in **Figure 3.1**.

The equipment and settings used in this study are described below. **Figure 3.2** shows an overview including the equipment used in this study. This figure shows the one-probe method, but the pitch catch method, which is a two-probe method, can also be applied by using another probe. Ultrasonic waves are transmitted from the ultrasonic pulser-receiver (**Figure 3.3**) to the probe, and

the probe receives the reflected wave from the object and sends it to the ultrasonic pulser-receiver. Filtering processing is possible within the ultrasonic pulser-receiver, but raw waveform data was acquired in this study in order to aim for reproducibility using equipment from different manufacturers. The transmitted waveform (pulse type) was a rectangular burst as shown in **Figure 3.4**, and the pulse wave number was 5 waves. The Pulse Repetition Frequency (PRF) was set so that the next pulse output would not be included in the observation width. The damping resistance was set to 100Ω and the sampling frequency was set to 100MHz. The frequency of the chirp wave is a geometric progression, and its common ratio is described by

$$\mathrm{R} = C_r^{(1/(n_w-1))} \tag{3-1}$$

where, C_r is the chirp ratio and n_w is the number of waves. The settings for the ultrasonic pulser-receiver used in this study are summarized in **Table 3.1**. There are two types of probes used in this chapter, and these are shown in **Figure 3.5**.

The frequency of the ultrasonic probe used in the study is 5MHz or 10MHz. The size of the bottom of the probe was set to 14 mm in diameter so that it could be installed avoiding the engraved bolts (**Figure 3.6**). A certain amount of machine oil (**Figure 3.7**) was applied to the contact point of the probe as the contact medium of the probe using a dropper. In order to prevent the size and shape of the received signal from changing depending on how the probe is pressed, fix the probe with a clamp with a spring as shown in **Figure 3.8**, and keep the length of the spring constant. So, I decided to fix the probe with a certain force. In addition, the gain was kept constant in all measurements. Both are single oscillator type vertical probes and have an internal structure as shown in **Figure 3.9**. By outputting the impulse voltage to the electrodes attached to both sides of the piezoelectric element, the piezoelectric element repeatedly expands and contracts and vibrates. The thinner the piezoelectric element, the higher the frequency of vibration, and the ultrasonic waves are transmitted from the probe. The transmitted ultrasonic waves are reflected at the interface, hits the piezoelectric element, is converted into a voltage, and is captured as a signal in the receiver. There are two types of ultrasonic measurement, contact type and non-contact type. As a non-contact ultrasonic method, a method using an electromagnetic ultrasonic probe [67], a laser ultrasonic waves [68-69], and an air propagation ultrasonic probe [70] was developed after 1960. However, compared to the contact type, it is difficult to meet the requirements for spatial resolution and high reliability, so the contact type was adopted in this study. The device for ultrasonic measurement described above was used in this study.

3.2.2. Conventional Bolt Axial Force Evaluation Method by Ultrasonic Measurement

Many studies on bolt axial force measurement using ultrasonic waves have been conducted, and the details are introduced in "Related Research" in Chapter 1. Among them, the bolt axial force measurement method that has been studied most is the measurement from the bolt head. The bolt length of high strength bolts increases when the bolt axial force is introduced. By using this property of the bolt, the conventional ultrasonic measurement method evaluates the bolt axial force by the Time of Flight (TOF). TOF assumes that there is a correlation between bolt elongation and ultrasonic velocity. The bolt axial force is evaluated from the time difference of the received wave by utilizing the fact that the time for receiving ultrasonic waves changes due to the elongation of the bolt. The calculation of TOF is explained below. The path of ultrasonic waves in ultrasonic measurement from the bolt head is shown in **Figure 3.10**. TOF is generally the time difference between the 1st reflection and the 2nd reflection as shown in **Figure 3.11**. The 1st rap time $\Delta_1$and the 2nd raps time Δ_2 are described below.

$$\Delta_1 = 2T_p + 2T_u \tag{3-2}$$

$$\Delta_2 = 2T_p + 4T_u \tag{3-3}$$

where, T_p is the one-way ultrasonic propagation time inside the probe, and T_u is the one-way ultrasonic propagation time inside the bolt. Since Δ_{TOF} is the time difference between Δ_1 and Δ_2, it is expressed as follows:

$$\Delta_{TOF} = \Delta_2 - \Delta_1 = 2T_u \tag{3-4}$$

where, T_u can be expressed by the ultrasonic velocity v and the volt length L so it is also described as follows:

$$\Delta_{TOF} = 2T_u = \frac{2L}{v} \tag{3-5}$$

However, it is difficult to evaluate the bolt axial force of existing bolts with high accuracy by this conventional ultrasonic measurement method using TOF. The reason is that the bottom of the bolt shank is drawn in the process of manufacturing the bolt [44]. Therefore, the initial length of each bolt is different. Therefore, in order to apply it to existing bolts, it is necessary to measure the initial length for all target bolts in advance.

Thus, it is required to construct a bolt axial force evaluation method for existing bolts that does not require prior measurement. In this study, it was attempted to solve the problem of bolt manufacturing error by focusing on the invariant information related to the bolt axial force.

3.3. Analytical Study to Investigate Bolt Axial Force and Related Invariant Information

In order to enable the evaluation of the bolt axial force of existing bolts, the invariant information related to the bolt axial force was investigated. Therefore, the analysis of high strength bolts in which bolt axial force was introduced was performed. The analytical model is a reproduction of the high strength bolt F10T M22 and is shown in **Figure 3.12**. Two types of bolt lengths, 95mm and 70mm, were compared and examined. Reproduction of the threaded part was omitted. The bottom of the washer was completely fixed. The introduction of bolt axial force was expressed by pulling the bottom of the slave bolt shank by forced displacement. The mesh size was set to 0.8mm for the 8-node solid element (hexahedron) in order to capture minute deformations. The slip coefficient of the contact surface with the washer was set to 0.5 with reference to the value proposed by Nishimura et al. [71], assuming inorganic zinc-rich paint. As for the material properties of bolts, the plastic strain is set to 0 up to a yield stress of 900N/mm^2. A deformation diagram when a bolt axial force of 220kN is introduced is shown in **Figure 3.13**. From this result, the deformation of the bolt head was confirmed. According to Nitta et al. [72], deformation of the bolt head has been confirmed, although the diameter and shape are different from those of the target bolt in this study. Taking advantage of this property, a strain gauge is attached to the bolt head to control the bolt axial force [73]. As can be seen from **Figure 3.13**, when a probe with a horizontal bottom is installed on the bolt head, a space is created between the probe and the surface of the bolt head. Since the probe has a diameter of 14 mm, the space between the probe and the surface of the bolt head is increased by the bolt axial force from the displacement of the surface of the bolt head with the bolt neck lengths of 95mm and 70mm shown in **Figure 3.14**. It became clear that they were different. It was also confirmed that the difference between

the bolt neck lengths of 95mm and 70mm has almost no effect on the amount of deformation of the bolt head.

In addition, Arakawa et al. [74] reported that when an ultrasonic vertical probe was installed on a curved surface for measurement, the contact conditions were different and the refraction angle changed, and the contact conditions were set during the initial time of the ultrasonic measurement waveform. It is possible that this change is included and is important information for evaluating the bolt axial force.

From the above, it is considered that the important information when evaluating the bolt axial force may be included in the initial time zone including the contact part between the ultrasonic probe and the high strength bolt.

3.4. Bolt Axial Force Measurement Experiment

For the bolt axial force evaluation experiment, the specimens modelled with basic bolted joints was created. In the bolt axial force evaluation experiment, the data of each bolt axial force was acquired. However, the bolt axial force is an uncertain parameter and constantly changes with the elapsed time. Therefore, it is necessary to always control the bolt axial force more accurately. In order to constantly monitor the bolt axial force, two strain gauges are attached to the bolt shank to control the bolt axial force (**Figure 3.15**). Deformation performance of each bolt differs depending on the manufacturing error. Thus, all bolts used in the experiment were calibrated. In this study, two bolts with a bolt length of 95mm and two bolts with a length of 70mm were used.

3.4.1. Bolt Axial Force Calibration of Bolts Used in the Experiment

To calibrate the bolt axial force, attached a bolt with a strain gauge used in the experiment to the bolt axial force meter shown in **Figure 3.16**, and tightened it by 10kN with a torque wrench. At that time, recorded the value of the strain gauge for each bolt axial force. The relationship between strain and bolt axial force was calculated by calibration as shown in **Figure 3.17**. From this result, it was confirmed that the relationship between strain and bolt axial force is slightly different for each bolt. In the bolt axial force evaluation experiment, the bolt axial force was introduced based on this result.

3.4.2. Specimens and Measurement Method

The specimens used in this chapter are basic bolted joints, and their outlines are shown in **Figure 3.18** and **Table 3.2**. The plate thickness was set based on the length under the neck of the bolt. The steel grade of the base plate and the splice plate was SS400, the surface treatment was the commonly used inorganic zinc-rich paint, and the bolts were F10T M22 of the same manufacturer and lot. The two bolts were located approximately in the center of the bolt hole (24.5mm) and had the same tightening conditions, but to distinguish between training and testing when applying machine learning, as shown in **Figure 3.18**, they are called Bolt 1 and Bolt 2. Measurements were taken from the top surface of the bolt head while avoiding marking of the bolt head by the one-probe method for the bolt of such specimens. At that time, the bolt head and shank were left in mill scale, the bolt axial force was introduced, and the measurement was performed in about 5 seconds per measurement after the probe was installed. The probe was removed after each measurement and re-installed for measurement. Since it has been reported that the bolt axial force varies at about 120kN or more due to the influence of aging [13], this study targeted the range of 120kN or more. For Bolts 1 and 2 of the same manufacturer and lot, the bolt axial force was measured in 11 steps in the range of 120kN to 220kN at a pitch of 10kN. In addition, each bolt was measured 5 times for each bolt axial force. In other words, each bolt was measured 55 times.

3.5. Extraction of Ultrasonic Waveforms Related to Bolt Axial Force

In the proposed method of this study, the axial force of the existing bolt is evaluated by using the waveform shape without using the information of the ultrasonic propagation time. As a result of the analysis by introducing the bolt axial force of the high strength bolt, it was confirmed that the bolt head was deformed by the bolt axial force. However, in the field of crack detection, it is said that the evaluation performance is inferior in the area near the probe [75]. This is because the reverberation of the dial tone generated during ultrasonic measurement, which is called the dead zone [76-77], is received directly under the probe, and the reflected signal from the crack is buried. However, the situation is considered to be different because this study attempted to extract the characteristics of the reflected wave by the shape of the reflecting surface instead of detecting

cracks. Thus, a detailed analysis was performed on the waveform of the time zone (Initial time zone) directly under the probe.

3.5.1. Extraction of Ultrasonic Waveforms Related to Bolt Axial Force Using Random Forest

First, it is necessary to confirm whether the signal related to the bolt axial force is included in the initial time zone. Therefore, the ultrasonic measurement waveform was divided into several zones, and bolt axial force evaluation was performed by applying machine learning to the raw waveform data of each zone, and the evaluation accuracy in the initial time zone was confirmed. The zones were set as shown in **Figure 3.19**, zone 1 is the entire ultrasonic measurement waveform, and Zone 2 and 3 are the first and second reflected waves from the bottom of the bolt axis, respectively. Zone 2 and 3 handle data for 4μs when measured with a 10MHz probe centered on the maximum amplitude value of the reflected wave, and for 6μs when measured with a 5MHz probe. Zone 4 is the data up to the reflected wave 1, and zone 5 is the time zone up to the first 6μs, which is the initial time zone including the dead zone.

Breiman [78] states that random forests are easier to implement than other classifiers such as NNs and SVMs, and have excellent evaluation capabilities without overfitting. Construction of a classification model by deep learning based on one-dimensional convolution operation [79] is also considered as an effective means, but in this research, the number of training samples is limited, and one-dimensional data such as time history waveforms are data-expanded. Since it is difficult to remove, the possibility that the model is overfitted cannot be denied. In addition, Hirokane et al. [80] hit a high strength bolt with a hammer and evaluated the residual axial force of the high strength bolt by various pattern recognition methods based on the obtained vibration waveform data. Four machine learning algorithms, NN, SVM, decision tree, and random forest, are used to evaluate the bolt axial force. And the random forest that used a large number of weak classifiers to determine the output, could be recognized with the highest accuracy.

With reference to the above research, by applying the random forest to the zone related to the bolt axial force in the ultrasonic measurement waveform, the zone related to the bolt axial force was extracted. For this zone survey, a study case is provided in **Table 3.3** using probes with frequencies of 5MHz and 10MHz. The raw waveform data measured by Bolt 1 is used as the training data, and the raw waveform data measured by Bolt 2 is used as the testing data. There

were 55 teacher data and 55 test data in each zone, and each was evaluated by the random forest to confirm its accuracy. The outline and evaluation results of Random Forest are described below.

Random forest is an algorithm based on ensemble learning bagging [81], which classifies by the results of multiple decision trees constructed from randomly selected training data and explanatory variables. Bagging is a method of learning multiple models in parallel by bootstrap that restores, extracts, and samples some data from training data. A conceptual diagram of the random forest is shown in **Figure 3.20**.

Each decision tree is randomly sampled from the teacher data, allowing duplication, and can reduce the probability of misclassification at the branch of the decision tree. On the other hand, there is a drawback that it is easy to overfit because it tries to classify training data completely, but Random Forest addresses this problem. Because multiple sampling data are generated by the bootstrap, the correlation between each decision tree is low. In addition, they are classified by majority vote, it is possible to reduce the effect of overfitting.

In Bolt 1, 10kN pitch waveform data measured from 120kN to 220kN of bolt axial force and labeled bolt axial force feed them into machine learning. Each zone of the study case is tested in the waveform data measured by Bolt 2. The random forest is used to evaluate with an accuracy of 10kN pitch. The waveform data was set to be sampled at a pitch of 0.01μs in order to focus on minute changes in the signal, and the Random Forest Classifier in the Python library sklearn.ensemble was used to evaluate the bolt axial force. In order to construct a simple method, the number of decision trees was set to 100, the character string was set to the Gini coefficient, and the other parameters were set to the default values. The correct answer rate of the bolt axial force evaluated in each case is shown in **Figure 3.21**.

In all cases, the accuracy rate was higher in the order of Zone 5, 4, 1, 2, and 3. Zone 5, which has the highest accuracy rate, contains only the reflected signal (Zone 5) from the vicinity of the bolt head including the dead zone, and the accuracy rate was about 50%. The dead zone is a region that has not been noticed until now because it has been difficult to detect flaws due to the width of the transmission pulse. Next, the accuracy rate is higher in the order of Zone 4 and 1, and these zones include other signals in addition to the initial time zone including the dead zone. The correct answer rate decreases as the number of signals other than the initial time zone is included, it is considered that the order is in the order of Zone 4 and 1. In addition, it is considered that the correct answer rate is lower in the case where the initial time zone is not included at all than in the case

where the teacher data includes the initial time zone. It is also considered that there is less information related to the bolt axial force in the reflected wave from the bottom of the bolt shank than in the initial time zone. From this result, it can be said that the initial time zone contains information related to the bolt axial force. Therefore, in this study, Zone 5 should be focused which is only the initial time zone.

3.5.2. Analysis of Ultrasonic Waveforms in the Initial Time Zone

From the above examination, it was confirmed that the initial time zone of the measured waveform data obtained by ultrasonic measurement from the bolt head includes a zone related to the bolt axial force. However, because the initial time zone includes waveforms other than the zone related to the bolt axial force, in order to evaluate the bolt axial force accurately, it is necessary to further select only the zone related to the bolt axial force from within the initial time zone. From this point onward, a study case was set up again in order to focus only on Zone 5 in **Table 3.3**. All of these study cases focus on the initial time zone (Zone 5). Therefore, the initial time zone of the ultrasonic measurement waveform was focused and it was confirmed the frequency band in that range. Furthermore, based on the results, only the zone containing the information related to the bolt axial force was selected by continuous one-dimensional wavelet transform (CWT).

In order to improve the bolt axial force evaluation accuracy and establish a bolt axial force evaluation method corresponding to the measurement of existing bolts, the ultrasonic measurement waveform in the initial time zone was analyzed and the frequency in the zone related to the bolt axial force was confirmed. The analysis focused on the data in the initial time zone obtained from the study cases shown in **Table 3.4**. **Figure 3.22** shows the raw waveform data of the initial time zone at 180kN in Cases A, B, and C. Case A and Case B are measured at 10MHz, 5 waves can be confirmed during the first 0.5μs, and Case C is measured at 5MHz, so 5 waves can be confirmed during the first 1μs. This is thought to be because the high voltage burst signals that drive the probe were recorded in an overlapping manner because transmission and reception were performed using the one-probe method. Therefore, it can be said that this burst wave does not contain information related to the bolt axial force. After the burst wave, a waveform with irregular period and amplitude can be confirmed. In this study, this waveform is called a beat waveform. After that, a waveform in which the period becomes constant and the amplitude decreases at a constant attenuation rate can be confirmed, and this is called the attenuation waveform. It is considered that the waveform

after the burst wave includes a zone related to the bolt axial force, frequency analysis was performed for that range and the frequency information in each time zone was confirmed. The frequency components of the beat waveform and the attenuation waveform are as shown in **Figure 3.23**, and it can be confirmed from (b) that the attenuation waveform is about 4MHz in each case. Also, from the beat waveform (a), it can be confirmed that signals in many frequency bands including the attenuation waveform frequency of 4MHz and the center frequency of the probe are mixed. **Figure 3.24** is a scalogram at a bolt axial force of 180kN plotted by CWT using Gabor, which is a general mother wavelet (MW). It can be confirmed that the attenuation waveform with a frequency of 4MHz is generated from the middle of the beat waveform. A frequency larger than 10MHz can be confirmed in the beat waveform, but this is because the data in the initial time zone has a large power and the amplitude is clipped as can be seen from the raw waveform data. From these frequency analysis results, it is considered that the damping waveform does not contain information related to the bolt axial force because the damping waveform is always a constant frequency. On the other hand, the beat waveform contains many characteristic components, it is possible that the zone related to the bolt axial force is in the beat waveform of the initial time zone. **Figure 3.25** shows the frequency band of each bolt axial force of the beat waveform. From this result, no linear change with the increase in bolt axial force could be confirmed. However, in Case A and Case B, the shape is different for each bolt axial force, so it is possible that the application of machine learning is effective.

In order to select only the beat waveform that is considered to be the zone related to the bolt axial force, it is needed to think about how to determine the boundary between the beat waveform and the attenuation waveform. The beginning of the beat waveform is after the burst wave, 0.5μs after Case A and Case B, and 1μs after Case C.

To select only the beat waveform, it is necessary to remove the frequency of the attenuation waveform. Therefore, from **Figure 3.24**, the bandpass was applied in the range of 7MHz to 10MHz excluding the frequency smaller than 7MHz of the decay waveform and the frequency larger than 10MHz due to clipping, and the result of applying CWT was the scalogram shown in **Figure 3.26**. Clipping is remarkable near the boundary between the burst wave and the humming waveform, but even after applying CWT, it was confirmed that the amplitude decreased at 0.5μs for Case A and Case B and 1μs for Case C. It is considered that the occurrence of clipping has a small effect on the analytical method of this study. The horizontal broken line shows the frequency at which

the amplitude peaks in each case, and the amplitude on the broken line is normalized and shown in **Figure 3.27**. Looking at the shape of each time zone in **Figure 3.27**, the shape becomes irregular after the maximum amplitude near the burst wave, and finally the amplitude decreases sharply and the shape is almost constant.

Therefore, in this study, in **Figure 3.27**, the zone with irregular shape was defined as the beat waveform, and the end of the beat waveform was set. In the zone where the shape of the latter half is almost constant, the place where the amplitude is first reduced by 90% was set as the end of the beat waveform.

3.6. Extraction of Characteristic Signals by Applying Signal Processing by Parasitic Discrete Wavelet Transform (P-DWT)

Among the components included in the measured waveform, in this study, it was aimed to improve the effect of machine learning by focusing on the high-frequency components that are thought to contain minute features such as time-localized signals. In order to acquire the high frequency components of the selected beat waveform, signal processing, especially P-DWT was chosen.

The following describes a method for extracting characteristic signals by applying signal processing using P-DWT [62-63]. Attention is paid to high-frequency components that are considered to contain minute characteristics in the extracted signal.

In order to acquire high-frequency components including minute characteristics of beat waveforms, signal processing by P-DWT, which is effective for signal processing with non-linearity, was performed. P-DWT is a method to acquire a feature signal that is to acquire the characteristic signal by adding the frequency characteristics of the real signal mother wavelet (RMW) created from the actually measured waveform to the decomposition flow of the conventional discrete wavelet transform (DWT) as a frequency domain filter. The target waveform and RMW are decomposed to the level where a filter is added by the base mother wavelet, it is possible to sufficiently remove extra data.

DWT, including P-DWT, can decompose the target signal into two components, Approximation on the low frequency side and Detail on the high frequency side, for each level. The waveforms selected in this study are unsteady waveforms, and in order to improve the accuracy of bolt axial force evaluation, it is necessary to capture subtle changes that occur at the bolt head. Therefore, it is important to pay attention to the Detail waveform, which is the detail of the selected waveform. The following describes the process from RMW design to acquisition of Detail waveform by P-DWT. There is no linear relationship between the waveform shape and the bolt axial force, but the reproducibility of the waveform obtained by each bolt axial force is high. Here, due to the large number of measured data, this chapter describes signal processing and machine learning by presenting figures from Case A at a bolt axial force of 180 kN as a representative example.

The RMW is created based on any one data measured by the training bolt. In this study, in order to acquire the feature signal from the important zone in the bolt axial force evaluation included in the initial time zone. First, take out the target range shown by the solid line in **Figure 3.28**. Multiply the waveform extracted from by a window function that becomes 0 sufficiently fast at a distance. For the window function, the Hanning window function (**Figure 3.29**) that is considered to be good in terms of both time resolution and frequency resolution is applied. Next, the Hanning window function constructs RMW ψ^R by normalizing the real waveform obtained by the above processing so that the norm becomes 1 in

$$\|\psi^R\| = \left[\int_{-\infty}^{\infty} \psi^R(t_1)^2 dt_1\right]^{1/2} = 1 \tag{3-6}$$

This RMW was created with bolt axial forces of 10kN pitch from 120kN to 220kN. **Figure 3.30** shows the RMW created by the above procedure. The calculation flow of P-DWT is shown in **Figure 3.31**. The RMW is decomposed by the base MW to the level where a filter is added, and the obtained time waveform data of the low frequency component or high frequency component is converted into frequency domain data by Fourier transform.

For the base mother wavelet used here, the optimum mother wavelet was selected according to the Akaike Information Criterion (AIC) [82]. In addition, since the signal processing capacity was the best in the measurement data of this study, the filter was decomposed to level 5 by MW in which RMW was selected by AIC. The frequency domain data of the obtained real part F_l^R and imaginary part F_l^I serve as a parasitic filter. The target waveform W is decomposed by DWT to

level -1 to which a filter is added using the same base mother wavelet as above. The Fourier transform of the obtained low frequency component or high frequency component waveform data is the real part P_{l-1}^{R} and the imaginary part P_{l-1}^{I}. Frequency domain data is obtained by filtering using parasitic filters F_l^R and F_l^I for P_{l-1}^{R} and P_{l-1}^{I}, respectively, and the approximation waveform is obtained by inverse Fourier transform. And the Detail waveform was acquired. The two types of waveforms obtained are shown in **Figure 3.32**. In this study, the Detail waveform was focused on in order to evaluate the bolt axial force based on the details of the selected bolt axial force and the related waveform.

3.7. Evaluation of Bolt Axial Force by Machine Learning

In order to evaluate the bolt axial force quantitatively, the bolt axial force is evaluated recursively by machine learning. First, the teacher data needs to be in a state where the waveform data and the bolt axial force are labeled, the classification was performed to give the information of the bolt axial force to each waveform data. Next, the teacher data labeled by classification was trained, and the bolt axial force was evaluated recursively by regression analysis [64-65] using supervised machine learning, and its accuracy was examined. Regression analysis used the linear_model of the most common Python library, sklearn. In order to propose a simple evaluation method, the set value was set as the default. In order to confirm the change in accuracy due to signal processing, the raw waveform and the Detail waveform after signal processing are compared and examined in each target range used as the teacher data of the study case. The classification and linear regression are described below, and then the survey results are described.

3.7.1. Evaluation of Bolt Axial Force by Linear Regression Algorithm

Label each measured data with bolt axial force and classified them according to the study cases in **Table 3.4**. Five teacher data were measured for each bolt axial force for Bolt 1 in **Figure 3.18**, and the bolt axial force was labeled for all 55 training data in total. All the labeled data feed to machine learning, and the bolt axial force is evaluated by the linear regression of the machine

learning algorithm from the testing data measured by Bolt 2 which has no learning history based on the training data classified.

In the research, multiple regression analysis is performed to predict one objective variable from multiple explanatory variables. Multiple regression analysis is an analytical method that calculates predicted values from data existing in M -dimensional space, and the model of multiple regression analysis is expressed as

$$y = \sum_{m=1}^{M} \beta_m x_m + \beta_0 \tag{3-7}$$

where, β_m is the partial regression coefficient, which is calculated by the least squares method, and β_0 represents the constant term. One coefficient is calculated for one explanatory variable, and the predicted value is calculated by adding them together. A partial regression coefficient is set for each value sampled at a pitch of 0.01μs, and they are added together to calculate the objective variable. By investigating the effect of each variable on the objective variable, it is possible to predict the numerical value between pitches from the training data of 10kN pitch.

In order to evaluate the bolt axial force recursively and confirm its accuracy, the accuracy of the evaluation method in this study is examined by investigating the error between the measured value (correct value) and the predicted value (evaluated value). **Figure 3.33** shows the mean absolute percentage error (MAPE) of each of the examined cases by comparing the case where the teacher data is the raw waveform and the case where the Detail waveform is used after signal processing.

As shown in **Figure 3.33**, it was confirmed that in all cases, when the Detail waveform after signal processing was used as the training data, the MAPE was smaller than when the raw waveform was used as the training data. In addition, it was shown that the proposed method of this study, which uses Detail waveforms as training data, can evaluate cases from 120kN to 220kN with a MAPE of 6% or less.

In **Figure 3.34**, the predicted values when the training data is the raw waveform and the Detail waveform are plotted. As a threshold value, a broken line is shown with the same slope as the solid line showing the measured value based on the error of MAPE 6% when the bolt axial force is 220kN. The predicted value when the teacher data was converted into a Detail waveform was sufficiently close to the measured value, and it was confirmed that the accuracy was improved by the signal processing of P-DWT. In Case A of **Figure 3.34**, the evaluation of 220kN when the

Detail waveform is used as the teacher data is greatly deviated, so the overall evaluation accuracy is low. The cause is the deviation of the probe installation position. It is conceivable that such a large error can be suppressed by making the installation position of the probe constant.

Case A and Case B used a 10MHz narrow band probe, and Case C used a 5MHz wide band probe, but except for 220kN, which had a large evaluation error for Case A, the Detail waveform was used as training data. The MAPE is 0.79%, and it can be said that the accuracy when the Detail waveform of each case is used as the training data is about the same. Therefore, it can be said that the pulse wave transmitted from the 10MHz narrow band probe and the 5MHz wide band probe has little effect on the evaluation accuracy in the proposed method of this study.

Except for 220kN of Case A, when the Detail waveform is used as the training data, it can be confirmed that all the evaluations of Case A and Case B in **Figure 3.34** are evaluated within the broken line which is the threshold value. Moreover, since the proposed method of this study focuses on the initial time zone, only the signal from the vicinity of the bolt head is included. From these facts, it is considered that the bolt length does not affect the bolt axial force evaluation proposed in this study.

3.7.2. Evaluation of Bolt Axial Force for Untrained Nominal Length Bolts

By supporting the measurement of existing bolts, the method proposed in this chapter focuses on the initial time zone and it is considered to be a method that is not easily affected by the bolt length. Therefore, the data obtained by measuring the bolt neck length of 95mm in Case A was used as the training data, and the bolt axial force was evaluated from the measured data of the bolt neck length of 70mm in Case B.

The result was shown in **Figure 3.35**. At 200kN it was evaluated significantly by about 30kN on average. In addition, because at 220kN it was evaluated significantly by 30kN or more, so it is out of the range of the vertical axis in **Figure 3.35**. This is related to the fact that only the evaluation of Case A at 220kN shown in **Figure 3.34** deviates significantly. It is considered that one of the factors is that the installation position of the probe was slightly deviated when the bolt axial force of Case A was measured at 220kN. Except 200kN and 220kN, it can be evaluated with an error of 7% or less.so it is expected that the evaluation accuracy will be improved by adjusting the installation position of the probe. In the future, a simple adjustment method for the installation position of the probe should be considered.

3.8. Proposal of Bolt Axial Force Evaluation Method for Bolt Oversized Hole

The bolt axial force evaluation method proposed in this chapter utilizes the deformation of the bolt head. It was shown that the bolt axial force can be evaluated with high accuracy when the standard bolt hole is 24.5mm. Thus, in the case of bolt with enlarged holes, the deformation of the bolt head may be different from that in the case of standard holes. Therefore, the accuracy of the evaluation in the case of bolt oversized holes is investigated here, and a bolt axial force evaluation method for bolt oversized holes was proposed.

An overview of the specimens reproducing the bolt oversized holes is shown in **Figure 3.36**. **Table 3.5** shows the two cases considered, with bolt hole sizes r of 26.5 mm and 32 mm. It is assumed that the effect on the displacement of the bolt head surface is small or large. The thickness of the specimen does not affect the deformed shape of the bolt head as long as it is within the range of tightening lengths determined according to the bolt length. In this consideration, the focus is not on the plate thickness but on the size of the bolt hole. In order to investigate the effect of bolt head deformation on the evaluation accuracy, the steel plates of the specimens were used in this experiment in the unpainted mill scale condition. Bolt 1 is for the training data and Bolt 2 is for the testing data, so that the bolts are tested with no learning history. In the case of the bolt oversized hole, the position of the bolt is misaligned significantly. Hence, the bolt was placed in the center of the bolt hole using the tool shown in **Figure 3.37**, which was fabricated by a 3D printer.

Before the experiment, the deformation of the bolt head was investigated by numerical analysis in the case of bolt oversized holes. In order to investigate the deformation of the bolt head in the case of a larger bolt hole, a case with a bolt hole of 32mm was analyzed. **Figure 3.38** shows the analytical model. The mesh shape is a hexahedron. To clarify the deformation of the bolt head, the mesh size was set to 0.8mm for the bolt and washer and 8 mm for the steel. By applying forced displacement to the bottom of the bolt shank, the tightening of the bolt was expressed. The deformation of the bolt head was confirmed up to a bolt axial force of 220kN. **Figure 3.39** shows the deformation diagram of the analysis results at 220kN. The deformation magnification is shown as 100 times, and it was confirmed that the bolt head deformed in the same way as in the case of a standard hole (**Figure 3.13**). The shape of the bolt head when the bolt axial force is introduced is shown in **Figure 3.40** in comparison with the case of the standard hole. In actuality, displacement in the loading direction occurs over the entire bolt head, but the displacement at both ends of the

bolt head is always set to 0 for comparison. In the bolt axial force evaluation considering the deformed shape of the bolt head, the influence of setting the displacements at both ends of the bolt head always to 0 is small, because the bolt axial force is evaluated by the curvature of the probe installation surface. It can be seen that the displacement of the bolt head surface is different from that of the standard hole because the reaction force by the washer is not sufficiently secured due to the large bolt hole and the steel sinks. Based on the results of the bolt head surface displacement, the accuracy of the bolt axial force evaluation in the case of bolt oversized holes was discussed.

The method of measuring the bolt axial force, signal processing, and evaluation method are the same as the procedure of the bolt axial force evaluation method proposed in this chapter. The probe used is a narrow band of 10MHz. Bolt axial forces were measured every 20kN from 120kN to 220kN. At each bolt axial force level, Bolt 1 and Bolt 2 were measured 5 times each. This means that there are 5 training data and 5 testing data for each bolt axial force level. The bolt axial forces were evaluated by machine learning using a linear regression algorithm.

Figure 3.41 shows the results of evaluating the data for the 32mm bolt hole from the data of the standard hole trained in 3.7. The predicted value was a larger evaluation of the bolt axial force than the measured value. In addition, **Figure 3.42** shows the result of evaluating the data of the bolt hole 26.5mm from the data of the standard hole. Although the evaluation accuracy is not high by any means, it was confirmed that the accuracy tends to be higher as the size of the oversized hole is smaller. Considering **Figure 3.40**, it is possible that the shape of the bolt head surface has a greater effect on the bolt axial force than the magnitude of the bolt head center displacement.

The data of 32mm bolt holes measured by Bolt 1 was used as training data, and the data of 32mm bolt holes measured by Bolt 2 was used as testing data. The results are shown in **Figure 3.43**. As in 3.7, the dashed line indicates the area where the error is 6%. The accuracy of the small bolt axial force was low, but it was confirmed that the accuracy was better than 140kN. Therefore, in the case of bolt oversized holes, it was shown that the bolt axial force could be evaluated by using the data of the oversized holes as training data.

3.9. Summary

This chapter proposed an axial force evaluation method for existing bolts focusing on the initial time zone among the data measured from the bolt head by the one-probe method using ultrasonic waves. By combining ultrasonic measurement, signal processing using P-DWT, and supervised machine learning, a new bolt axial force evaluation method was conducted and its accuracy was confirmed. The conclusions obtained are as follows:

1. Among the ultrasonic measurement waveform data obtained from the bolt head, the beat waveform in the initial time zone contains information related to the bolt axial force.
2. An analytical investigation of the high strength bolts when the bolt axial force was introduced confirmed that the effect of the bolt length on the amount of deformation of the bolt head was small. Therefore, because the ultrasonic measurement data targets the data in the initial time zone measured near the bolt head, it is considered that this method is not easily affected by the bolt length
3. As a result of applying the proposed method in this chapter to bolts of the same manufacturer and lot, it was shown that MAPE can be evaluated at 6% or less when the bolt length of the teacher data is the same. Because it was difficult to correct the deviation of the probe installation position by the signal processing performed in this study, if it is different from the bolt length of the teacher data, there is a possibility that the evaluation accuracy can be improved by keeping the installation position of the probe constant.
4. It is considered that the information indicating the bolt axial force is more influenced by the shape of the bolt head surface, which is the reflecting surface of the ultrasonic wave, than by the displacement of bolt head center. It was shown that the bolt oversized hole could be evaluated by using the data of the oversized hole as training data.

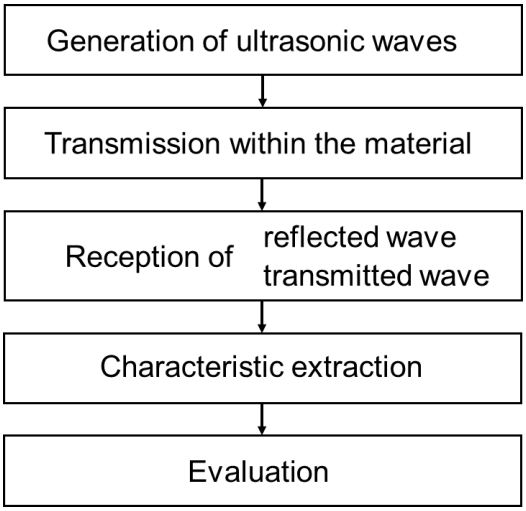

Figure 3.1 General ultrasonic measurement procedure

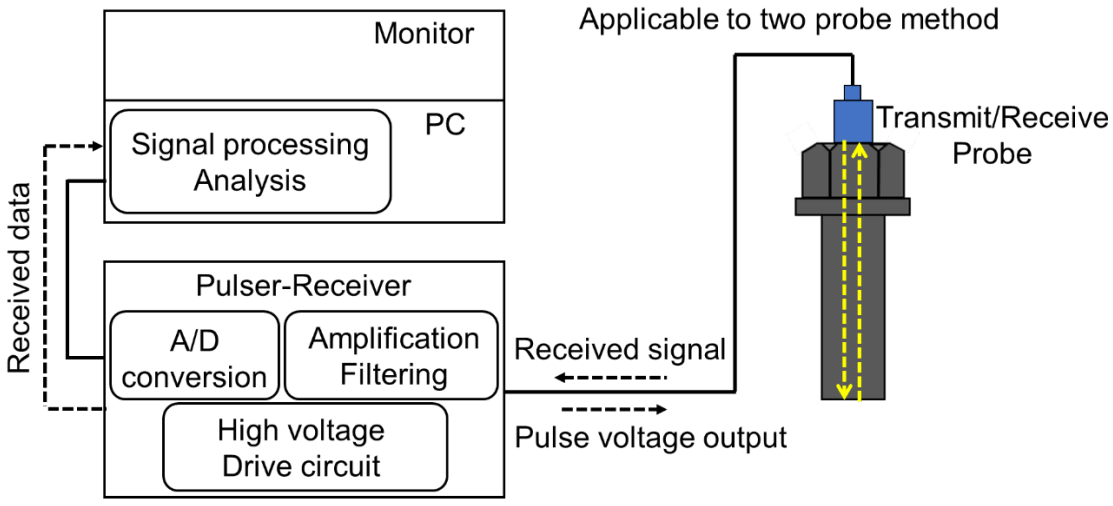

Figure 3.2 Outline of ultrasonic transmission and reception (One probe method)

Figure 3.3 Ultrasonic pulser-receiver

Table 3.1 Pulser settings

Item	Specifications
Pulse type	Rectangle burst
Pulse voltage	50[V]
Pulse frequency	5 or 10[MHz]
Number of pulse waves	5 waves
Damping resistance	100[Ω]
Chirp ratio	100[%]
Resolution capacity	10[bit]
Sampling rate	100[MS/s]

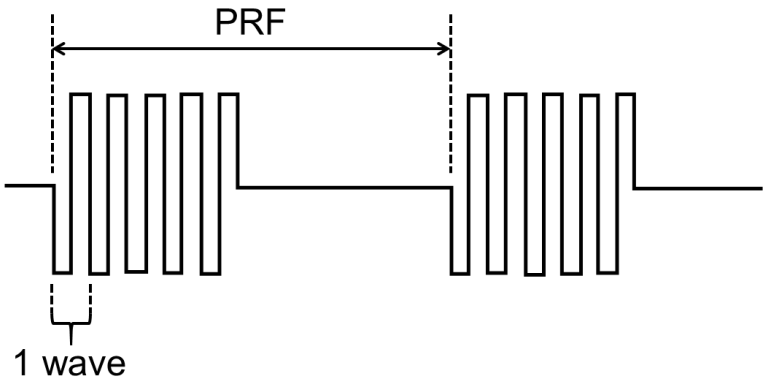

Figure 3.4 Rectangle burst (5 waves)

Figure 3.5 Ultrasonic probes used in Chapter 3

Figure 3.6 Engraved bolt head

Figure 3.7 Machine oil (Ultrasonic probe contact medium)

Figure 3.8 State of the experiment

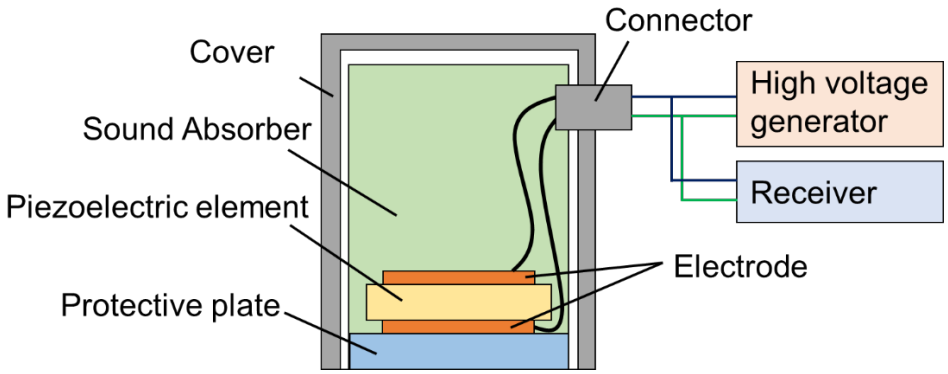

Figure 3.9 Structure of the single crystal vertical probe

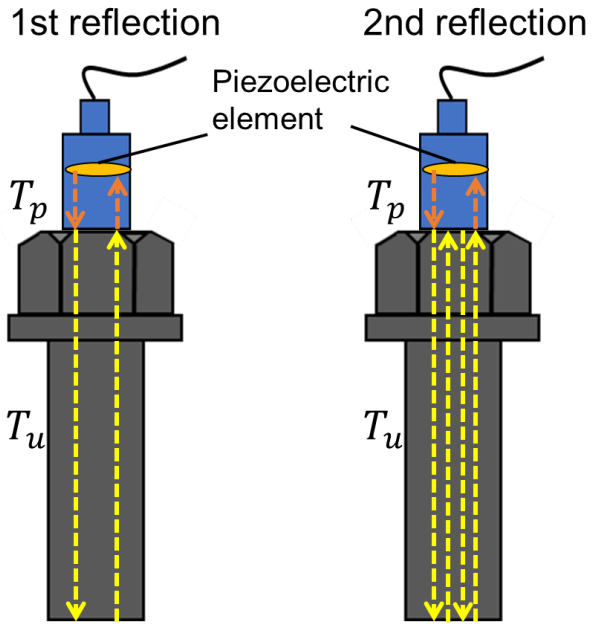

Figure 3.10 Path of ultrasonic waves in ultrasonic measurement from a bolt head

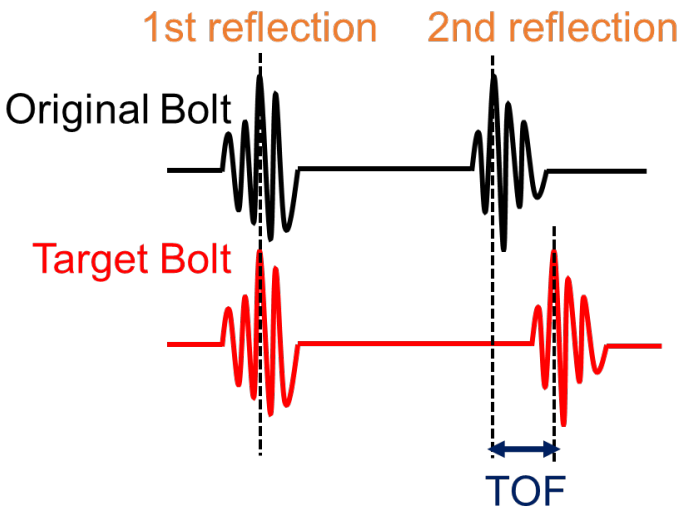

Figure 3.11 Time Of Flight (TOF)

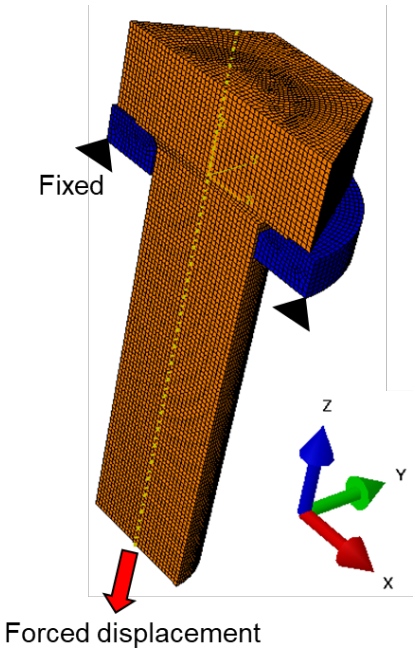

Figure 3.12 Analytical model for tightening high strength bolt

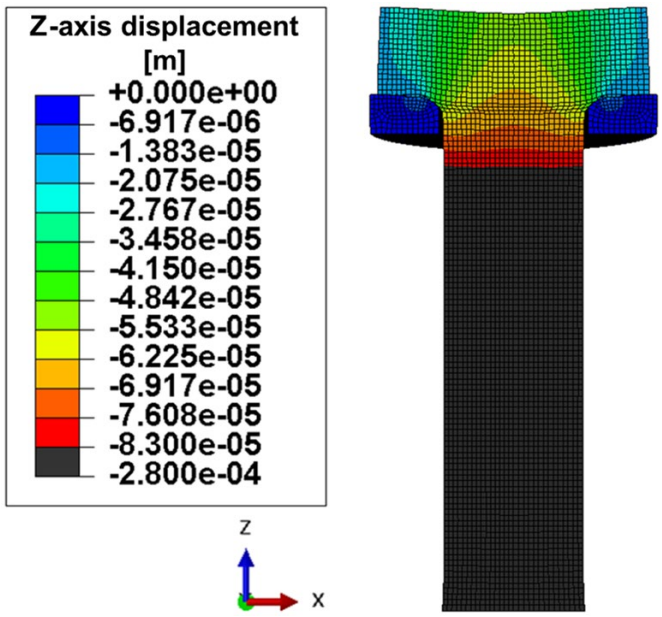

Figure 3.13 Deformation when bolt axial force 220kN (Deformation magnification ×30)

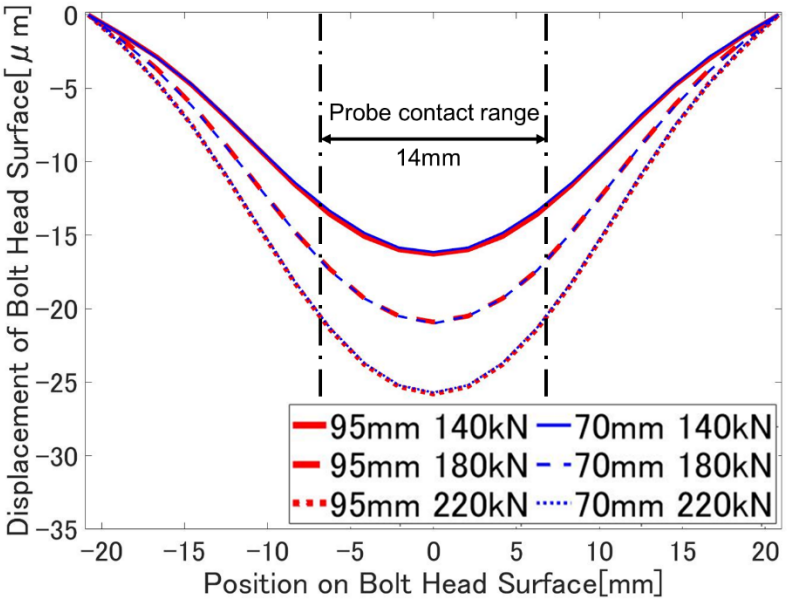

Figure 3.14 Displacement of the bolt head surface

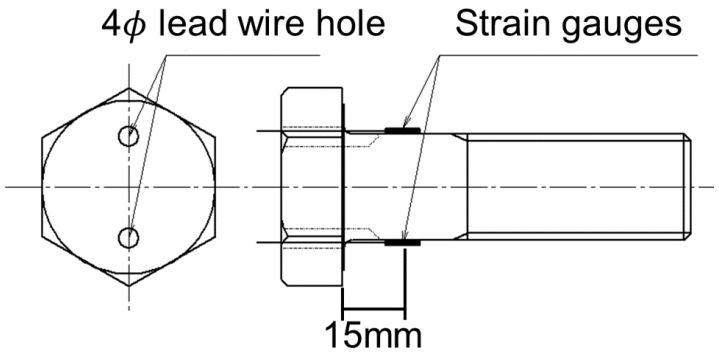

Figure 3.15 The position where strain gauges are attached

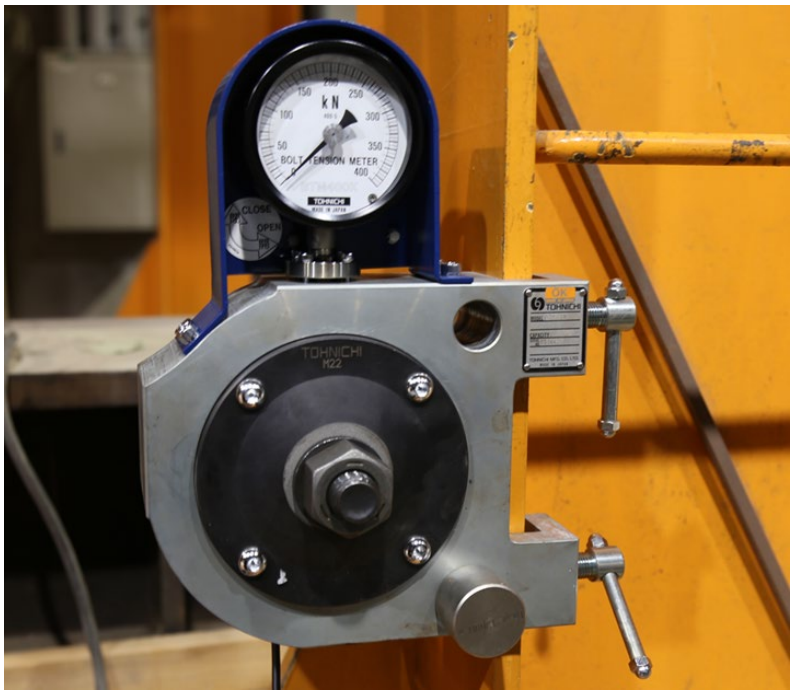

Figure 3.16 Bolt axial force measuring instrument

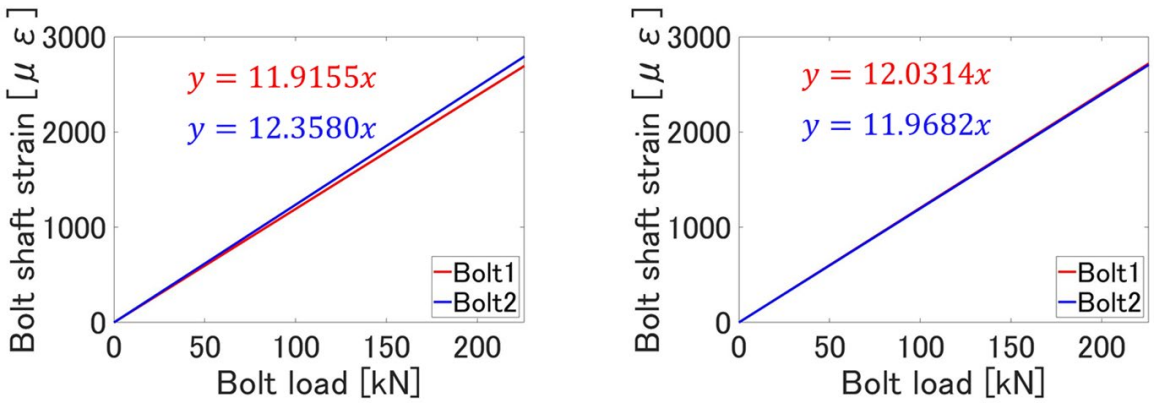

(a) Bolt length 95mm (b) Bolt length 70mm

Figure 3.17 Results of bolt axial force calibration

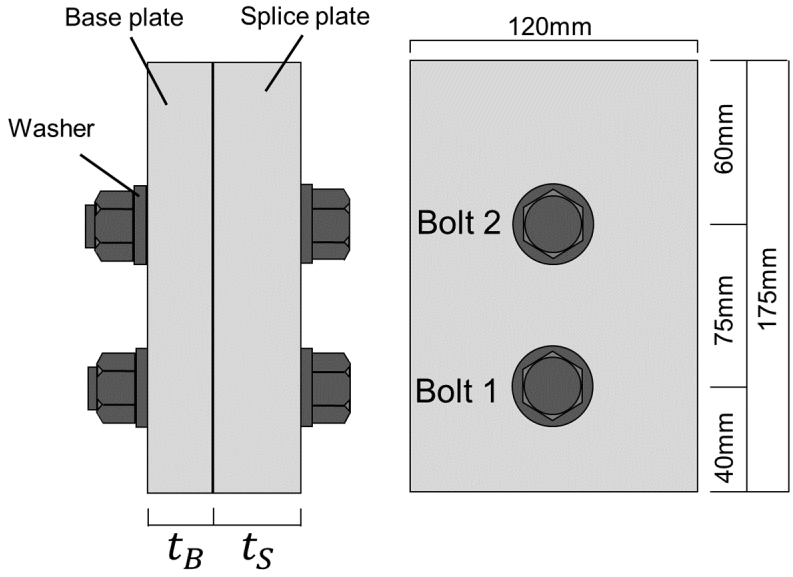

Figure 3.18 Outline of specimens

Table 3.2 Study case

Case	Plate thickness		Bolt shank length
	t_B [mm]	t_S [mm]	L [mm]
t22	22	22	95
t9	9	16	70

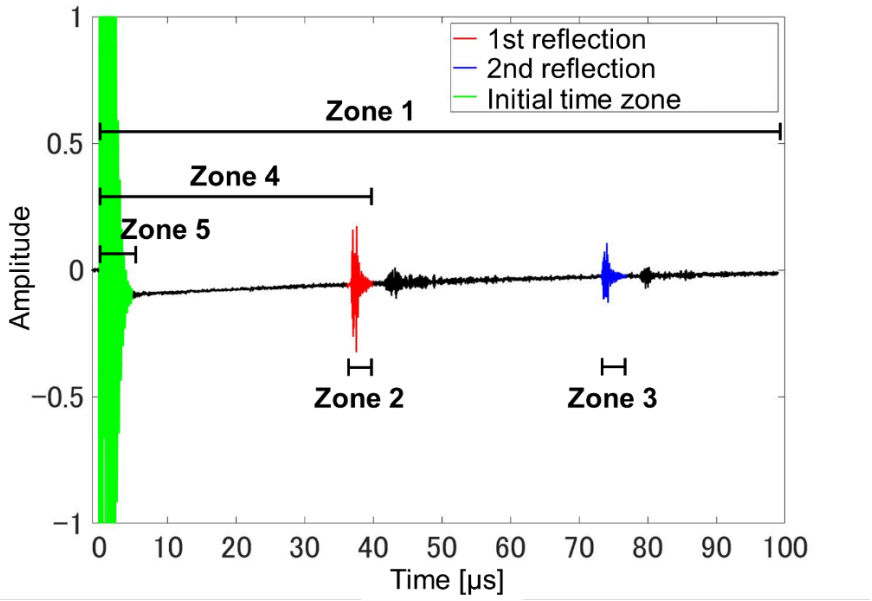

Figure 3.19 Examination zone divided for zone extraction related to bolt axial force

Table 3.3 Study case for zone investigation related to bolt axial force

Case	Probe type	Bolt shank length [mm]	Zone
A	10MHz Narrow band	95	1
			2
			3
			4
			5
B		70	1
			2
			3
			4
			5
C	5MHz Wide band	95	1
			2
			3
			4
			5

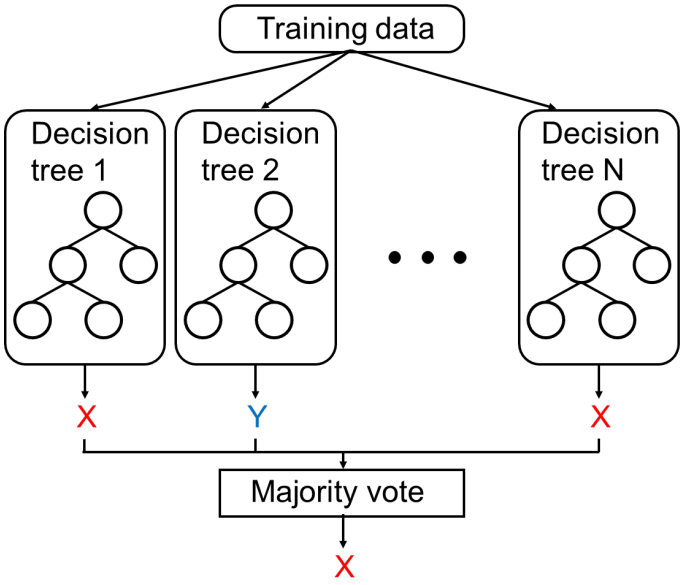

Figure 3.20 Outline of random forest

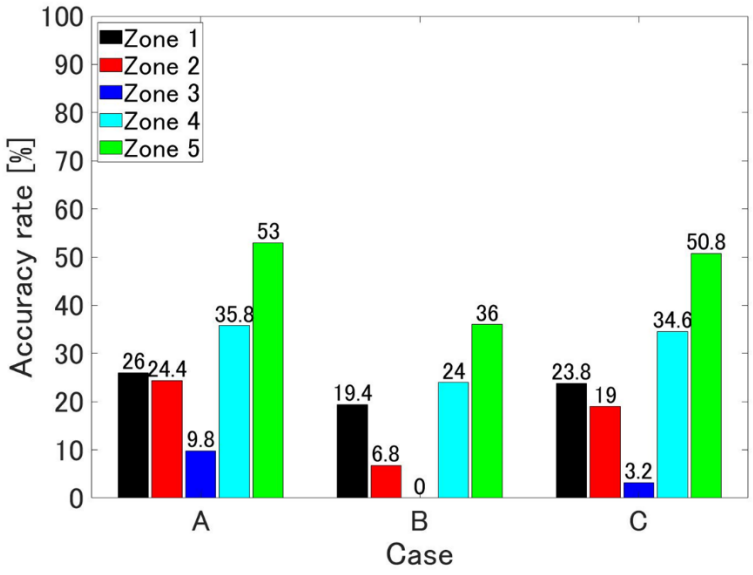

Figure 3.21 Evaluation result of bolt axial force by random forest

Table 3.4 Study case for bolt axial force evaluation

Case	Specimen	Probe type	Target bolt
A	t22	10MHz Narrow band	M22 95mm
B	t9		M22 70mm
C	t22	5MHz Wide band	M22 95mm

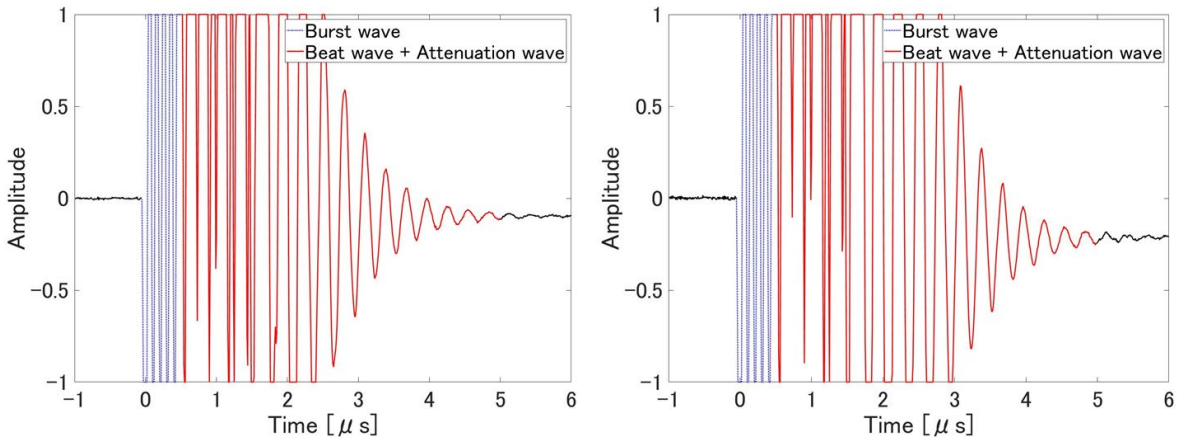

(a) Case A

(b) Case B

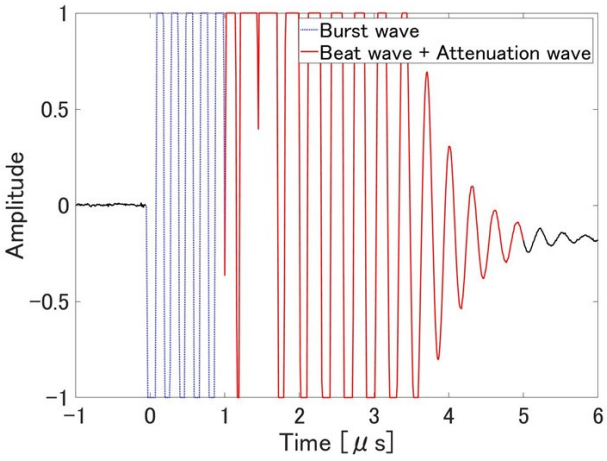

(c) Case C

Figure 3.22 Raw wave of initial time zone (180kN)

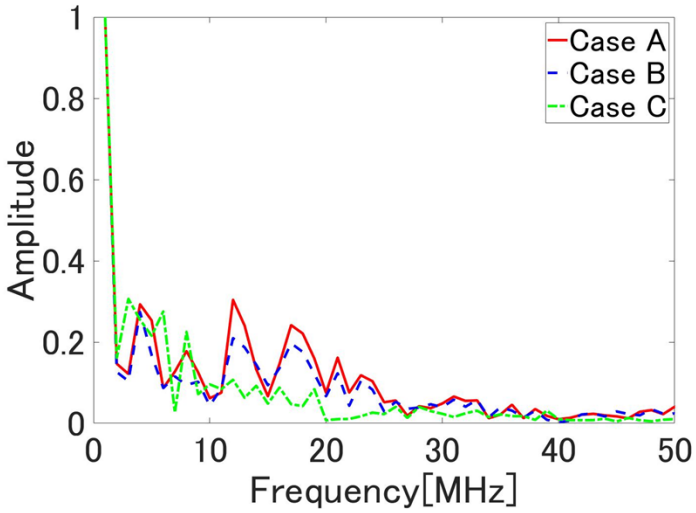

(a) Frequency band of beat wave

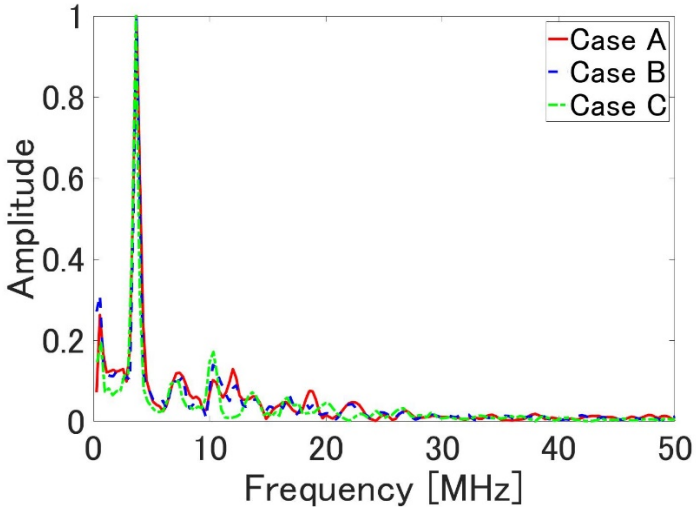

(b) Frequency band of attenuation wave

Figure 3.23 Frequency band of beat wave and attenuation wave

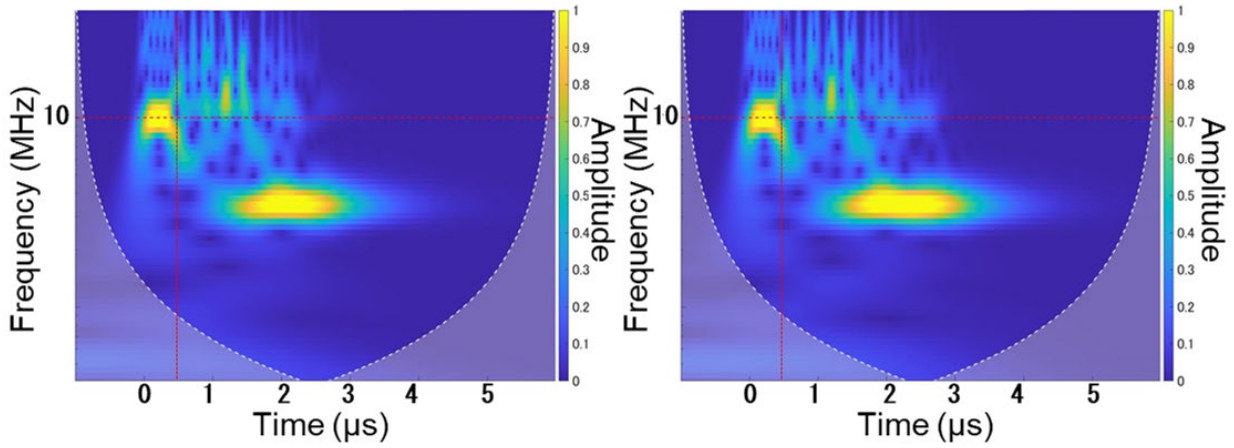

(a) Case A

(b) Case B

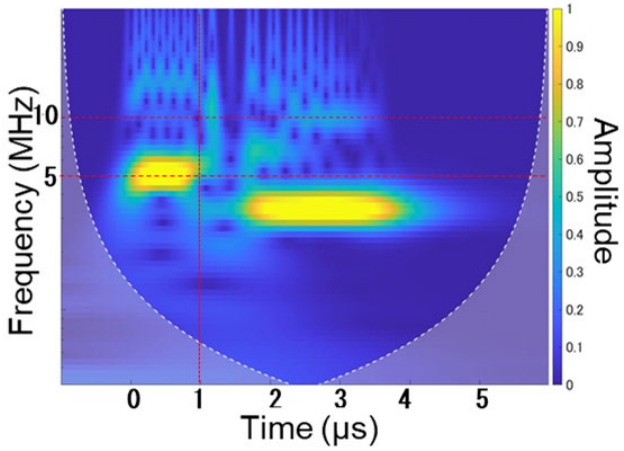

(c) Case C

Figure 3.24 Scalogram after applying CWT (180kN)

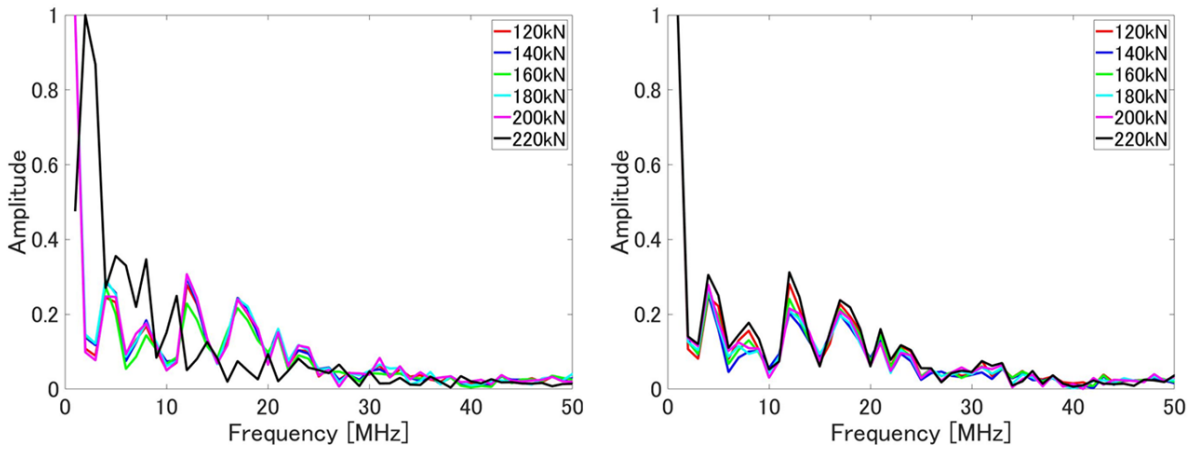

(a) Case A

(b) Case B

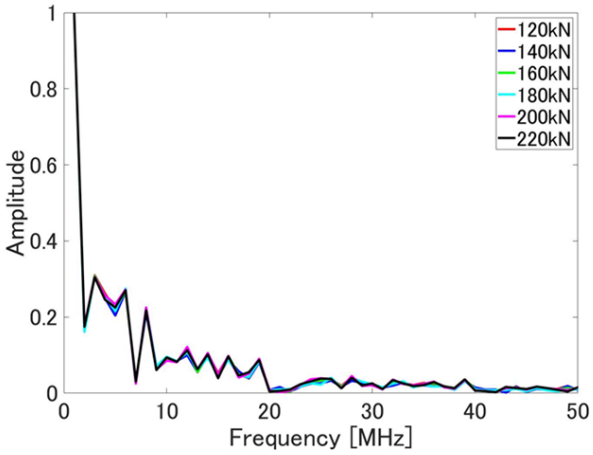

(c) Case C

Figure 3.25 Frequency band of each bolt axial force in beat waveform

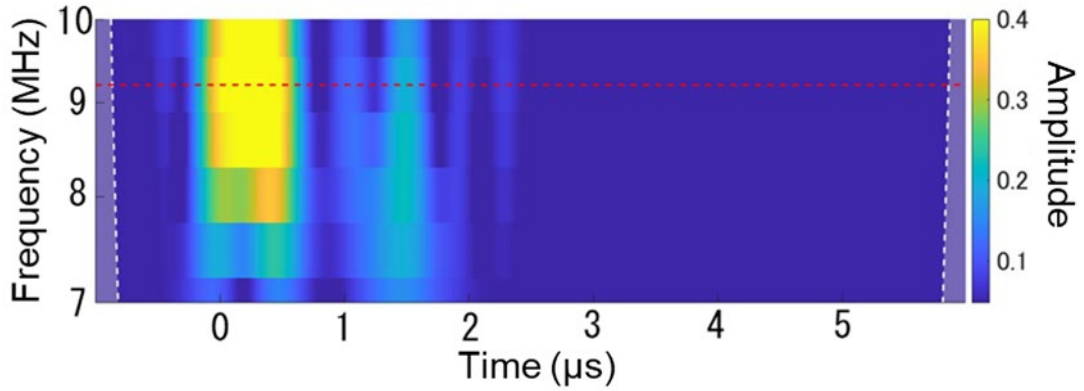

(a) Case A

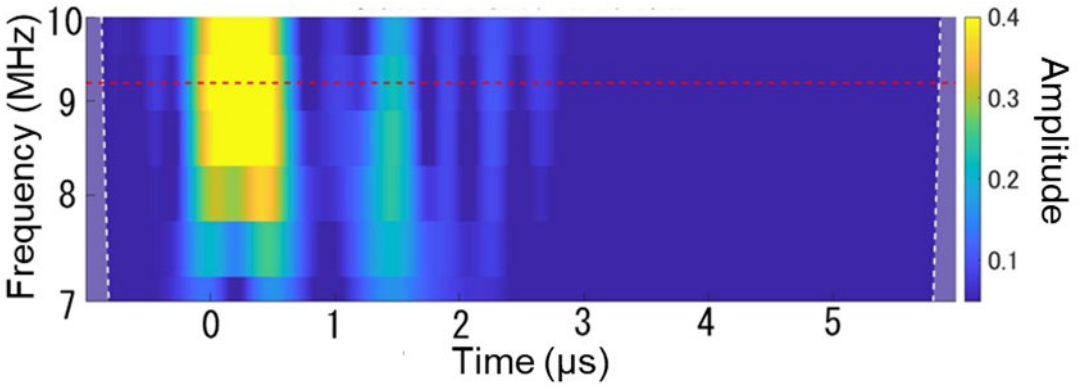

(b) Case B

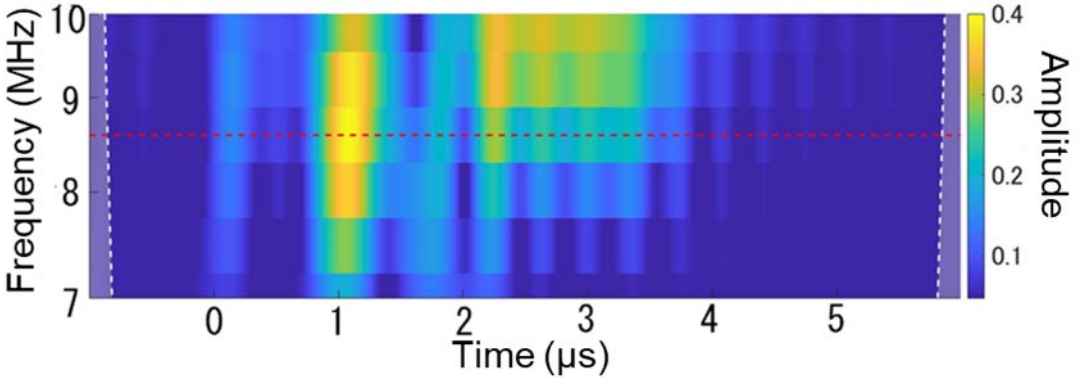

(c) Case C

Figure 3.26 Scalogram after applying bandpass and CWT (180kN)

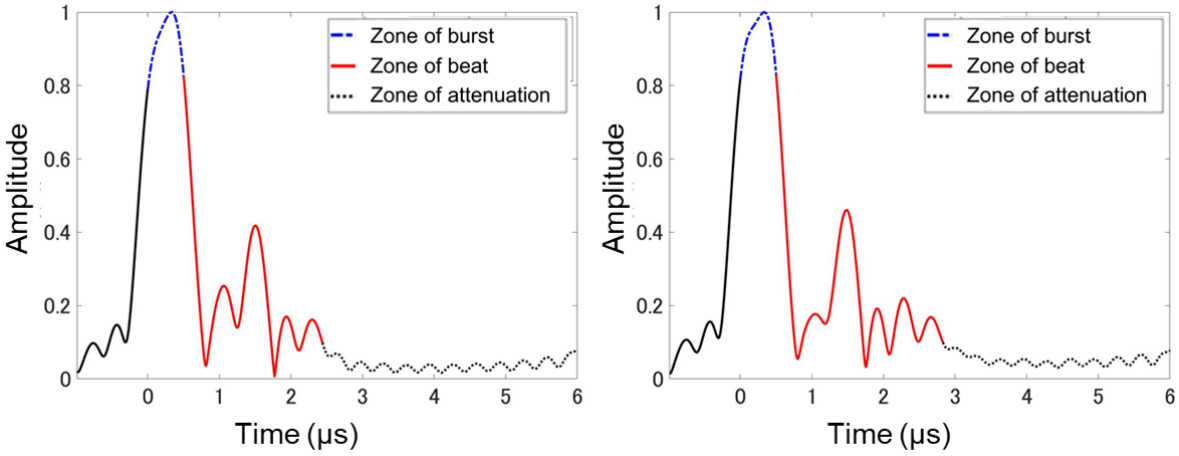

(a) Case A

(b) Case B

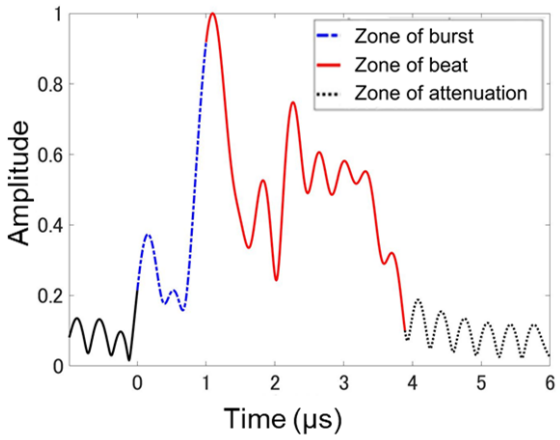

(c) Case C

Figure 3.27 Scalogram after applying bandpass and CWT (180kN)

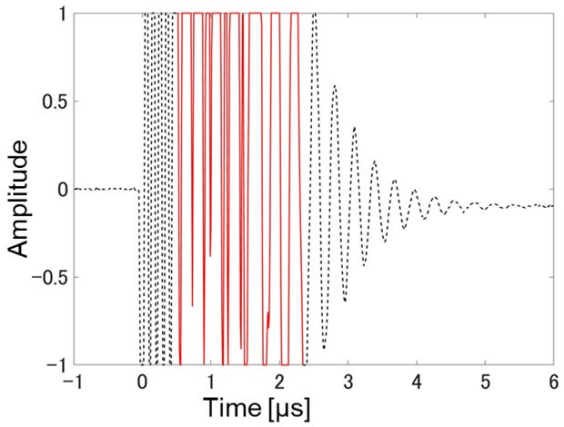

Figure 3.28 Beat waveform to be taken out (180kN)

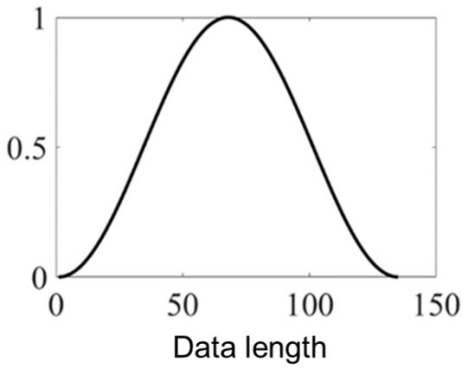

Figure 3.29 Hanning window function

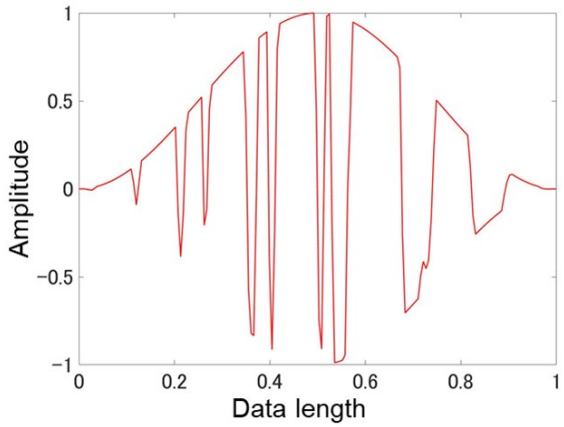

Figure 3.30 RMW (180kN)

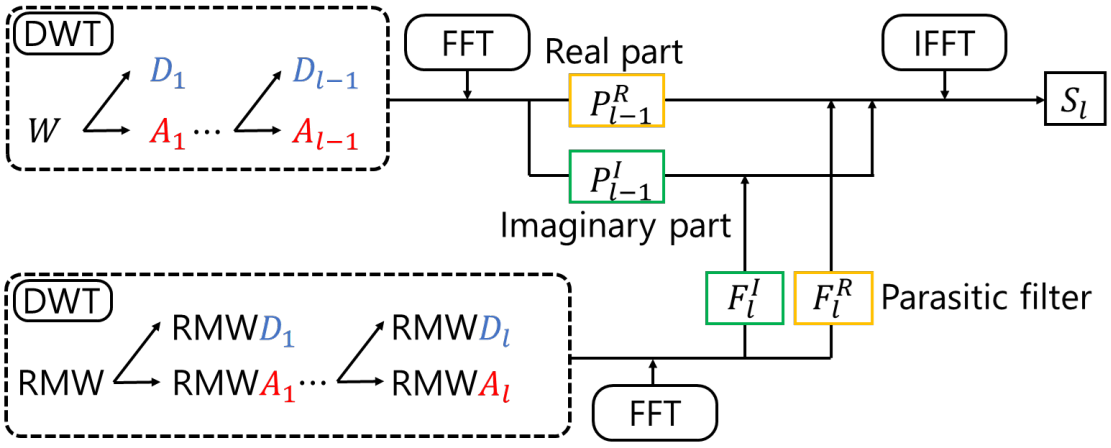

Figure 3.31 P-DWT calculation flow

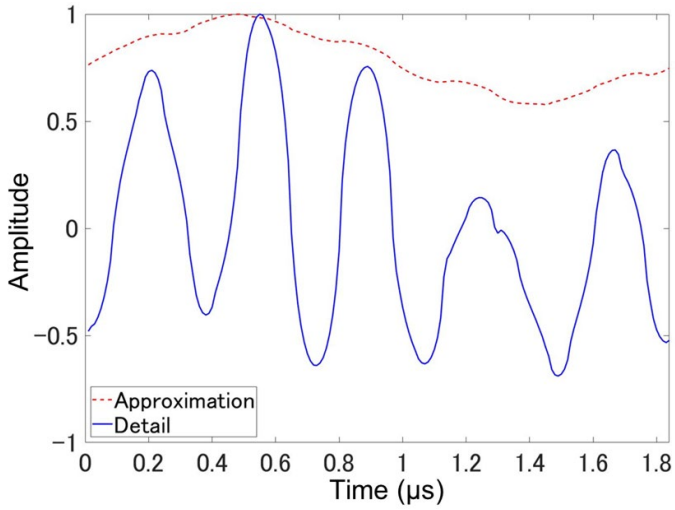

Figure 3.32 Approximation and Detail (180kN)

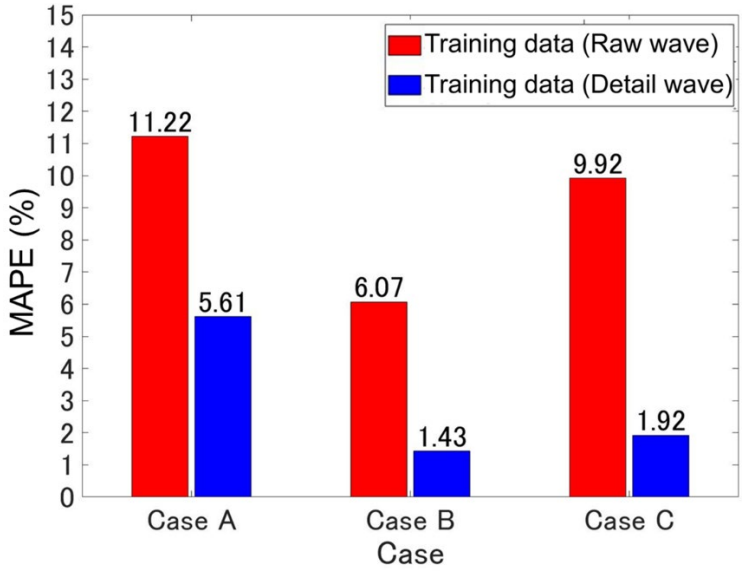

Figure 3.33 MAPE for each case

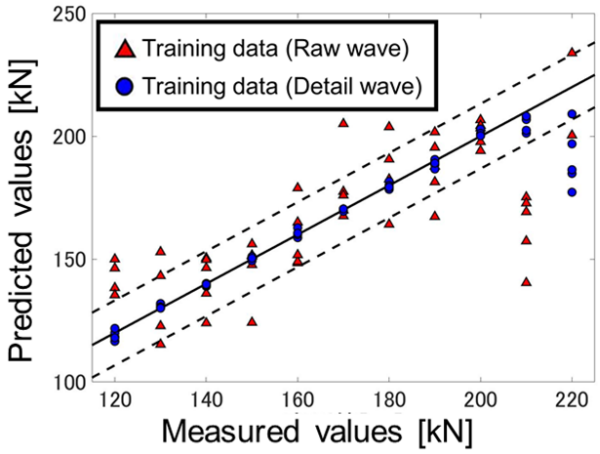

(a) Case A

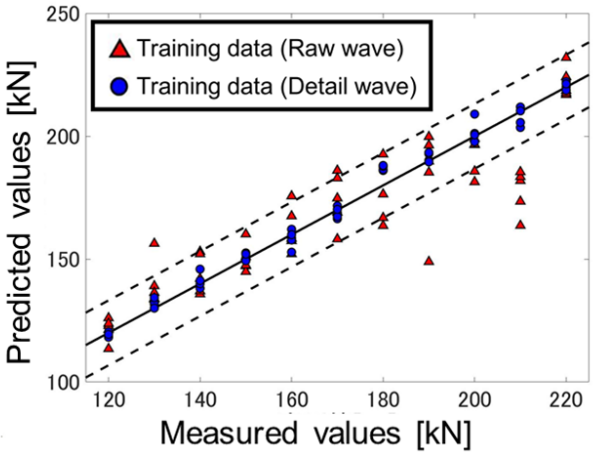

(b) Case B

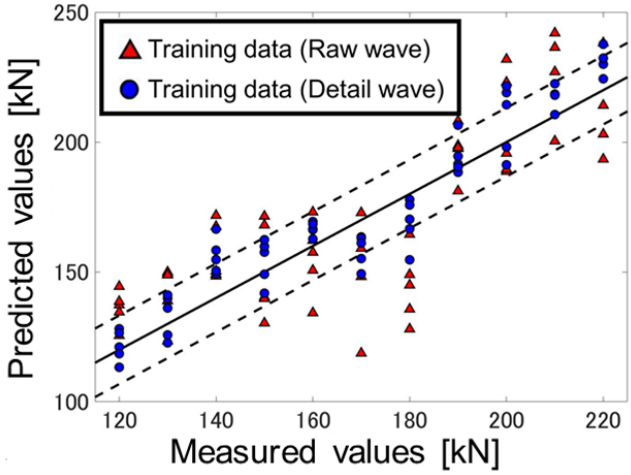

(c) Case C

Figure 3.34 Predicted values and Measured values for each case

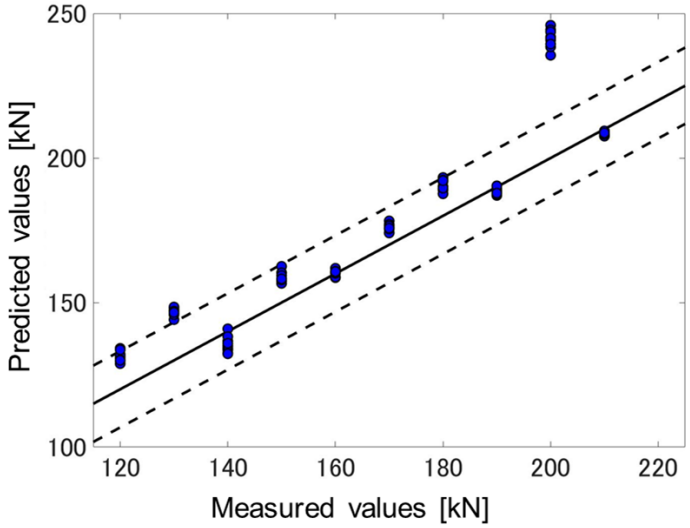

Figure 3.35 95mm bolts were trained and 70mm bolts were tested

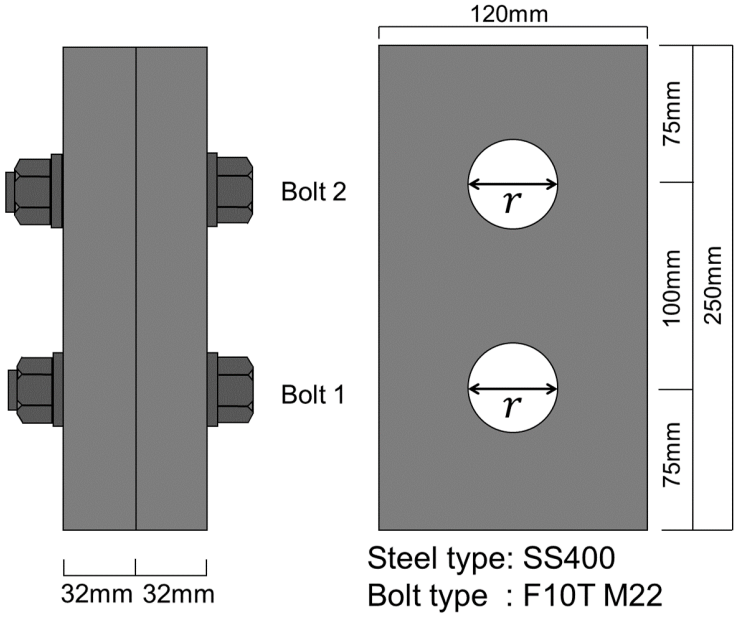

Figure 3.36 Specimen that reproduces the oversized bolt hole

Table 3.5 Considered bolt hole size

Case	Bolt hole diameter r [mm]
r26.5	26.5
r32	32

Figure 3.37 Tool for placing the bolt in the center of the bolt hole

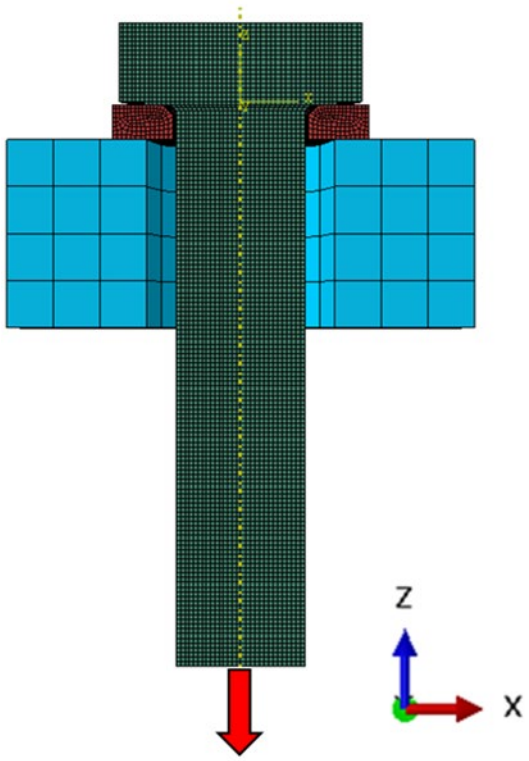

Figure 3.38 Analytical model for bolt hole 32 mm

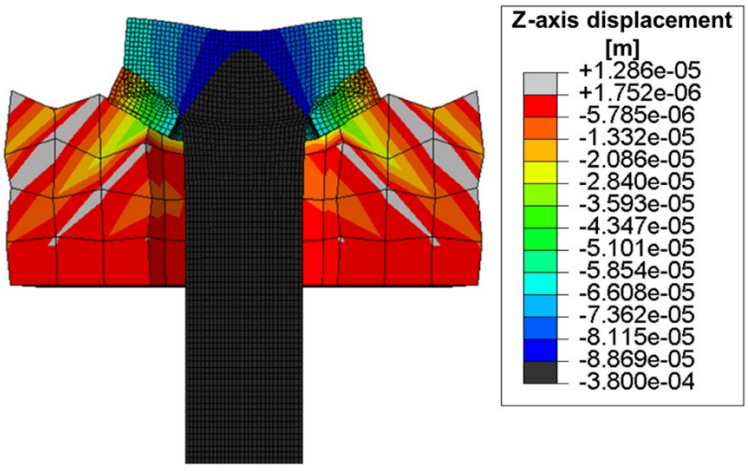

Figure 3.39 Deformation when bolt axial force 220kN (Deformation magnification ×100)

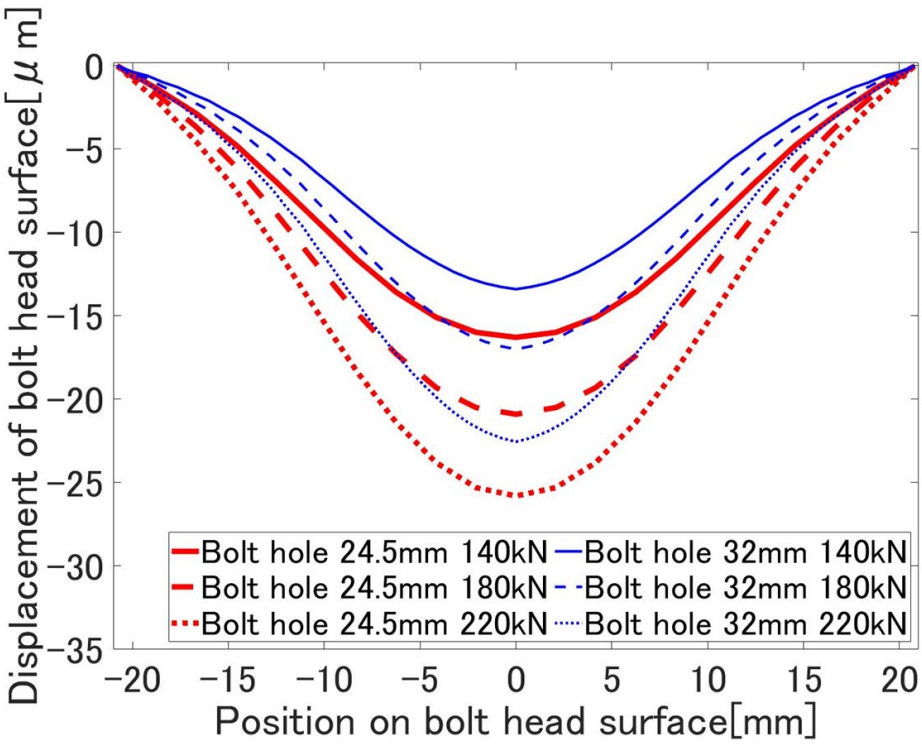

Figure 3.40 Displacement of the bolt head surface when standard hole and oversized hole

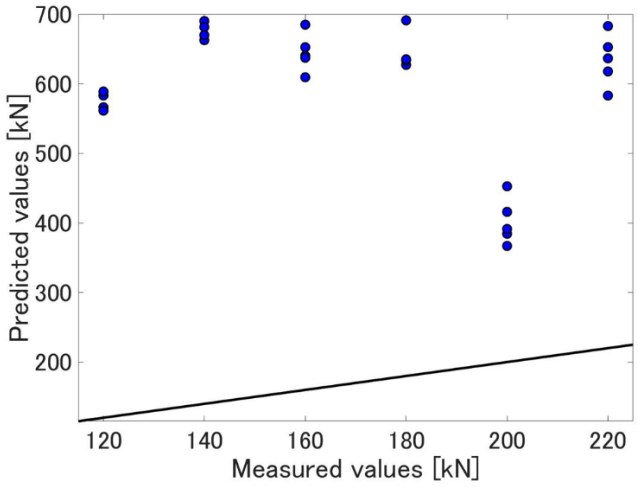

Figure 3.41 Results of bolt axial force evaluation when learning standard hole data and testing bolt hole 32mm data

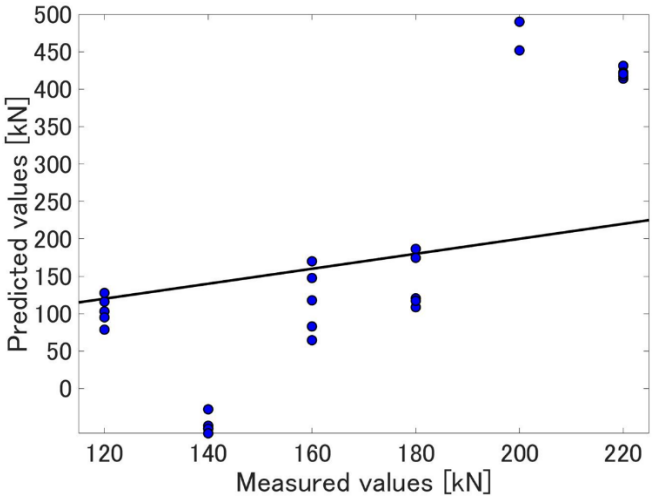

Figure 3.42 Results of bolt axial force evaluation when learning standard hole data and testing bolt hole 26.5mm data

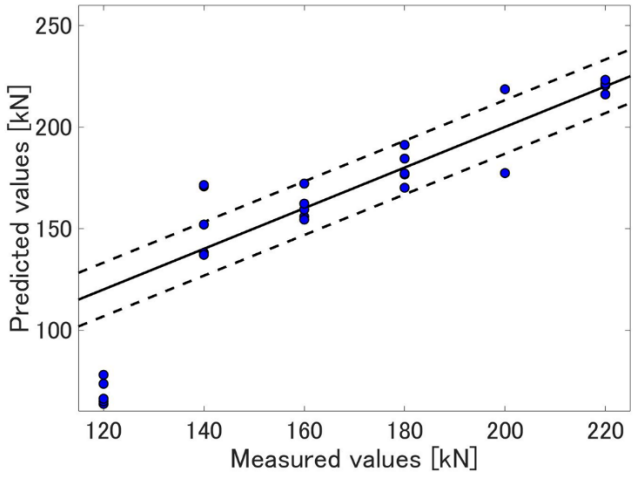

Figure 3.43 Results of bolt axial force evaluation when learning bolt hole 32mm data and testing bolt hole 32mm data

References (Chapter 3)

[1] Nishimura, A., Taido, Y., Sera, S., Hozumi, S. and Mitani, T.: On the Scattering of Clamping Forces of High-Strength Bolts in Actual Structural Joints, *Proceedings of the JSCE*, No.180, pp.1-9, 1970.8.

[2] Fukuoka, T. and Takai, T.: Mechanical Behaviors of Bolted Joint During Tightening Using Torque Control, *JSME International Journal Series A Solid Mechanics and Material Engineering*, Vol.41, No.2, pp.185-191, 1998.

[3] You, R., Ren, L. and Song, G.: A Novel Comparative Study of European, Chinese and American Codes on Bolt Tightening Sequence Using Smart Bolts, *International Journal of Steel Structures*, Vol.20, No.3, pp.910-918, 2020.

[4] Wang, Y.Q., Wu, J.K., Liu, H.B. and Xu, S.T.: Modeling and Numerical Analysis of Multi-Bolt Elastic Interaction with Bolt Stress Relaxation, *Proceedings of the Institution of Mechanical Engineers, Part C: Journal of Mechanical Engineering Science*, Vol.230, No.15, pp.2579-2587, 2015.

[5] Minami, K., Tamura, H., Uchida, D., Shirahata, H., Yoshioka, N., Tsutsui, K. and Fujino, D.: A Study on Initial Value Setting Method for Relaxation Tests in High Strength Bolted Joints, *Journal of JSCE A1 (Structural Engineering & Earthquake Engineering)*, Vol.76, No.3, pp.496-509, 2020.

[6] Abid, M., Khalil, M.S. and Wajid, H.A.: An Experimental Study on the Relaxation of Bolts, *IIUM Engineering Journal*, Vol.16, No.1, pp.43-52, 2015.

[7] Ishihara, Y., Kobayashi, G., Minada, O. and Nishimura, N.: Characteristic Investigation and Cyclic Slip Experiment of HSFG Bolted Joints Which were Damaged by Earthquake, *Journal of the JSCE A1*, No.745, I-65, pp.53-64, 2003.10.

[8] Wang, F., Ho, S.C.M. and Song, G.: Monitoring of Early Looseness of Multi-Bolt Connection: A New Entropy-Based Active Sensing Method Without Saturation, *Smart Materials and Structures*, Vol.28, No.10, pp.1-7, 2019.

[9] Marshall, M.B., Lewis, R., Howard, T. and Brunskill, H.: Ultrasonic Measurement of Self-Loosening in Bolted Joints, *Proceedings of the Institution of Mechanical Engineers, Part C: Journal of Mechanical Engineering Science*, 2011.

[10] Jiang, Y., Zhang, M. and Lee, C.H.: A Study of Early Stage Self-Loosening of Bolted Joints, *Journal of Mechanical Design, Transactions of the ASME*, Vol.125, pp.518-526, 2003.

[11] Tanihira, T., Kamei, M., Ishihara, Y. and Taido, Y.: Carrying Capacity Test for Friction Joint of High-Strength Bolt from a Removed Foot-Way Bridge Used Under 17 Years, *JSCE Journal of Structural Engineering*, Vol.36 A, pp.1087-1096, 1990.3.

[12] Kanou, M., Tanihira, T., Ishihara, Y., Kobayashi, G. and Nishio, H.: 高力ボルト軸力の経年変化に関する実験的研究, *JSCE* 第 56 回年次学術講演会, I-B162, pp.324-325, 2001.10.

[13] Ishihara, Y., Kobayashi, G., Kano, M., Kamei, M. and Tanihira, T.: The Influence of Reduction and Variation of Bolt Tensions by Aging on Limit States of HSFG Bolted Joint, *Journal of JSCE*, Vol.763, VI-63, pp.33-42, 2014.6.

[14] Temitope, S.J.: Condition Monitoring of Bolted Joints, Ph.D. *Thesis, University of Sheffield*, Sheffield, UK, 2015.6.

[15] Rafik, V., Combes, B., Daidié, A. and Chirol, C.: Experimental and Numerical Study of the Self-Loosening of a Bolted Assembly, *Advances on Mechanics, Design Engineering and Manufacturing II*, pp.85-94, 2019.

[16] Kikukawa, S., Murata, K. and Nishimura, A.: Secular Changes of Slip Resistance of Friction-Type Bolted Joints in Structural Members, *Kawasaki Steel Giho*, Vol.11, No.4, pp.127-135, 1979.

[17] Takai, T., Yamaguchi, T. and Yamashina, K.: Analytical Study on Influence of Irregularity on Slip Strength of High Strength Bolted Friction Type Joint, *JSCE Journal of Structural Engineering*, Vol.61 A, pp.605-613, 2015.3.

[18] Takai, T., Peng, X. and Yamaguchi, T.: An Analytical Study on Load Carrying Characteristic of High Strength Bolted Friction Type Joint with Thick Filler Plate, *Journal of JSCE A1 (Structural Engineering & Earthquake Engineering)*, Vol.71, No.1, pp.1-9, 2015.

[19] Tanaka, A., Masuda, H., Wakiyama, K., Tsujioka, S., Hirai, K. and Tateyama, E.: Experimental Study on High Strength Bolted Friction Joints with Oversized and Slotted Holes, *JSSC Steel Construction Engineering*, Vol.5, No.20, pp.35-44, 1998.12.

[20] Mori, T., Yamazaki, N. and Yamaguchi, J.: Slip and Yield Resistance of Friction Type of High Strength Bolted Connections with Over-Sized Holes, *Journal of the JSCE*, No.794, I-72, pp.157-169, 2005.7.

[21] Murakoshi, J., Sawada, M., Yamaguchi, T., Peng, X. and Ootake, A.: Slip Resistance Tests of Friction-Type High-Strength Multi Bolted Joints with Coated Contact Surfaces by Inorganic Zinc Rich Paint on Thick Plate, *Journal of JSCE A1 (Structural Engineering & Earthquake Engineering)*, Vol.70, No.1, pp.94-104, 2014.

[22] Peng, X., Yamaguchi, T., Takai, T., Murakoshi, J. and Sawada, M.: FEA Study on the Slip Behavior of High Strength Multi Bolted Friction Type Joints with Thick Plates by Structural Dimensions, *Journal of JSCE A1 (Structural Engineering & Earthquake Engineering)*, Vol.69, No.3, pp.452-466, 2013.

[23] Kamei, Y., Matsuno, M. and Nishimura, N.: An Analytical Study on Slip Strength of Multi HSFG Bolted Joints in Tention, *Journal of JSCE*, No.640, I-50, pp.49-60, 2000.

[24] Geoffrey, L.K., John, W.F. and John, H.A.S.: Guide to Design Criteria for Bolted and Riveted Joints, Second Edition, *American Institute of Steel Construction, Inc.*, 1987.

[25] Tamura, H., Minami, K., Yoshioka, N., Uchida, D., Moro, M., Hama, T. and Hirao, K.: Applicability of Pretensioned Bolted Joints Including Different Contact Faces, *Journal of JSCE A1 (Structural Engineering & Earthquake Engineering)*, Vol.76, No.2, pp.255-274, 2020.4.

[26] Murakoshi, J., Sawada, M., Yamashina, K., Yamaguchi, T. and Ishihara, D.: Study of Influence on Slip Coefficient of High Strength Bolted Friction Type Joints by Painting Condition and Exposure Term, *Journal of JSCE A1 (Structural Engineering & Earthquake Engineering)*, Vol.73, No.1, pp.40-53, 2017.

[27] Minami, K., Mori, T. and Sugiya, T.: 摩擦面の状態が高力ボルト継手のすべり耐力に及ぼす影響, *JSCE* 第 59 回年次学術講演会, I-587, pp.1171-1172, 2004.9.

[28] Tajima, J.: 高力ボルト摩擦接合概説, 第 2 版, 技報堂, 1966.11.

[29] Miao, R., Shen, R., Zhang, S. and Xue, S.: A Review of Bolt Tightening Force Measurement and Loosening Detection, *sensors*, Vol.20, No.11, 3165, 2020.6.

[30] Jhang, K.Y., Quan, H.H., Ha, J. and Kim, N.Y.: Estimation of Clamping Force in High-Tension Bolts Through Ultrasonic Velocity Measurement, *Ultrasonics*, Vol.44, pp.e1339-e1342, 2006.12.

[31] Minakuchi, Y. and Nawa, T.: Ultrasonic Measurement of the Bolt Axial Force of a Bolted Joint after Tightening, *Journal of the Japanese Society for Non-Destructive Inspection*, Vol.54, No.7, pp.365-371, 2005.7.

[32] Joshi, S.G. and Pathare, R.G.: Ultrasonic Instrument for Measuring Bolt Stress, *Ultrasonics*, Vol.22, pp.261-269, 1984.11.

[33] Sakai, T., Makino, T. and Toriyama, H.: 超音波を利用したボルト軸力の測定, *Journal of JSME*, Vol.43, No.366, pp.723-729, 1977.2.

[34] Takahashi, M., Fukuda, M. and Imano, K.: A Method for Evaluation of Fastened Condition of Bolt – Nut Using Ultrasonic Waves, *SICE Tohoku Chapter* 第 285 回研究集会, No.285-9, pp.1-5, 2013.12.

[35] Argatov, I. and Sevostianov, I.: Health Monitoring of Bolted Joints Via Electrical Conductivity Measurements, *Int. J. Eng. Sci.*, Vol.48, pp.874-887, 2010.

[36] Ritdumrongkul, S., Abe, M., Fujino, Y. and Miyashita, T.: Quantitative Health Monitoring of Bolted Joints Using a Piezoceramic Actuator–Sensor, *Smart Materials and Structures*, Vol.13, pp.20-29, 2004.

[37] Daniel, M.P., Park, G. and Daniel, J.I.: Improving Accessibility of the Impedance-Based Structural Health Monitoring Method, *J. Intelligent Material Systems and Structures*, Vol.15, pp.129-139, 2004.2.

[38] Tao, W., Shaopeng, L., Junhua, S. and Yourong, L.: Health Monitoring of Bolted Joints Using the Time Reversal Method and Piezoelectric Transducers, *Smart Materials and Structures*, Vol.25, No.2, 025010, 2016.1.

[39] Hosoya, N., Niikura, T., Hashimura, S., Kajiwara, I. and Giorgio-Serchi, F.: Axial Force Measurement of the Bolt/Nut Assemblies Based on the Bending Mode Shape Frequency of the Protruding Thread Part Using Ultrasonic Modal Analysis, *Measurement: Journal of the International Measurement Confederation*, Vol.162, pp.1-10, 2020.10.

[40] Hosoya, N., Hosokawa, T., Kajiwara, I., Hashimura, S. and Huda, F.: Evaluation of the Clamping Force of Bolted Joints Using Local Mode Characteristics of a Bolt Head, *Journal of Nondestructive Evaluation*, Vol.37, No.4, 2018.

[41] Park, S., Yun, C.B. and Roh, Y.: Active Sensing-Based Real-Time Nondestructive Evaluations for Steel Bridge Members, *KSCE J. Civ. Eng.*, Vol.10, pp.33-39, 2006.

[42] Marshall, M.B., Zainal, I. and Lewis, R.: Influence of the Interfacial Pressure Distribution on Loosening of Bolted Joints, *An International Journal for Experimental Mechanics, Strain*, Vol.47, I-s2, pp.65-78, 2011.12.

[43] Akutsu, A., Bajracharya, S., Sasaki, E., Shimozato, T. and Tai, M.: Eddy Current Based Evaluation of Axial Force of High-Strength Bolts, *IABSE Congress: Resilient technologies for sustainable infrastructure*, pp.1-9, Christchurch, New Zealand, 2020.9.

[44] JSCE 鋼構造委員会, 高力ボルト摩擦接合継手の設計・施工・維持管理指針(案), 鋼構造シリーズ 15, 2006.12.

[45] Kong, Q., Zhu, J., Ho, S.C.M. and Song, G.: Tapping and Listening: A New Approach to Bolt Looseness Monitoring, *Smart Materials and Structures*, Vol.27, No.7, 07LT02, 2018.6.

[46] Kuramoto, N. and Chun, P.J.: Detection of Pavement Crack from Image by Decision Tree Learning, *Journal of JSCE A2 (Applied Mechanics)*, Vol.71, No.2, pp.I_823-I_830, 2015.

[47] Chun, P.J. and Igo, A.: Crack Detection from Image Using Random Forest, *Journal of JSCE F3 (Civil Engineering Informatics)*, Vol.71, No.2, pp. I_1-I_8, 2015.

[48] Wang, F. and Song, G.: Monitoring of Multi-Bolt Connection Looseness Using a Novel Vibro-Acoustic Method, *Nonlinear Dynamics*, Vol.100, No.10, pp.243-254, 2020.2.

[49] Chun, P.J., Igo, A., Namera, Y., Kuroki, K. and Okubo, K.: Deep Learning Based Crack Ratio Evaluation on Asphalt Pavement from Image Taken by Car-Mounted Camera, *Journal of JSCE E1 (Pavement Engineering)*, Vol.73, No.3, pp. I_97-I_105, 2017.

[50] Yuan, C., Wang, S., Qi, Y. and Kong, Q.: Automated Structural Bolt Looseness Detection Using Deep Learning-Based Prediction Model, *Structural Control Health Monitoring*, e2899, 2021.

[51] Zhao, X., Zhang, Y. and Wang, N.: Bolt Loosening Angle Detection Technology Using Deep Learning, *Structural Control Health Monitoring*, Vol.26, No.1, e2292, 2019.1.

[52] Mikami, I., Tanaka, S., Hiwatashi, T. and Yamaura, T.: A System for Inferring Axial Force of High-Strength Bolts on Steel Bridges, *Journal of JSCE*, No.549, I-37, pp. 77-90, 1996.10.

[53] Tran, D.Q., Kim, J.W., Tola, K.D., Kim, W. and Park, S.: Artificial Intelligence-Based Bolt Loosening Diagnosis Using Deep Learning Algorithms for Laser Ultrasonic Wave Propagation Data, *Sensors*, Vol.20, No.18, 5329, 2020.9.

[54] Cha, Y.J., Choi, W., Suh, G. and Mahmoudkhani, S.: Autonomous Structural Visual Inspection Using Region-Based Deep Learning for Detecting Multiple Damage Types, *Comput.-Aided Civ. Infrastruct. Eng., Special Issue:Health Monitoring of Structures*, Vol.33, No.9, pp.731-747, 2018.9.

[55] Cha, Y.J., Choi, W. and Büyüköztürk, O.: Deep Learning-Based Crack Damage Detection Using Convolutional Neural Networks, *Comput.-Aided Civ. Infrastruct. Eng.*, Vol.32, No.5, pp.361-378, 2017.5.

[56] Huynh, T.C., Park, J.H., Jung, H.J. and Kim, J.T.: Quasi-Autonomous Bolt-Loosening Detection Method Using Vision-Based Deep Learning and Image Processing, *Autom. Constr.*, Vol.105, 102844, 2019.9.

[57] Zhang, Y., Sun, X., Loh, K.J., Su, W., Xue, Z. and Zhao, X.: Autonomous Bolt Loosening Detection Using Deep Learning, *Struct. Health Monit.*, Vol.19, No.1, pp.105-122, 2020.

[58] Kiranyaz, S., Ince, T., Abdeljaber, O., Avci, O. and Gab-bouj, M.: 1-D Convolutional Neural Networks for Signal Processing Applications, *ICASSP 2019 IEEE*, pp.8360-8364, 2019.

[59] Tsuji, H., Suzuki, K. and Hirata, H.: 機械学習を援用したコンクリート内鉄筋の腐食判別の試み, *JSCE* 第 75 回年次学術講演会, 2020.

[60] Cha, Y.J., You, K. and Choi, W.: Vision-Based Detection of Loosened Bolts Using the Hough Transform and Support Vector Machines, *Autom. Constr.*, Vol.71, pp.181-188, 2016.11.

[61] Tsuji, Y., Hirokane, M., Hayashi, I. and Konishi, H.: Analysis of Characteristics for Diagnosing Axial Force of High-Strength Bolts, *Journal of JSCE F6 (Safety Problem)*, Vol.72, No.2, pp. I_177-I_182, 2016.

[62] Zhang, Z., Ikeuchi, H., Saiki, N., Imamura, T., Ishii, H., Toda, H. and Miyake, T.: Parasitic Discrete Wavelet Transform and its Application on Abnormal Signal Detection, *Transactions of the JSME (C)*, Vol.75, No.757, pp.163-170, 2009.9.

[63] Tsunoda, T. and Suzuki, K.: Image Sharpening of Concrete Voids With The Application of Parasitic Discrete Wavelet Transform, *Journal of JSCE A2 (Applied Mechanics)*, Vol.73, No.2, pp.I_691-I_698, 2017.

[64] Asamoto, S., Okazaki, Y., Okazaki, S. and Chun, P.J.: Regression Analysis of Concrete Shrinkage and Creep Laboratory Data by Machine Learning, *Intelligence, Informatics and Infrastructure*, Vol.1, I-J1, pp.122-131, 2020.

[65] Miguel-Hurtado, O., Guest, R., Stevenage, S.V., Neil, G.J. and Black, S.: Comparing machine learning classifiers and linear/logistic regression to explore the relationship between hand dimensions and demographic characteristics, *PLOS ONE*, Vol.11, No.11, 2016.11.

[66] Kawashima, K.: ものづくりのための超音波非破壊材料評価・検査, 養賢堂, 2009.

[67] Meredith, D.J., Watts-Tobin, R.J. and Dobbs, E.R.: Electromagnetic Generation of Ultrasonic Waves in Metals, *The Journal of the Acoustical Society of America*, Vol.45, No.6, pp.1393-1401, 1969.

[68] Scruby, C.B. and Drain, L.E.: Laser Ultrasonics Techniques and Applications, *Adam Hiler*, 1990.

[69] Kang, K.C. and Park, K.K.: Noncontact Laser Ultrasound Detection of Cracks Using Hydrophone, *Sensors*, Vol.21, No.10, Article No.3371, 2021.5.

[70] Bhardwaj, M.C.: Non-Contact Ultrasound, *Secondwave Systems*, 2002.

[71] Nishimura, N., Akiyama, H. and Kamei, Y.: Trend of Studies on High-Strength Friction Grip Bolt Joint, *Journal of the JSCE*, No.675, I-55, pp.1-14, 2001.4.

[72] Nitta, I., Matsuzaki, Y., Abe, M. and Miyajima, T.: A Measurement Method of Bolt Loads Based on Deformation of a Top Surface of a Bolt Head, *Transactions of the Japan Society of Mechanical Engineers Series C*, Vol.73, No.733, pp.2612-2618, 2007.

[73] Pan, C., Yamaguchi, T. and Suzuki, Y.: ひずみゲージを用いた高力ボルト軸力の測定法に関する検討, *JSCE* 第 65 回年次学術講演会, 2010.9.

[74] Arakawa, T., Fukumoto, S. and Ooba, Y.: 丸棒などの曲率が超音波探傷に及ぼす影響, *IIC REVIEW*, No.58, pp.42-47, 2017.10.

[75] Tanimura, Y.: 絵とき「超音波探傷」基礎のきそ, *Nikkan Kogyo Shimbun, LTD., Chapter 3*, 2013.11.

[76] Birring, A.S.: TOFD principle, limitations, calibration and inspection, *e-journal of Nondestructive Testing*, ISSN 1435-4934, pp.1-8, 2020.6.

[77] Gauthier, B., Painchaud-April, G., Duff, A.L. and Bélanger, P.: Towards an alternative to time of flight diffraction using instantaneous phase coherence imaging for characterization of crack-like defects, *Sensors*, Vol.21, No.3, 730, 2021.1.

[78] Breiman, L.: Random forests, Machine Learning, Vol.45, No.1, pp.5-32, 2001.4.

[79] Kiranyaz, S., Ince, T., Abdeljaber, O., Avci, O. and Gabbouj, M.: 1-D convolutional neural networks for signal processing applications, ICASSP 2019 IEEE, pp.8360-8364, 2019.

[80] Hirokane, M., Nakata, H., Konishi, H. and Suzuki, N.: Diagnosis for Axial Force of High-Strength Bolts Using Pattern Recognition, *Journal of JSSC F6 (Safety Problem)*, Vol.69, No.2, pp.I_69-I_74, 2013.

[81] Breiman, L.: Bagging Predictors, Machine Learning, Vol.24, pp.123-140, 1996.

[82] Tsunoda, T. and Suzuki, K.: Image Sharpening of Linearized Inverse Scattering Method for Concrete Voids, *Journal of JSCE A2 (Applied Mechanics)*, Vol.75, No.1, pp.23-36, 2019.

Chapter 4
Evaluation of Faying Surface Contact Condition

4.1.Overview

The study of faying surface contact states has a long history, and it is a field that has been studied since the time of Leonardo Da Vinci (1452-1519) [1]. Based on Da Vinci's research, Amontons and Coulomb further developed the technology. They proposed Amonton-Coulomb's law [2], which clearly states that "The force of friction is independent of the apparent area of contact." The apparent area of contact is given by

$$A_t = \frac{W_v}{P_{\bar{y}}} \tag{4-1}$$

where W_v is the vertical force and $P_{\bar{y}}$ is the average yield pressure. As shown in **Figure 4.1**, the real contact area, which is the total area of the real contact points, is proportional to the load W_v and does not depend on the apparent contact area, and the total adhesion force is proportional to the real contact area, which means that Amonton-Coulomb's law is valid. However, Rubinstein et al. [3-4] reported that, as a result of macroscopic investigation of object slipping, it was confirmed that a large number of small slips occurred up to the slip resistance R_s (**Figure 4.2**). Based on their research, some reports have suggested that there are exceptions to Amonton-Coulomb's law [5]. Therefore, it is considered that local slipping occurs repeatedly up to the static friction force, and the faying surface is scraped by wear each time. The protruding part of the faying surface repeatedly deforms elastically to form a real contact point [6]. Considering this fact, the inorganic zinc-rich paints commonly applied to bolted joints in recent years have increased the number of uncertain parameters. In the case of a bolted joint where the faying surface is coated with a paint such as inorganic zinc-rich paint, the paint is scraped off by a load smaller than the slip resistance. In other words, the faying surface contact condition is always changing at the load level where no slip occurs. Under such conditions, various phenomena occur in the bolted joints, and it is considered that the structural performance of bolted joints may be unclear, and the importance of accurately evaluating the faying surface contact condition is increasing. Therefore, it is very important to evaluate the faying surface contact condition of bolts in existing joints coated with inorganic zinc-rich paint.

The faying surface contact condition due to bolt tightening in Chapter 2 was clarified analytically. Therefore, in this chapter, it was investigated whether the condition of the analysis actually occurs. In the case of a plate coated with inorganic zinc-rich paint, the faying surface

contact condition may be different from that of an uncoated plate due to the peeling of the paint. In such a situation, the distribution of contact pressure was confirmed by scanning the ultrasonic probe on the plate surface in a bolted joint coated with inorganic zinc-rich paint. Furthermore, Minami et al. [7] pointed out that the coating thickness of inorganic zinc-rich paint affects the slip coefficient. Hence, specimens with different coating thickness on backside of steel plate and bolted joint faying surfaces were used, and data for each coating thickness was obtained. These data were fed into machine learning to quantitatively evaluate the coating thickness.

4.2. Reproduction of Actual Faying Surface Contact Condition by Analysis

In Chapter 2, the faying surface contact condition of the 1 by 2 bolt joint was confirmed when the bolt was tightened. The analysis revealed that the distribution of contact pressure was concentrated just below the washer. It was confirmed that the contact pressure spread concentrically around the bolt, and the contact pressure at the edge was completely zero. A weak contact pressure was confirmed by overlapping two small contact pressures between the bolts. The bolt pitch p is limited by

$$p = 12t \tag{4-2}$$

A maximum bolt pitch of 144mm is possible when the 12mm splice plate used in this study is the target. Therefore, the faying surface contact condition for the case of long bolt pitch was investigated and compared with the case of short bolt pitch again.

The analytical model is shown in **Figure 4.3**. 205kN bolt axial force was introduced for all bolts. Only the top face of the base plate was fixed. The symmetry condition was set for the nut side. In this analysis, a slip coefficient of 0.6, which is the average value of a large number of experiments conducted in [8-9], was set as the slip coefficient. However, since the analysis was conducted without tensile or compressive loading, the slip coefficient is not considered to have a significant effect. The mechanical properties and plate thickness configuration were set to be the same as in the analysis of Chapter 2. The mesh was set to be an 8-node solid element (hexahedron) with a size of 2mm, since more detailed contact pressure and stress distributions were to be investigated in this analysis. No load was applied, and only the bolt axial force was introduced in the numerical analysis.

The distribution of contact pressure at the faying surface of the base plate obtained from the analysis is shown in **Figure 4.4**. The range of low contact pressure, below 10MPa, was indicated by black scale. A large contact pressure is observed just below the washer, and the pressure spreads in concentric circles around the bolt, but the damping rate is large. The stress distribution in the longitudinal direction of the splice plate is shown in **Figure 4.5**. For the case with short bolt pitch, the stress at the center between bolts is large, and for the case with long bolt pitch, it can be confirmed that the stress spreads greatly in the x-axis direction between bolts. In other words, when several bolts are arranged in a bolted joint, the force between the bolts is considered to be acting in the direction that the splice plate is separated from the base plate. This phenomenon can be seen in the deformation diagram in **Figure 4.6**. The distances between the base plate and the splice plate between the bolts were confirmed when a bolt axial force of 205kN was introduced to the two bolts. In the case of the bolt pitch of 75mm, the distance was 57.69μm, and in the case of the bolt pitch of 144mm, it was 5081.66μm. Since the coating thickness of inorganic zinc-rich paint is usually 75μm, it is possible that the base plate and the splice plate are far apart when the bolt pitch is long.

4.3. Effect of Actual Faying Surface Contact Condition on the Structural Performance of Bolted Joints

In the analysis of bolt axial force introduction only, it was confirmed that most of the friction forces in the bolted joint acted directly under the washer. In the conventional analysis of bolted joints, a uniform slip coefficient is often set for the faying surface. However, it is not clear how the slip resistance of bolted joints is affected when the slip coefficient may vary with the contact pressure distribution. Therefore, the difference between the structural performance evaluated when the slip coefficient is set to match the distribution of the analytical results and the structural performance evaluated when the slip coefficient is set to be constant for all faying surfaces is clarified.

Figure 4.7 shows the cases that were compared. The case where all faying surfaces are set to 0.6, which is the conventional method, is designated as Case 1. The case where the contact pressure

is set to $\mu = 0.6$ for areas where the contact pressure is larger than 0Pa, and $\mu = 0$ for areas where the contact pressure was 0Pa is called Case 2. In addition, Case 3 is the case in which the slip coefficient is divided into three types based on the contact pressure distribution. Case 3 is that $\mu = 0.6$ is directly under the washer, i.e., the same as the size of the washer. $\mu = 0.4$ is the area where the contact pressure is greater than 0Pa, and $\mu = 0$ is the area where the contact pressure was 0Pa. The analytical model with a bolt pitch of 75mm shown in **Figure 4.3** was used. The bottom of the splice plate was changed to the fixed side, and a tensile load was introduced at the top of the base plate.

The load at which the relative displacement between the base plate and the splice plate is 0.2mm was compared as the slip resistance. The results of the analysis are shown in **Figure 4.8**. According to **Figure 4.8**, it was confirmed that the slip resistance of Case 1 and Case 2 were approximately the same. In other words, it can be said that only the area where the contact pressure around the bottom of the washer is applied is important in evaluating the slip resistance. In Case 3, it was confirmed that the slip resistance was significantly reduced. Therefore, it is clear that slip coefficient for the area with contact pressure governs slip resistance. In the current regulations [10], the entire faying surface is defined by a constant slip coefficient. In addition, most of the studies are based on it for experiments and analyses. However, the results of the analysis in this study revealed that the contact pressure spreads concentrically around the bolt. Based on the results of this analysis, the case where inorganic zinc-rich paint is applied is considered. The faying surface coated with inorganic zinc-rich paint is subjected to contact pressure, which causes it to peel and crumble. As a result, it can be said that the slip coefficient is not constant because the faying surface condition changes. Therefore, if research is conducted to evaluate the structural performance of bolted joints with high accuracy, it is considered important to define the slip coefficient for each contact pressure distribution. In addition, by considering the distribution of contact pressure, there is a possibility of clarifying the process of load transfer in bolted joints under various conditions. Identification of contact pressure distribution is important for structural performance of bolted joints. Therefore, in this chapter, the method to evaluate the distribution of contact pressure was considered.

4.4. Evaluation of Contact Pressure for Different Bolt Axial Force Level

Up to the above, the faying surface contact condition was confirmed analytically. As a result of the analysis, it was confirmed that when the bolt axial force was introduced into the bolt joint, the force acted in the direction of peeling of the plates between the bolts. It was also confirmed that most of the frictional force of the bolted joint was borne around the washer. Identification of contact pressure distribution is important for structural performance of bolted joints. Thus, it is necessary to establish a method to evaluate the distribution of contact pressure. Therefore, in this chapter, an experiment was conducted to evaluate the contact pressure according to the bolt axial force level, focusing on the space between bolts in a bolted joint. It is believed that the higher the adhesion of the interface, the higher the transmittance of the ultrasonic wave and the higher the power of the received wave [10-11]. Then, considering the results of the analysis in this study, the theory of ultrasonic characteristics is as shown in **Figure 4.9** for the two-probe method. If the bolt axial force is large, the Intensity of the received wave signal will be weak or zero because the plate between the bolts will be less adherent. On the other hand, when the bolt axial force is small, the plate between the bolts has a high degree of adhesion, so the ultrasonic transmission is high, and a signal with a large Intensity is received. Based on this law, experiments were conducted.

4.4.1. Specimen and Measurement Method

When the faying surface is coated with inorganic zinc-rich paint, there are many uncertain parameters such as roughness and coating thickness, which may prevent the accurate measurement of contact pressure. Thus, the unpainted mill scale specimen was used in this experiment. An overview of the specimen is shown in **Figure 4.10**. Based on the results of the analysis, the specimen was modeled with a bolt pitch that can easily reproduce plate to plate delamination between bolts. The ultrasound equipment used was the same as the one used in Chapter 3. Both the transmitter and receiver were 10MHz ultrasonic probes. The transmitting ultrasonic waves were set as shown in **Table 4.1**.

In order to accurately control the bolt axial force, the relationship between the strain value of the strain gauges and the bolt axial force was calculated in advance using an axial force gauge [12]. Calibration of the bolt axial force was performed for all the bolts used. Since the total plate thickness of the specimen used in this experiment was 64 mm, the bolts used in this experiment

had a neck length of 100mm. The results of the bolt axial force calibration are shown in **Figure 4.11**. The mechanical properties and torque coefficient values of the bolts used (F10T M22) are shown in **Table 4.2**. The bolt axial force was introduced at a pitch of 20kN from 120kN to 220kN. A torque wrench was used to tighten the bolts, referring to the values of the strain gauges. Five measurements were conducted at each bolt axial force level. Two probes were placed between the two plates between the bolts and the measurements were conducted using the two-probe method. In order to conduct the measurement under the same conditions, a technique was devised to keep the force of the probe constant. It is possible that the pushing force of the ultrasonic probe affects the Intensity of the received signal. For this reason, it is necessary to keep the force of the ultrasonic probe constant during the measurement. To keep this in mind, we devised a method to keep the force of the probe constant in order to conduct the measurement under the same conditions. A spring-loaded jig made by a 3D printer, as shown in **Figure 4.12**, was used to keep the force of the probe constant. Machine oil was used as the contact medium between the probe and the plate, and a certain amount was applied to the bottom of the probe using a dropper.

4.4.2. Evaluation of Contact Pressure by Intensity of Received Wave and Frequency Level

The raw waveform data measured at each bolt axial force level is shown in **Figure 4.13**. These raw waveform data are the average of five measurements. The frequency bands are shown in **Figure 4.14**. These data were normalized by the value of the largest received signal. Therefore, the Intensity of the signal indicates the magnitude of the contact pressure. No linear variation with bolt axial force level was observed. Hence, it was difficult to prove the theory of ultrasonic characteristics described above from the two figures. According to the results, transmission waves could not be received when the bolt axial force was 0 kN. Therefore, it is presumed that the plates are close to non-contacting each other. However, it is considered difficult to evaluate the contact pressure quantitatively in the case of the mill scale specimens, where the steel has no coating. Since the frequency bands are almost the same for all bolt axial forces and no signal can be identified at the frequency of multiples, it is considered that no harmonics [13-14] are generated. Harmonics are said to be generated at the interface between steels. If the adhesion between steels is strong, the two steels are completely integrated and the same frequency will reach the receiver. If the adhesion between the steels is weak, the longitudinal vibrations of the ultrasonic waves cause

the steels to slightly separate and stick together, and the frequency at the interface is said to change by an integer factor. This is the mechanism of harmonic generation.

4.5. Evaluation of Contact Pressure Distribution on Faying Surface

It was confirmed that it is difficult to evaluate the contact pressure in the bolted joints with mill scale using the above measurement method. However, the faying surface contact condition may be different for bolted joints coated with inorganic zinc-rich paint. The inorganic zinc-rich paint is usually 75μm thick. When inorganic zinc-rich paint is subjected to pressure by tightening bolts, the coating thickness could change in response to the contact pressure. In this chapter, the distribution of contact pressure on bolted joints coated with inorganic zinc-rich paint is experimentally evaluated. The specimen used and the measurement methods are described below.

4.5.1. Specimen and Measurement Method

In order to experimentally clarify the distribution of contact pressure magnitude and contact pressure, a specimen (**Figure 4.15**) was prepared with a bolt axial force of 205kN, the design bolt axial force, introduced. The bolt axial force was accurately introduced by strain gauge control. **Figure 4.16** shows the points to be measured and the measurement method. The measurement method was a two-probe method, in which ultrasonic probes were placed on the front and back of the plate, and separate probes were used for transmission and reception. There are 13 measurement points as shown in **Figure 4.16**. In order to reduce the variation of the measurement data, each point was measured 3 times. A 5 MHz broadband probe was used for transmission, and a 10MHz broadband probe was used for reception. The frequency characteristics of each are shown in **Figure 4.17** and **Figure 4.18**. The reason why the receiving side was set to high frequency was to consider the possibility of harmonics [13-14] being generated at the interface of the plates. The ultrasonic characteristics are the same as in **Table 4.1**.

4.5.2. Evaluation of Contact Pressure Distribution on Faying Surface

In this investigation, the Intensity of the received ultrasonic signal is important. When the two-probe method using ultrasonic waves is applied, the law of **Figure 4.19** devised by the author is

expected. When the plates are not in contact with each other, ultrasonic waves can be transmitted between the steels as the inorganic zinc-rich paint is extruded and hardened, but the Intensity is low. When the plates are in contact with each other, a large intensity is observed. Therefore, the higher the contact pressure, the higher the Intensity.

Thus, the raw waveform data measured at each measurement point is shown in **Figure 4.20**. These raw waveform data are the average of the data obtained from three measurements. Overall, P1, the one with the shorter edge distance, had the highest Intensity. This experiment is evaluated based on the law of **Figure 4.19**. Therefore, it can be said that the contact pressure of P1 is high. In P5, P6, and P7, which have longer edge distances on the opposite side, we can see that the Intensity gradually weakens toward the edge. Similarly, P11, P12, and P13 showed a gradual decrease in Intensity toward the outside, and no transmitted waves were received for P8, P9, and P10 except for P8. In other words, inorganic zinc-rich paint is flowing into the material due to the low contact pressure. There was almost no difference in the magnitude of Intensity between the bolts P2, P3 and P4. The Intensity is also similar to P5 and P11. When the faying surface was coated with inorganic zinc-rich paint, no contact was suggested between the bolts, except for P1, where the outermost bolts, P7, P10 and P13, had an Intensity of 0, indicating no contact. The reason for the large P1 may be the short edge distance. The fact that the outer contact pressure was 0Pa suggests that the numerical analysis conducted in Chapter 2 and this chapter was approximately accurate. However, no contact was observed between the bolts, indicating that the bolt pitch of 75mm was not completely non-contact. It is also possible that the plates between the bolts became in contact due to the crushing of the coating under the washers. It is conceivable that, contrary to expectations, the slip resistance may have increased. This is truly an uncertain influential parameter. Therefore, it is considered very important to evaluate the structural performance of inorganic zinc-rich paint when it is applied. **Figure 4.21** shows the two-dimensional contours of contact pressure created based on the raw waveform in **Figure 4.20**. The magnitude and damping of the contact pressure are also almost the same as the results of the analysis. Due to the small number of measurement points, the figure is angular, but the distribution of contact pressure is almost the same as the analysis. Hence, the possibility of understanding the faying surface contact condition by ultrasonic measurement was demonstrated.

4.6. Evaluation of Inorganic Zinc-Rich Paint Thickness on Backside of Steel Plate and Faying Surface

The contact pressure distribution of bolted joints coated with inorganic zinc-rich paint can be evaluated by the above experiment, and it is confirmed that Base plate and Splice plate are in contact between bolts when the bolt pitch is 75mm. In the case of contact between inorganic zinc-rich paints, the coating thickness is one of the factors that affect the slip coefficient of bolted joints. In this section, an attempt was made to evaluate the coating thickness on faying surfaces, which is assumed to influence the slip coefficient. This study was based on related research on coating thickness measurement.

4.6.1. Relationship Between Coating Thickness on the Faying Surface and the Slip Coefficient and Related Research on the Coating Thickness Measurement

In the current Japanese design standards for steel roadway bridges [15], the design slip coefficient of a bolted joint is determined by the faying surface treatment during construction, and if the faying surface is coated with inorganic zinc-rich paint, the slip coefficient is 0.45 regardless of the coating thickness. However, it has been reported that the slip coefficient depends on the coating thickness of the faying surface [7, 16], and the ISO design standard specifies [17] the slip coefficient depending on the coating thickness of inorganic zinc-rich paint. The specification for road bridges sets the slip coefficient at 0.45 for coating thicknesses of 50 μm or more, and some standards suggest a slip coefficient of 0.6 for coating thicknesses of 60 μm or more. On the other hand, it has also been observed that the slip coefficient decreases if the coating thickness is too large. Thus, there is a need for a method to accurately determine the coating thickness of bolts in existing joints.

The coating thickness of the inorganic zinc-rich paint coated on bolted joints is said to decrease with age and slipping due to earthquakes. The authors [18] conducted a slip resistance test on bolted joint specimens with inorganic zinc-rich paint coated on the faying surface, and found that the paint thickness decreased after the test. In addition, Ishihara et al. [19] reported the variation of the slip coefficient when repeated slip occurred in the bolted joint, assuming actual earthquake damage, and experimentally clarified that the slip coefficient changed with each slip.

As described above, it is said that the slip coefficient differs depending on the coating thickness of the faying surface in bolts in existing joints. However, since the coating on the faying surface

is on the back side of the steel, it is difficult to evaluate the coating thickness accurately without dismantling the bolted joint, and the evaluation method has not yet been established. Coating thickness measurements are generally made on surface coatings, and techniques have been developed to measure coating thickness using spectral interference [20], electromagnets [21], eddy currents [22], infrared [23], and ultrasonic waves [24]. Contact-type electromagnetic thickness gauges have been developed for measuring the thickness of dried and solidified coatings, including inorganic zinc-rich paints, and are often used to measure the thickness of magnetic materials such as bolted joints.

Thus, conventional coating thickness evaluation is based on formulas using correlations between light interference intensity, electric current, etc. and coating thickness, mainly for the purpose of measuring surface coating thickness. However, none of them can be applied to the measurement of the faying surface coating thickness on the backside of steel plate.

Studies have been conducted to evaluate the coating thickness on the backside of a steel plate. Tohmyou et al. [25-29] conducted ultrasonic measurements from the surface of steel plates to evaluate the coating thickness of steel plates and other materials with bag structures for industrial products. There, acoustic resonance phenomenon was used and a method was proposed to evaluate the coating thickness on backside of the steel plate. At frequencies of several 10 MHz, measurement of coating thicknesses below 100 μm, which is equivalent to the wavelength, becomes difficult due to superposition of reflected waves. Thus, the use of high-frequency ultrasonic waves of 100 MHz suppresses the superposition of reflected waves and enables the evaluation of coating thicknesses of several 10 μm. In this study, the evaluation of coating thickness is attempted by considering the superposition of reflected waves that occur at coating thicknesses of 100 μm or less, since the study is conducted using a 10 MHz ultrasonic probe, which is commonly used. Recently, studies have been conducted to evaluate the features of measured waveforms by learning them as training data and using machine learning [30]. It is possible that not only the coating thickness on the backside of a steel plate but also the coating thickness on the bolted joint faying surface can be evaluated. By superposition of reflected waves, the waveform shape during the time period including the reflected waves from the bolted joint faying surface changes with coating thickness, which is learned and analyzed by machine learning.

In machine learning, evaluation with random forests, which are easier to implement than other classifiers such as NNs or SVMs and have features that reduce overfitting, is considered.

While Tohmyou et al. were able to evaluate the coating thickness on the backside of a single steel plate using 100 MHz ultrasonic waves, this study uses the more common 10 MHz ultrasonic waves to evaluate the coating thickness on backside of steel plate and bolted joint faying surfaces. Hence, an ultrasonic measurement method for coating thickness on the backside of steel plates and bolted joint faying surfaces is established by applying machine learning. First, the coating thickness on the backside of steel plate is evaluated. Next, an attempt is made to evaluate the coating thickness on the faying surface of two plates, such as bolted joints, using the same method as that used for the evaluation of the coating thickness on the backside of steel plates.

4.6.2. Overview of each interface of bolted joints and ultrasonic measurements

In a two-media transmission system, when an ultrasonic wave is vertically incident on a certain medium 1 and transmitted to medium 2, the transmission coefficient t_{12} and reflection coefficient r_{12} of the sound pressure at the interface between medium 1 and medium 2 are determined by the acoustic impedance Z of each medium and can be expressed as follows [31].

$$t_{12} = \frac{2Z_2}{Z_1 + Z_2} \tag{4-3}$$

$$r_{12} = \frac{Z_2 - Z_1}{Z_1 + Z_2} \tag{4-4}$$

In this study, the double-plate coated with inorganic zinc-rich paint are connected to each other and ultrasonic waves are injected from one surface (**Figure 4.22**). In general, the acoustic impedance of steel is 46 and that of air is very small, 0.0004. In addition, the acoustic impedance of the inorganic zinc-rich paint used in this study is 6.55. Hence, the transmission coefficient of sound pressure from inorganic zinc-rich paint to steel is about 1.75 times, and that from steel to inorganic zinc-rich paint is about 0.25 times. If the interface is air, the wave is reflected with the same sound pressure as the incident wave.

Therefore, the ultrasonic wave transmitted through the interface 2 and reflected at the interface 3 with the sound pressure about 1.31 times larger than that of the ultrasonic wave at the incident. However, the ultrasonic wave with a sound pressure about 0.44 times larger than that of the incident ultrasonic wave is considered to reach the faying surface, which is interface 4. The interface 4 is the contact between the coating films. The surface of the inorganic zinc-rich paint is unevenness [18], and according to tribology [32], a field concerned with friction, wear, and lubrication, the contact condition may be as shown in **Figure 4.23**. This figure shows that the true

contact area is sufficiently smaller than the apparent contact area. In general, the true contact area depends on the load, but the sum of the true contact areas is only a few hundred thousandths to a few hundredths of the apparent contact area. Therefore, at interface 4, the proportion of air is large, and most of the ultrasonic waves are reflected and received as reflected signals.

The coating to be measured in this study is the coating on backside of a single steel plate and the coating on the measurement side of the faying surface of two plates, which is assumed to be a bolted joint, and will be referred to as the target coating in this study. **Figures 4.24** and **Figures 4.22** show images of ultrasonic measurements on one and two plates, where ultrasonic measurements are conducted using the single probe method, where transmission and reception are conducted with a single probe. Interface 1 is the measurement surface, interface 2 is the interface between the measurement surface coating and the steel plate, and interface 3 is the interface between the steel plate and the target coating. Interface 4 is the backside surface in the case of a single plate or the faying surface in the case of two plates.

In this study, an ultrasonic pulser receiver is used to output high-voltage pulses and transmit and receive longitudinal ultrasound waves with a 14 mm diameter 10 MHz ultrasonic vertical probe (PN 10C10N, Japan Probe). The settings of the ultrasonic pulser receiver are shown in **Table 4.3**. Also, no filtering process was performed in the ultrasonic pulser receiver, and the raw waveform data was acquired as it was. A certain amount of machine oil was applied to the probe contact point using a dropper as the probe contact medium. To constant the pushing force of the probe, a 1 kg weight was placed on top of the probe as shown in **Figure 4.25**. Measurements were made after waiting for about 5 seconds per measurement for the probe to settle. The gain was kept constant for all measurements.

4.6.3. Effects of superimposed reflected waves on the target waveform

In order to evaluate the target coating thickness, this study focuses on a group of reflected waves generated during a time period when ultrasonic waves make a single round trip to the steel plate on the measurement side. In this paper, this group of reflected waves is called the target waveform. The use of general 10 MHz ultrasonic waves may result in the superposition of reflected waves that are difficult to separate from the target waveform. An example of superposition of reflected waves that can be expected to be superimposed on the target waveform is shown in **Figure 4.26**. It is also possible that the information on target coating thickness might be buried by

the superposition of reflected waves, as shown in **Figure 4.27**, due to multiple reflections between each interface. Therefore, preliminary experiments were conducted on two steel plates to clarify the effect of each interface on the target waveform based on the reflection wave assumed in **Figure 4.26**. The same steel plate was used for the measurement side in the preliminary experiments, with a thickness of 28 mm.

a). Influence of the measurement surface coating on the target waveform

To clarify the effect of the target coating on the target waveform, ultrasonic measurements were performed on a single plate with (**Figure 4.24**) and without (**Figure 4.28**) target coating on the measurement surface, and the target waveforms with and without target coatings are shown in **Figure 4.29** for comparison. When there is a coating on the measurement surface, the amplitude is significantly reduced. It is considered that the transmitted and received waves penetrate the interface 2 twice, resulting in attenuation of the energy. The waveform shape is relatively stable when there is no coating on the measurement surface, whereas when there is a coating on the measurement surface, the wavelength collapses and an interference reaction can be observed in the vicinity of approximately 10 μs. This can be assumed to be due to the multiple reflections at interface 1 and interface 2 shown in **Figure 4.26**. If there is a coating on the measurement surface, the waveform shape changes according to the target coating thickness, which could affect the target coating thickness evaluation. Therefore, in this study, the coating on the measurement surface is removed.

b). Influence of the target coating on the target waveform

To confirm that the shape of the target waveform changes with target coating thickness, ultrasonic measurements were performed on a single plate as shown in **Figure 4.28** with target coating and **Figure 4.30** without target coating, and the target waveforms are compared in **Figure 4.31**. The amplitude is lower when there is a target coating. The rise time of the reflected wave is the same, suggesting that both waves are first reflected at interface 3.

c). Influence of plates being joined to each other

Measurements were taken with a single plate as shown in **Figure 4.28** and with two plates as shown in **Figure 4.32** to confirm the effect of the plates being joined together. two plates were

joined using F10T M22 high-strength bolts, tightened with an axial bolt force of 205 kN. **Figure 4.33** compares the target waveforms measured with one and two plates. Ultrasonic waves transmitted through interface 3 are almost totally reflected at interface 4 in the case of a single plate, but in the case of two plates, some ultrasonic waves are transmitted through interface 4 according to the contact pressure distribution, and a decrease in amplitude can be observed. When transmitted through the faying surface, the superposition of reflected waves from the interface 5 may be superposed on the target waveform, but there is almost no change in wavelength or waveform shape, and the two waveform shapes are similar. This suggests that if the two plates are joined, the transmittance at interface 4 may be small. However, the effect of contact pressure on the target waveform should be investigated in the future.

4.6.4. Outline of specimens for evaluation of coating thickness

To evaluate the coating thickness on the backside of steel plate and on the faying surface, ultrasonic measurements are conducted on a single plate and on two plates. To evaluate the backside of steel plate, steel plates with different coating thicknesses were used only between the bolts on the backside, as shown in **Figure 4.34**. To evaluate the faying surface coating thickness, steel plates with two bolt holes were used and specimens were fabricated with a combination of two different plate thicknesses, 28 mm and 16 mm. **Figure 4.35** shows an overview of the two plates specimen. Five different coating thicknesses were applied between the bolts on the faying surface, since the distance between the bolts was used as the measurement position. The steel plates used for the specimens were coated with approximately 80 μm inorganic zinc-rich paint over the entire surface of the steel plates with the mill scale removed. Case A has a coating thickness of 80 μm. Except for Case A, the coating thicknesses in the order of Case B, C, D, and E were 60, 40, 20, and 0 μm, respectively, and the thicknesses were gradually reduced using sandpaper while checking with an electromagnetic coating thickness meter (**Figure 4.36**). The maximum error of coating thickness within and around the black frame in **Figure 4.34** should not exceed 20 μm. Before measuring the specimens, the coating thickness was again measured at the five locations shown in **Figure 4.37** in the range where the coating thickness was adjusted using an electromagnetic coating thickness meter. **Figure 4.38** and **Figure 4.39** show the coating thicknesses at the five locations measured from a steel plate 28 mm and 16 mm thick, respectively. The five values in each case are the values at measurement positions 1 to 5 from the left,

corresponding to the measurement positions in **Figure 4.37**. The dashed lines indicate the targeted coating thickness when the coating was removed. The five objective variables for machine learning were 80, 60, 40, 20, and 0 μm. For the steel plate surface, only the coating on the measurement surface was completely removed to eliminate the influence of the coating on the measurement surface. The two plates specimens were made up of two different thicknesses of the same coating thickness, and were joined to each other by tightening F10T M22 high-strength bolts with bolt axial force of 205 kN. The mechanical properties of the specimens are shown in **Table 4.4**.

4.6.5. Overview of machine learning for coating thickness evaluation

For target coating thickness evaluation, the "RandomForestClassifier" of the "sklearn.ensemble" library in Python 3.7.6 was used. In order to establish a simple method, the number of decision trees is 100 and the decision trees are split using the measure of impurity, which is calculated as the Gini coefficient. This divides the child nodes so that the difference between the impurity of the parent and child nodes is maximised. The minimum number of samples required to form a leaf was set to 1, and other parameters were set to default. Since the results of the evaluation by the random forest [33, 34] are different each time, the evaluation is repeated 100 times and the probability of the value predicted by each testing data is calculated.

For the construction of classification models, evaluating the application of deep learning based on one-dimensional convolutional neural networks (1DCNN) etc. [35] can be considered as an effective means, but the number of training samples is limited in this study, and one-dimensional data such as time history waveforms are difficult to expand, so there is a possibility that overfitting could occur. Therefore, the application of a random forest was attempted in this evaluation method.

The k-fold cross-validation [36, 37] is carried out by dividing all the acquired ultrasound measurement data into k pieces, one of which is the testing data and the remaining k-1 pieces are the training data. During data partitioning, the data are randomly assembled and evaluated using a random forest. By calculating the average accuracy, which is the average of k evaluations, it is confirmed that this method is not overfitting and that it is versatile.

4.6.6. Evaluation of coating thickness on the backside of steel plate

In this study, the target coating thickness is evaluated from the waveform shape using machine learning without separating the multiple reflected waves in the target waveform. For this purpose,

ultrasonic measurements were conducted on specimens with different target coating thicknesses, and the acquired ultrasonic measurement data were divided into training data and testing data.

The five objective variables for machine learning were 80, 60, 40, 20 and 0 μm. For the steel plate surface, the coating on the measurement surface was completely removed only at the measurement position in order to remove the influence of the coating on the measurement surface. A total of 10 specimens were used, with two different plate thicknesses and five different coating thicknesses.

Ultrasonic measurements were conducted on five specimens each of a 28 mm steel plate and a 16 mm steel plate as shown in **Figure 4.28**, each at five measurement points as shown in **Figure 4.37**. In other words, 25 ultrasonic measurement data were obtained from each of the 28 mm and 16 mm steel plates. The normalized target waveforms acquired from the 28 mm and 16 mm steel plates are compared for each case in **Figure 4.40**. Here, the ultrasonic measurement data measured at measurement position 3 are compared, showing the waveforms in the state to be applied to machine learning.

A comparison between a 28 mm steel plate and a 16 mm steel plate shows that the wavelengths are almost identical between 1.5 μs. Comparison of the cases shows that in each case there is an interference response in the waveform at about 0.5 μs, and that the shape is different in each case. These waveforms were applied to machine learning to evaluate the coating thickness on the backside of steel plate, and cross-validation confirmed the accuracy of the evaluation method considered in this study.

First, 25 reflection signals acquired from a 28 mm steel plate were used as training data and 25 reflection signals acquired from a 16 mm steel plate were used as testing data for evaluation using a random forest. The evaluation was repeated 100 times and the probabilities of the values predicted by each testing data are shown in **Table 4.5**. It was observed that the higher the backside of steel plate coating thickness, the higher the percentage of correct responses. The probability of the value being evaluated as 0 μm tended to be higher when the coating thickness on the backside of steel plate was less than 40 μm. The reason for this is thought to be that, under 40 μm, interface 3 and interface 4 are extremely close to each other and the time difference between the generation of each reflected wave becomes small, making it difficult for changes to appear as a waveform shape. In the Specifications for Highway Bridges, the coating thickness that ensures a slip coefficient of 0.45 is 50 μm, so the evaluation accuracy over 50 μm, which is important in practice,

is considered to have the potential to be sufficiently accurate. Furthermore, the fact that steel plates of different thicknesses are evaluated as testing data suggests the possibility of using steel plates of any thickness to obtain coating thickness training data, which could be applied irrespective of plate thickness.

Next, k-fold cross-validation was conducted by dividing the 50 acquired ultrasonic measurement data into 10 parts. k-fold cross-validation results showed an average accuracy of 0.82 for the single plate specimens used in this study.

4.6.7. Evaluation of coating thickness on faying surface

The 25 data measured from the 28 mm steel plates of each specimen were used as training data, and the 25 data measured from the 16 mm steel plates of each specimen were used as testing data for evaluation using random forests.

The normalized target waveforms for evaluation obtained from a 28 mm steel plate and a 16 mm steel plate are compared for each case in **Figure 4.41**. Here the ultrasonic measurement data measured at measurement position 3 are compared, showing the waveforms in the state to be applied to machine learning.

The evaluation by random forest was repeated 100 times, and the probabilities of the values predicted by each testing data are shown in **Table 4.6**. we observed that for values over 40 μm there was an accuracy rate of over 80 %. For all coating thicknesses, the maximum error in the predicted value was 20 μm, which is different by one step, and no error of more than two steps occurred. The time difference between the generation of each reflected wave is small at 20 μm or less because the interface 3 and 4 are extremely close, and it is difficult to see changes in the waveform shape, which may be the reason for the low accuracy. 40 μm, as shown in **Figure 4.41**, the characteristics of the interference were greatly expressed at around 0.5 μs, which may be the reason for the high accuracy of the evaluation. This is considered to be the reason for the high accuracy of the evaluation.

Furthermore, k-fold cross-validation was applied by dividing the 50 acquired ultrasonic measurement data into 10 parts. k-fold cross-validation results showed an average accuracy of 0.84 for the specimens used in this study. A possible reason for the improved accuracy compared to the evaluation of the coating thickness on the backside of a single steel plate is that the narrower range

of measurement positions results in a smaller variation of the coating thickness on the faying surfaces.

4.7. Summary

In this chapter, the quantitative evaluation of the distribution of contact pressure and the coating thickness of inorganic zinc-rich paint was considered in order to evaluate the faying surface contact condition, which is uncertain influential parameters in bolted joints. The slip coefficient acting on the faying surface should be considered based on the distribution of the contact pressure. In the case of a bolted joint where a bolt axial force of 205kN was introduced, it was confirmed that the slip coefficient according to the distribution of contact pressure governed the slip resistance. If slip coefficients can have variation with contact pressure, slip resistance will be affected by such effect. Identification of contact pressure distribution is important for structural performance of bolted joints. Therefore, there is a need to establish a method to evaluate the distribution of contact pressure. The importance of evaluating the faying surface contact condition was confirmed.

The contact pressure of the bolted joint was evaluated according to the level of bolt axial force. The evaluation of unpainted bolted joints was difficult. However, when the surface is coated with inorganic zinc-rich paint, the conditions for ultrasonic measurement are different because the inorganic zinc-rich paint flows into the area with low contact pressure. The signal transmitted through the faying surface was investigated by the two-probe method using ultrasonic waves. As a result, a large signal was observed around the bolt, while no contact was observed in other. The results of the analysis and the experiment were in almost same, indicating that there may be a correlative relationship between the intensity of the steel adhesion and the transmitted ultrasonic waves. In addition, it was found that the distribution of contact pressure could be evaluated.

The determination of the slip coefficient of a bolted joint is determined by the faying surface contact condition. Therefore, in this chapter, a method is developed to evaluate coating thickness of high-strength bolted joint faying surfaces coated with inorganic zinc-rich paints by ultrasonic measurement with the application of machine learning. Measurements were conducted on specimens with five different coating thicknesses reproduced in the experiment. The ultrasonic measurement from the steel plate surface focused on a group of reflected waves generated during

the time when the ultrasonic waves make a single round trip on the measurement side of a single plate, and machine learning with random forests was applied to evaluate the coating thickness on the backside of steel plate and the faying surface.

When 10 MHz ultrasonic waves are used to evaluate target coating thickness, the larger the coating thickness, the higher the evaluation accuracy tends to be, and for coating thicknesses of 20 μm or less, changes in waveform shape are unlikely to be apparent. In addition, the evaluation method studied in this study has the potential to be applied regardless of the plate thickness of bolted joints by acquiring coating thickness training data using steel plates of arbitrary thickness.

In order to construct a simpler method for evaluating coating thickness, an ultrasonic measurement method that applies machine learning based on the shape of the raw waveforms was attempted. However, further improvement of the accuracy requires the extraction of characteristic signals by signal processing.

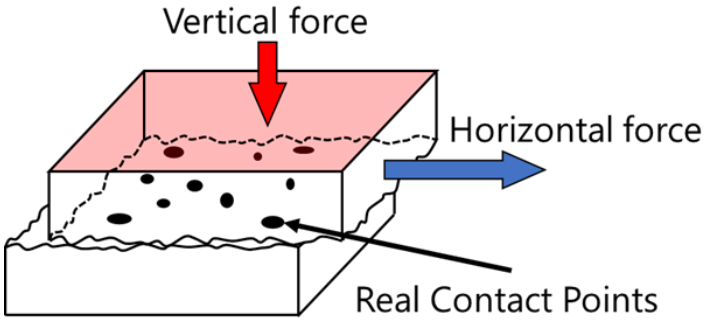

Figure 4.1 Solid surface and real contact points

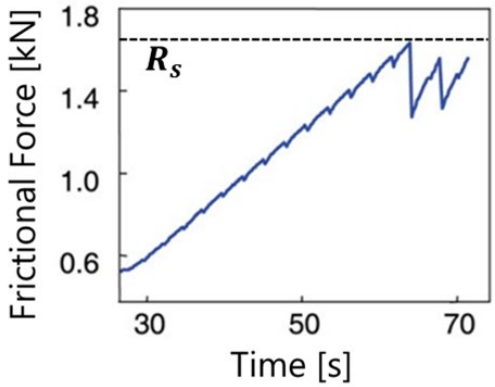

Figure 4.2 Occurrence of local slip (Relationship between frictional force and time)

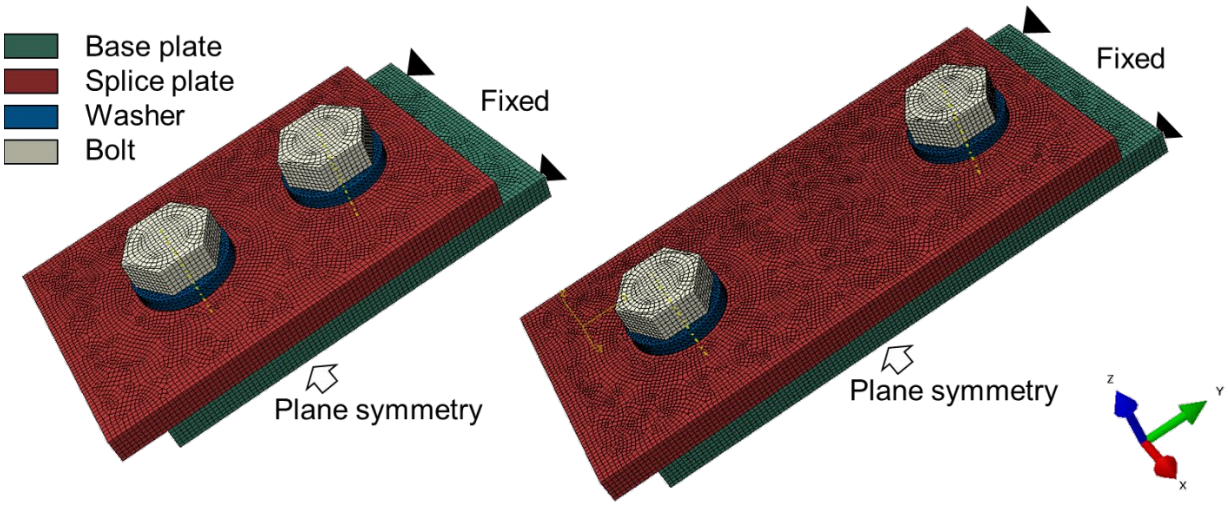

(a)$p = 75mm$ (b) $p = 144mm$

Figure 4.3 Bolt tightening analysis model

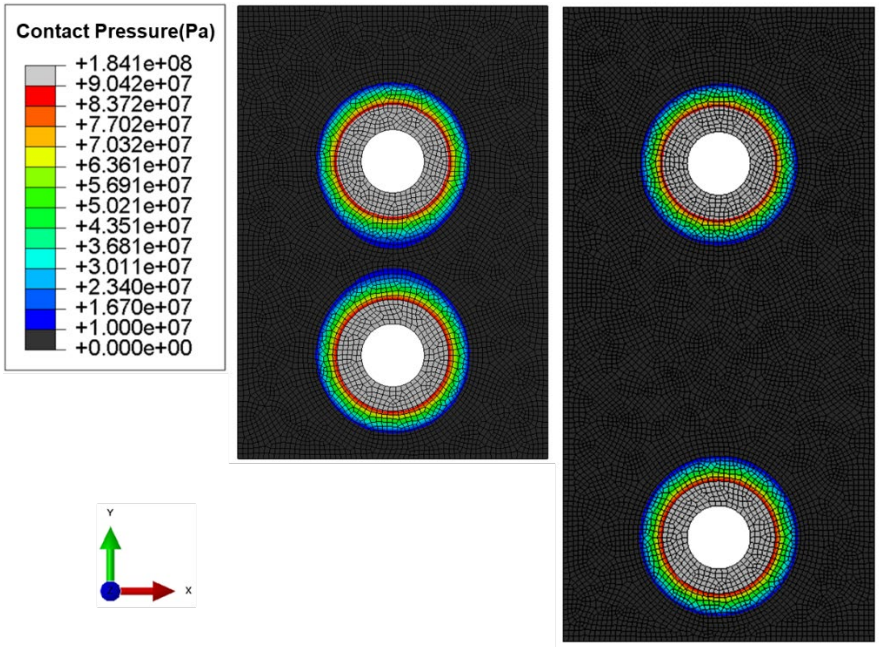

(a)$p = 75mm$ (b) $p = 144mm$

Figure 4.4 Distribution of contact surface pressure in faying surface of the base plate

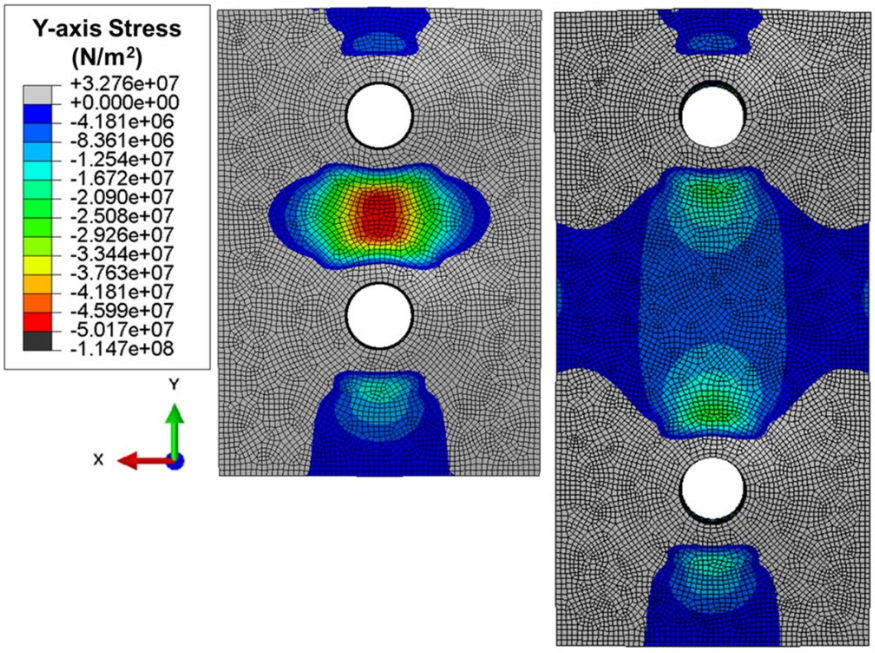

(a) $p = 75mm$ (b) $p = 144mm$

Figure 4.5 Stress distribution in the load direction on faying surface of the splice plate

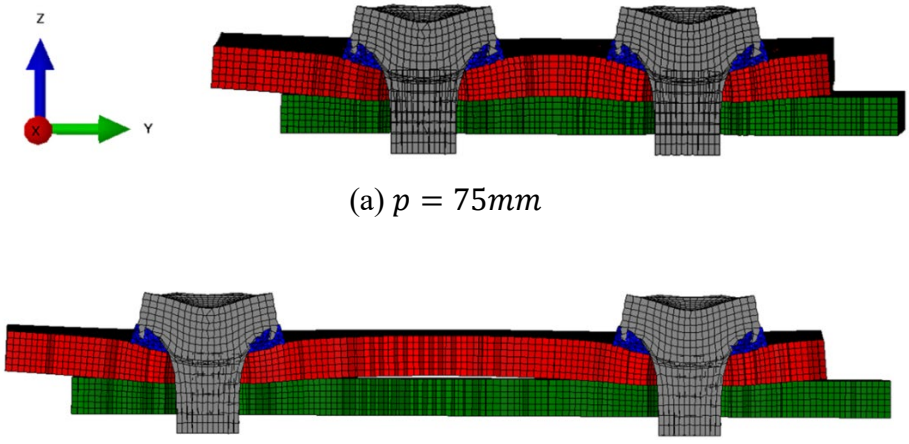

(a) $p = 75mm$

(b) $p = 144mm$

Figure 4.6 Deformed shape of splicing plate due to introduction of bolt axial force (Deformation magnification ×200)

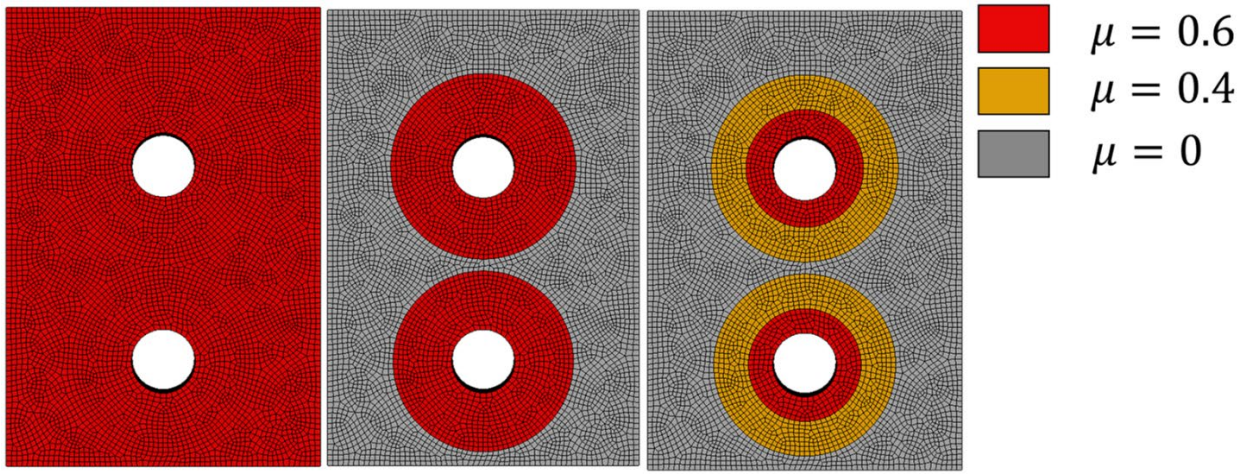

(a) Case 1 (b) Case 2 (c) Case 3

Figure 4.7 Slip coefficient distribution map of the study case

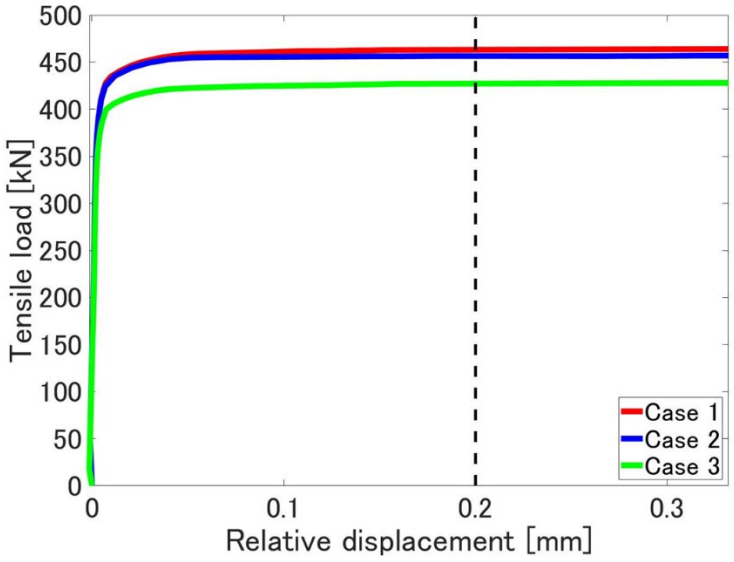

Figure 4.8 Comparison of slip resistance between the conventional method and the method that reproduces the actual state

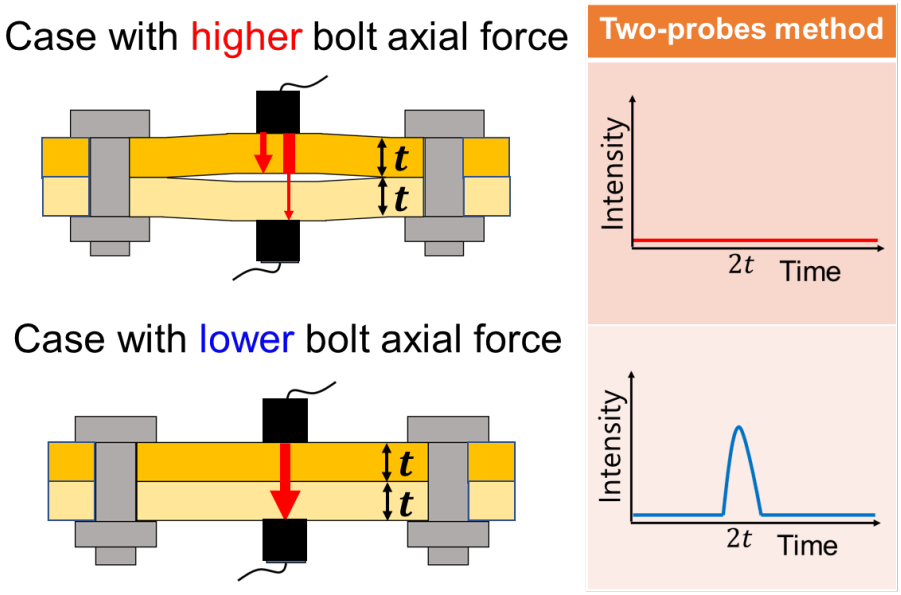

Figure 4.9 Ultrasonic characteristic theory assumed from the analysis results of this study

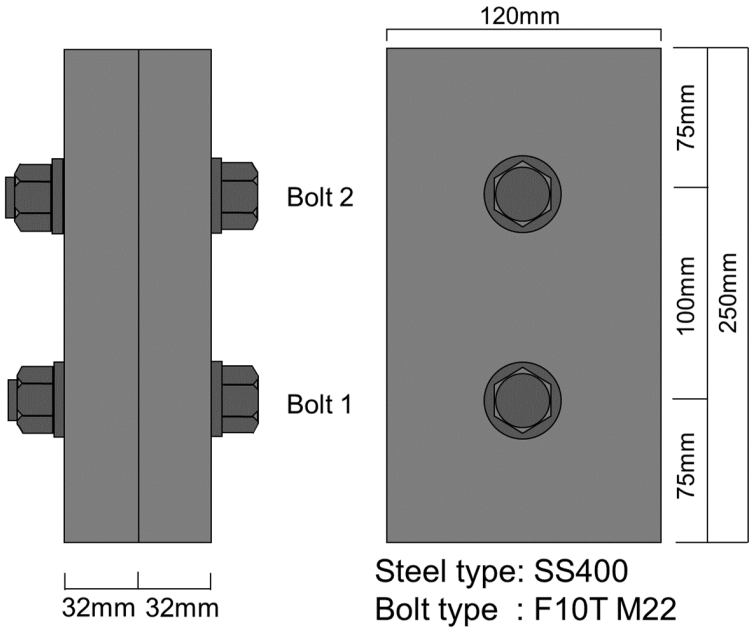

Figure 4.10 Outline of mill scale specimen

Table 4.1 Ultrasonic characteristics

Pulse type	Rectangle burst
Pulse frequency	5 waves
Damping resistance	100Ω
Sampling frequency	100MHz

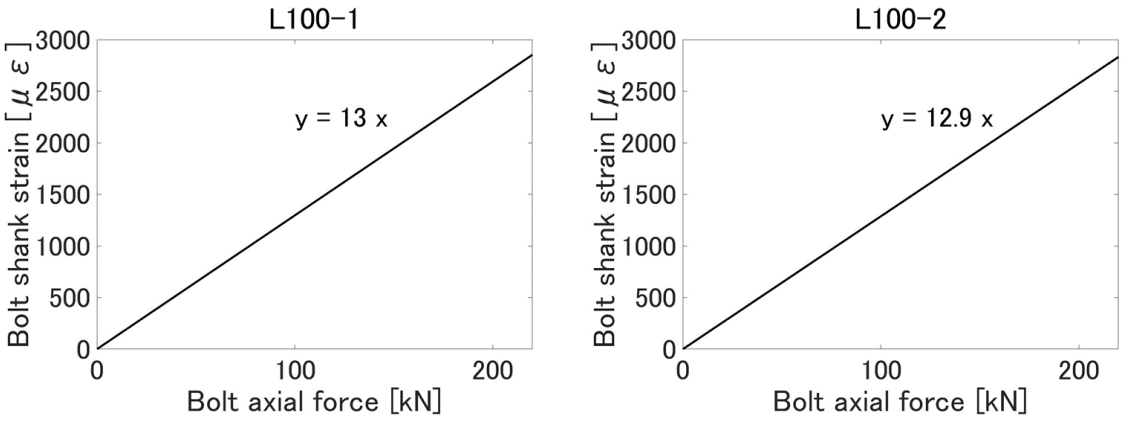

(a) Bolt 1 (b) Bolt 2

Figure 4.11 Results of bolt axial force calibration with a bolt length neck of 100 mm

Table 4.2 Mechanical properties and torque coefficient values of bolts used

Test piece				Product		Torque coefficient
Strength [N/mm2]	Yield strength [N/mm^2]	Stretch [%]	Aperture [%]	Tensile load [kN]	Hardness HRC	
1061	1104	22	69	335	35	0.137

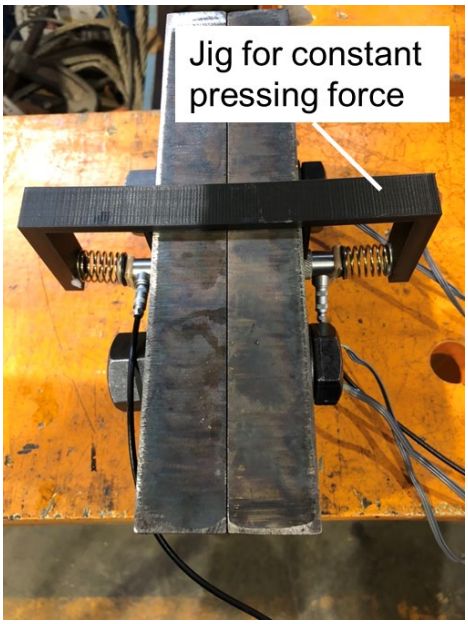

Figure 4.12 State of ultrasonic measurement experiment

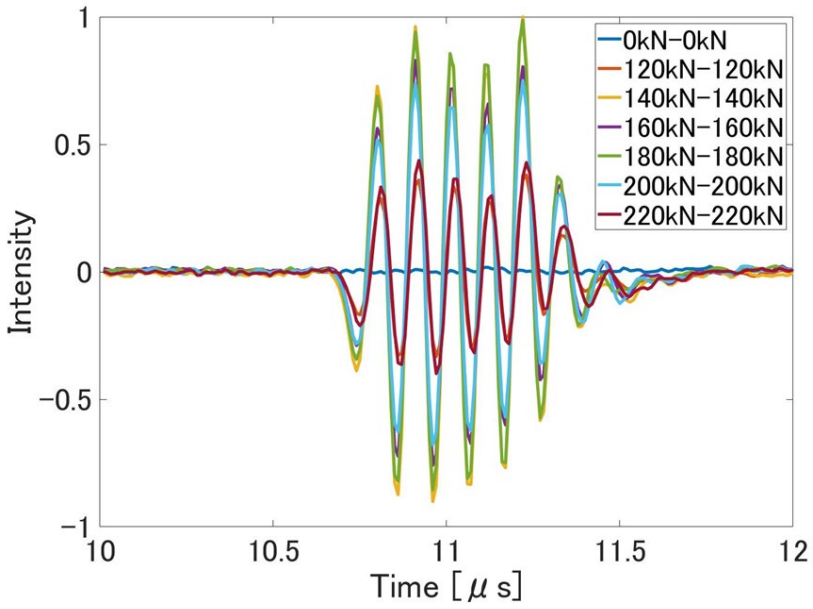

Figure 4.13 Raw waveforms at each bolt axial force level

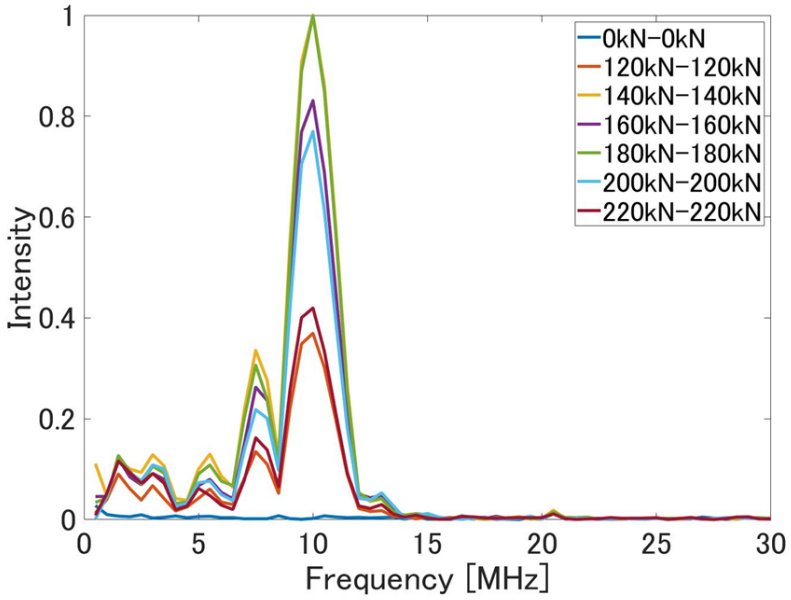

Figure 4.14 Frequency bands at each bolt axial force level

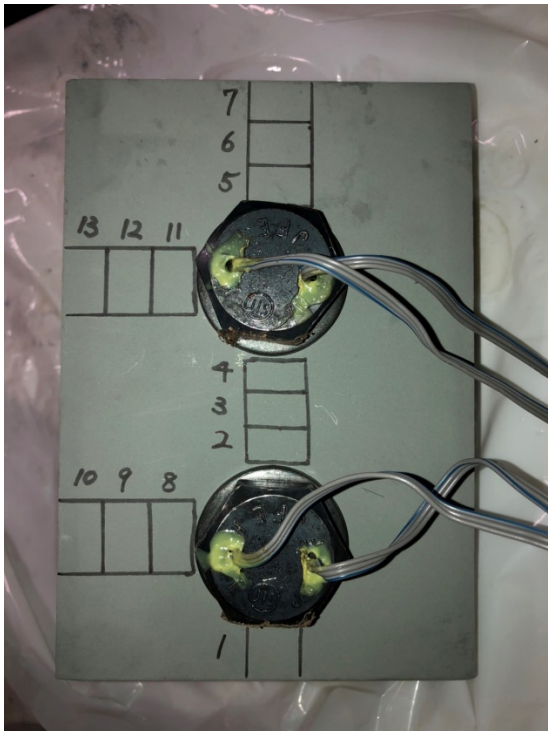

Figure 4.15 Specimen for evaluation of faying surface contact condition

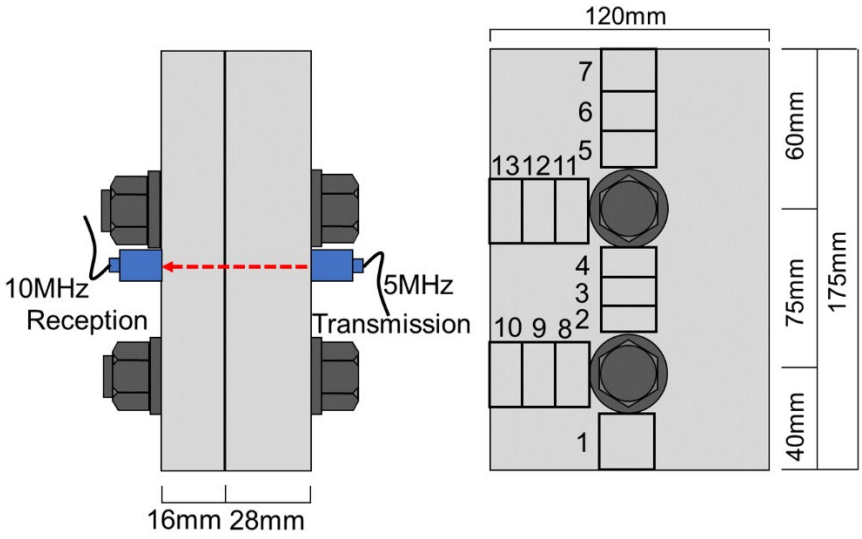

Figure 4.16 Measurement points and measurement methods

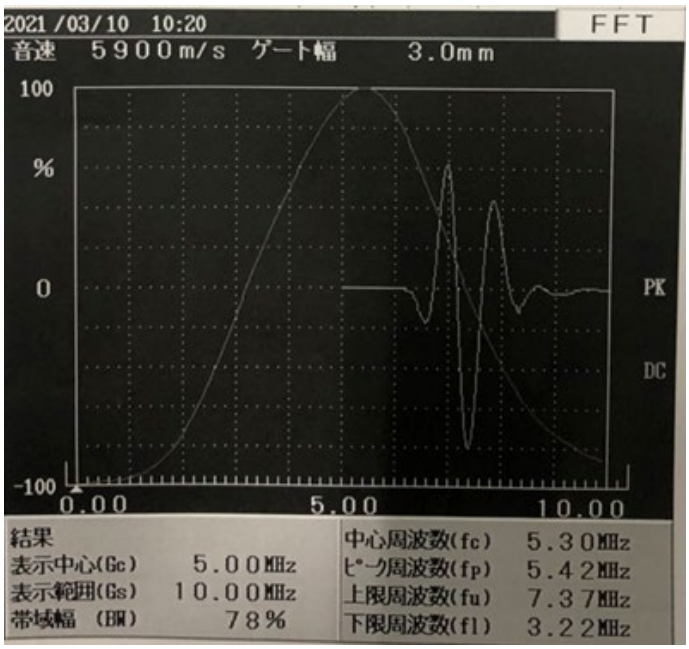

Figure 4.17 Frequency characteristic of 5MHz wide band probe

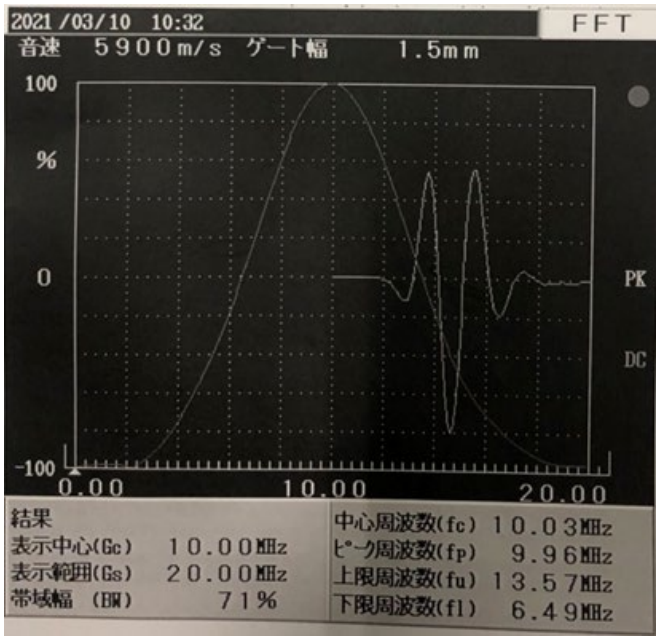

Figure 4.18 Frequency characteristic of 10MHz wide band probe

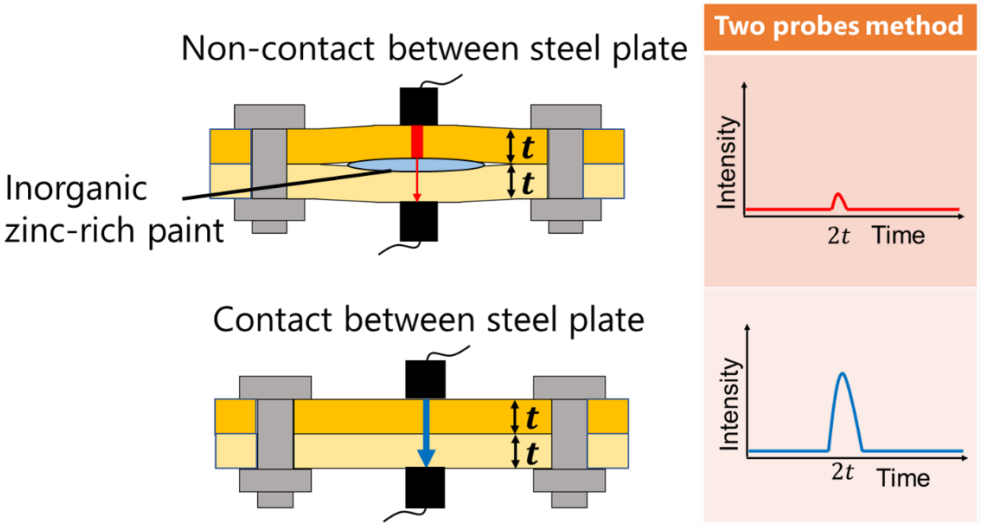

Figure 4.19 Ultrasonic measurement when inorganic zinc-rich paint is applied to the faying surface

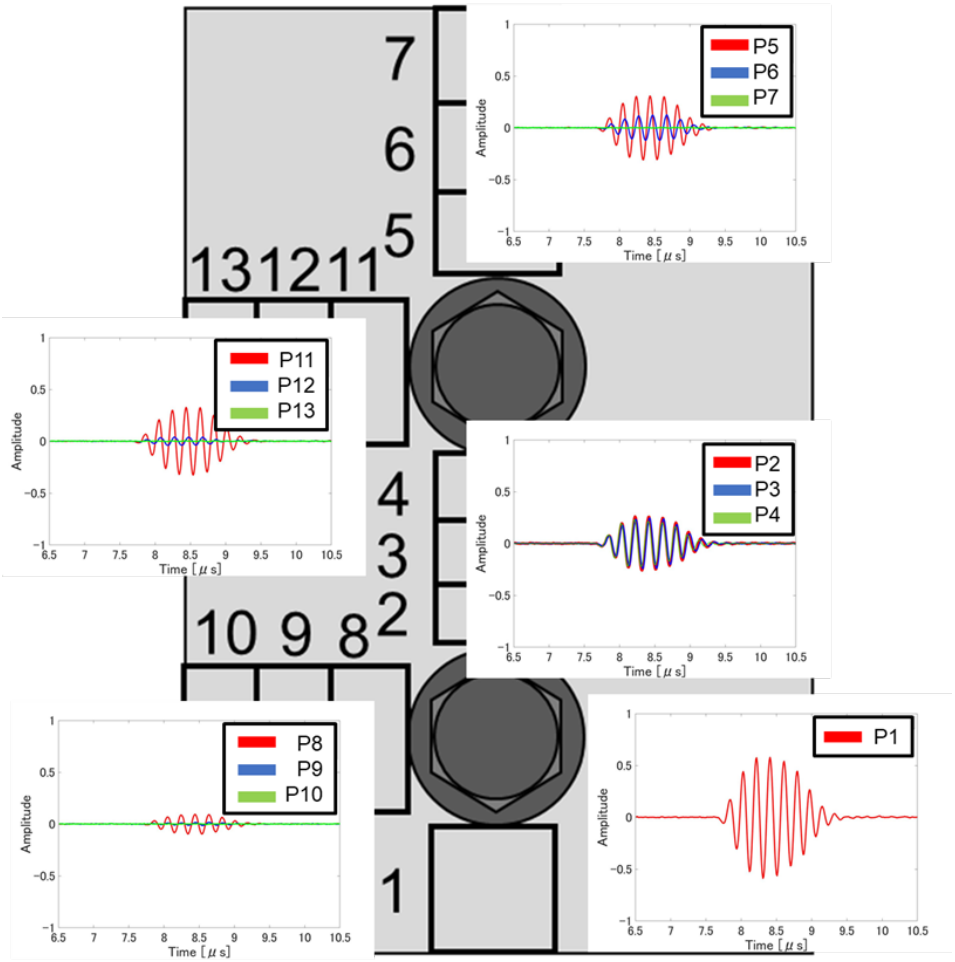

Figure 4.20 Raw waveform data at each measurement point

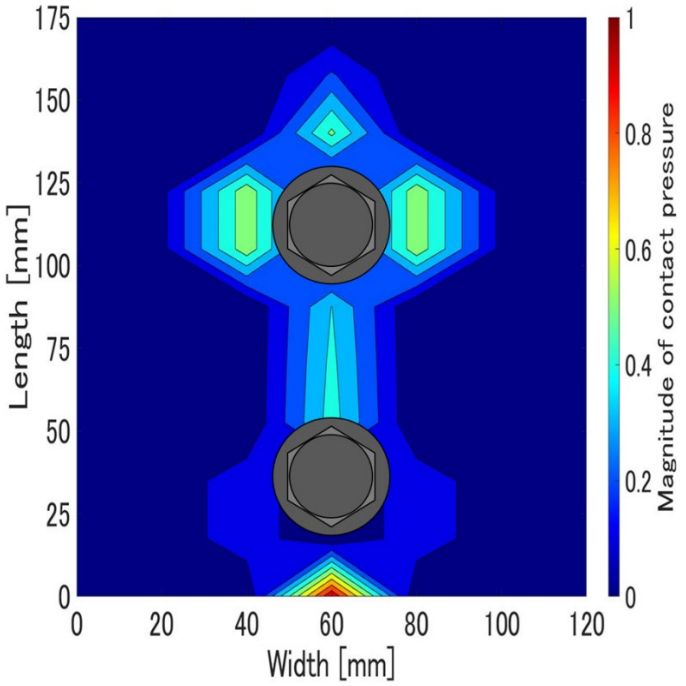

Figure 4.21 Two-dimensional contour diagram of contact pressure

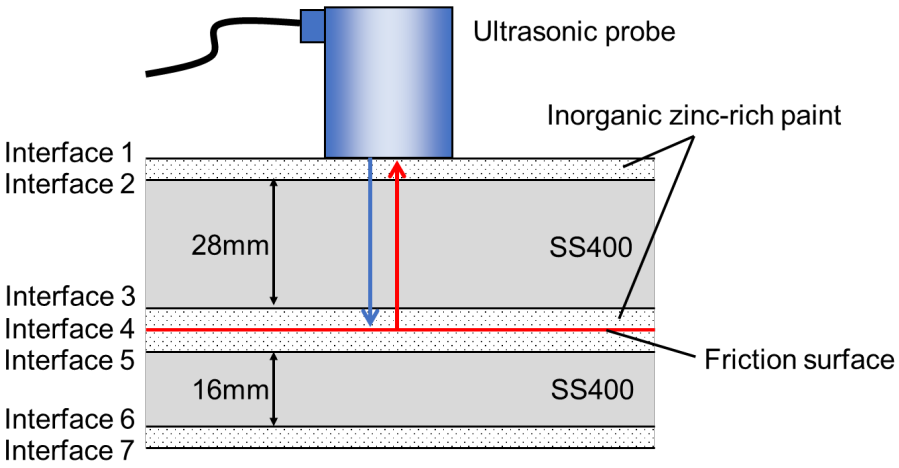

Figure 4.22 Ultrasonic transmission and reception for evaluation of coating thickness on faying surface

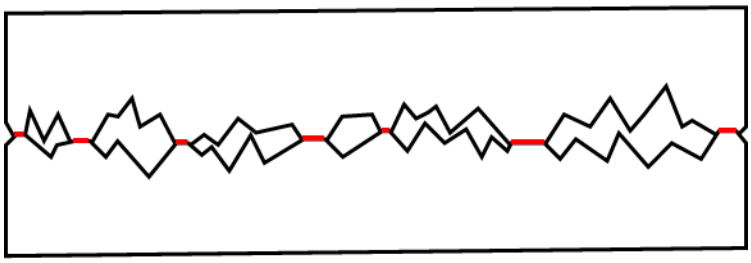

Figure 4.23 Image of true contact area based on tribology

Table 4.3 Ultrasonic pulser receiver setting value

Item	Specifications
Pulse type	Rectangle burst
Pulse voltage	50[V]
Pulse frequency	10[MHz]
Number of pulse waves	5 waves
Damping resistance	100[Ω]
Chirp ratio	100[%]
Resolution capacity	10[bit]
Sampling rate	100[MS/s]

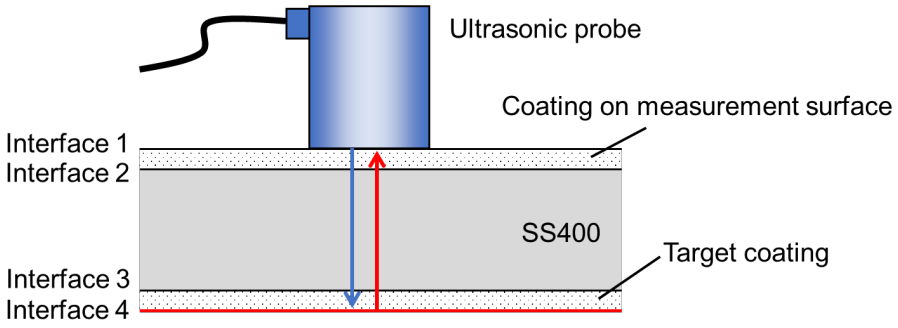

Figure 4.24 Ultrasonic measurement on a single plate

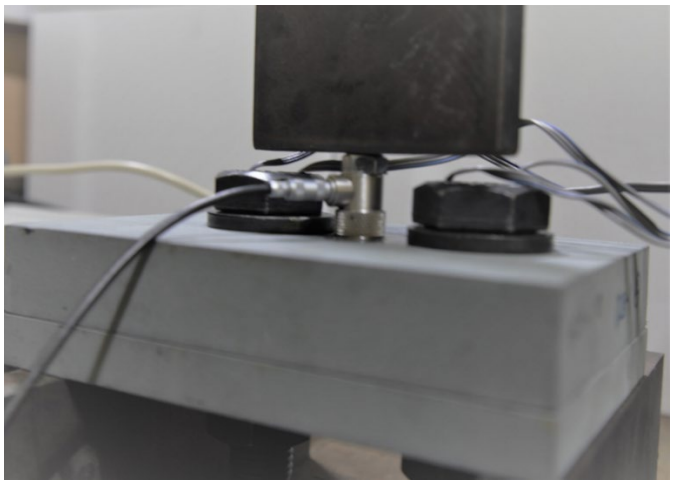

Figure 4.25 Ultrasonic measurement with constant pushing force of the probe

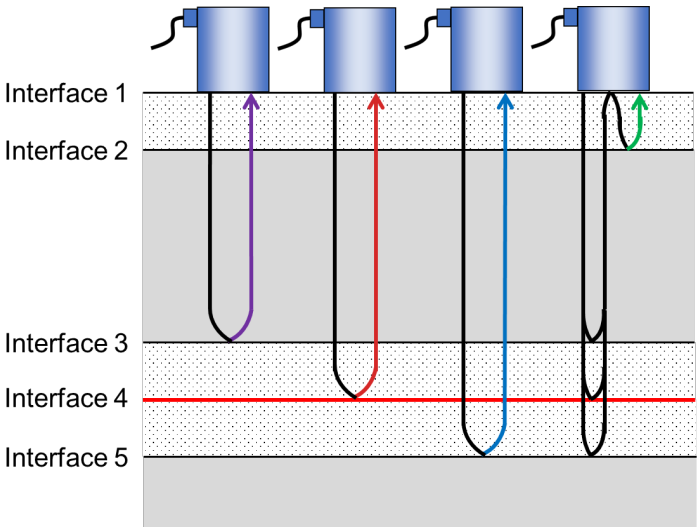

Figure 4.26 Reflected waves that are expected to be superposed of reflected waves from interface 4

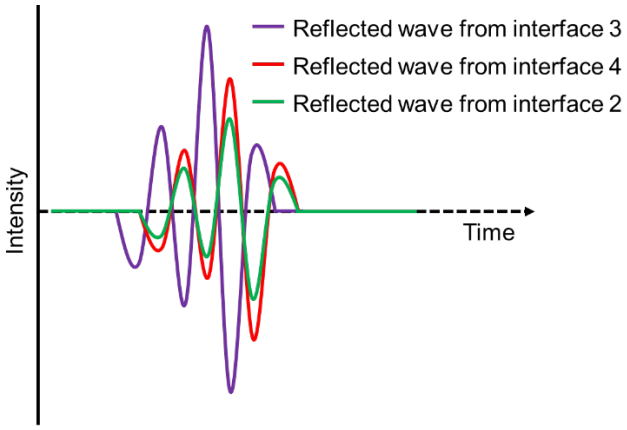

Figure 4.27 Image of superposition of reflected waves

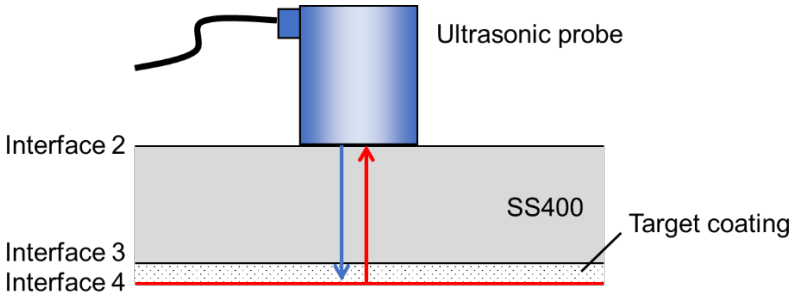

Figure 4.28 Ultrasonic measurement on a single plate (without coating on measurement surface)

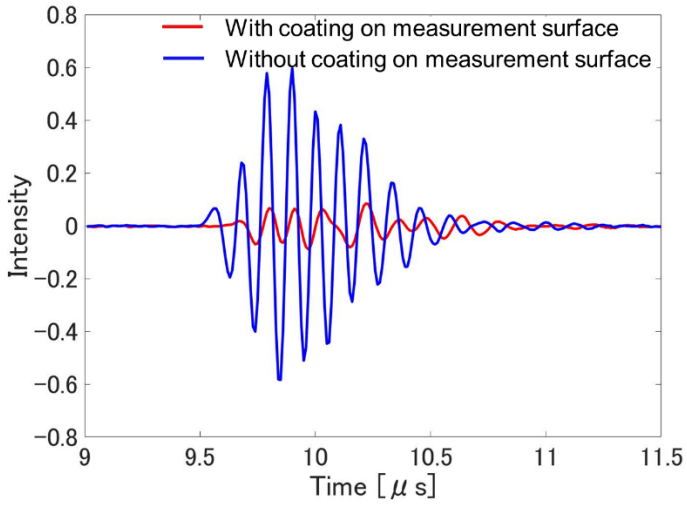

Figure 4.29 Comparison of target waveforms with and without target coating on the measurement surface

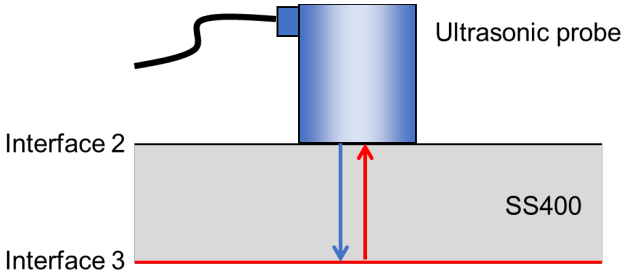

Figure 4.30 Ultrasonic measurement of a single plate without target coating

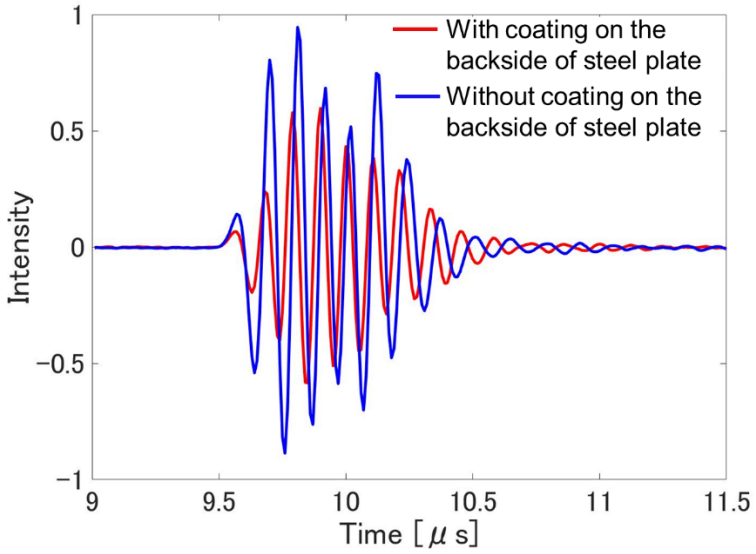

Figure 4.31 Comparison of target waveforms with and without target coating on the backside of steel plate

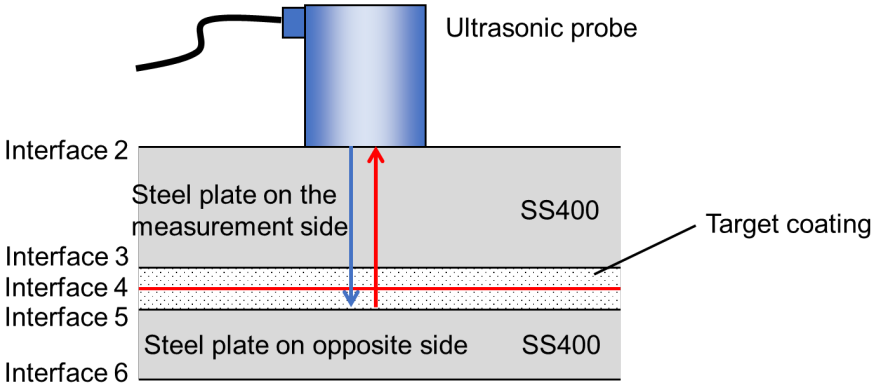

Figure 4.32 Ultrasonic measurement of two plates without coating on the measurement surface

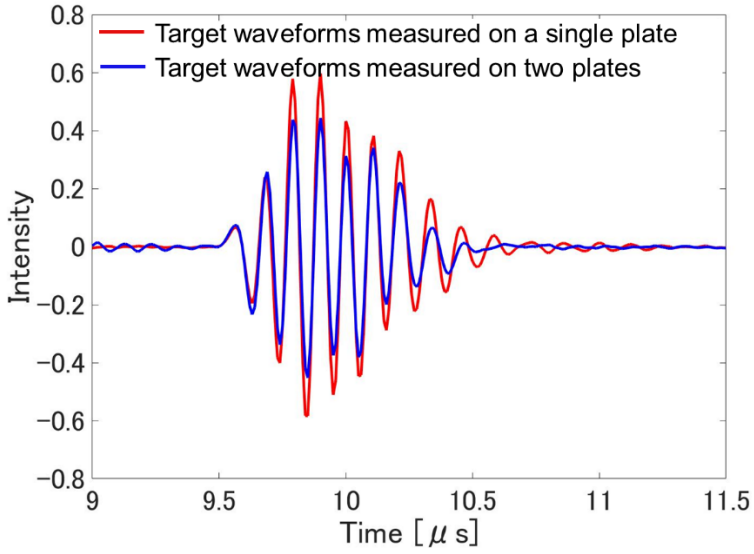

Figure 4.33 Comparison of target waveforms measured on a single plate and two plates

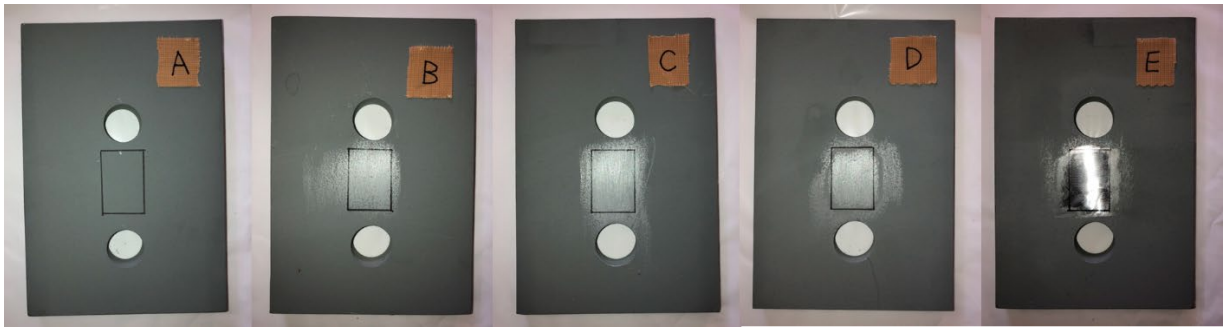

Figure 4.34 Condition of backside of steel plate and faying surface for each study case

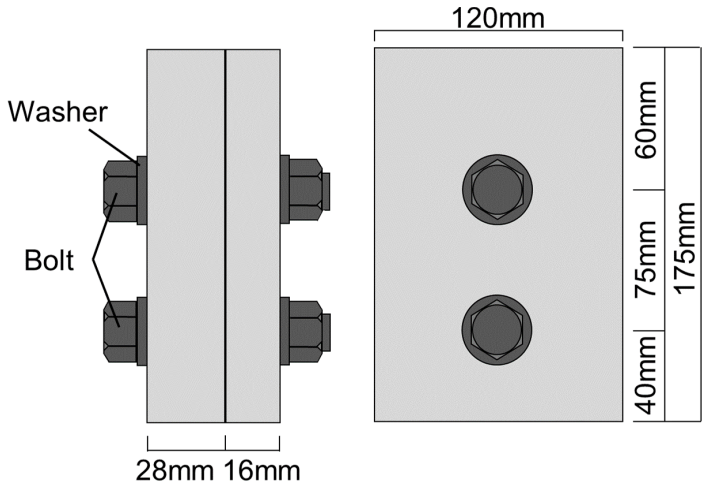

Figure 4.35 Overview of specimens for evaluation of coating thickness on faying surface

Figure 4.36 Contact type electromagnetic coating thickness meter

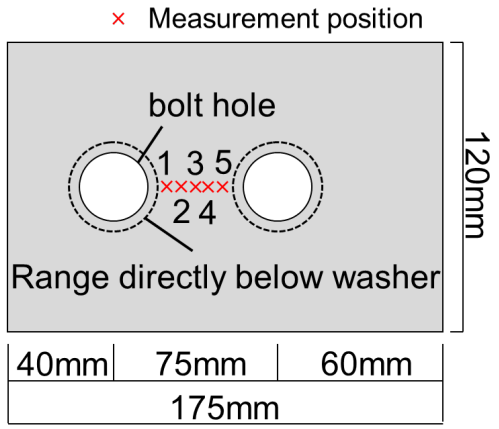

Figure 4.37 Coating thickness measurement position

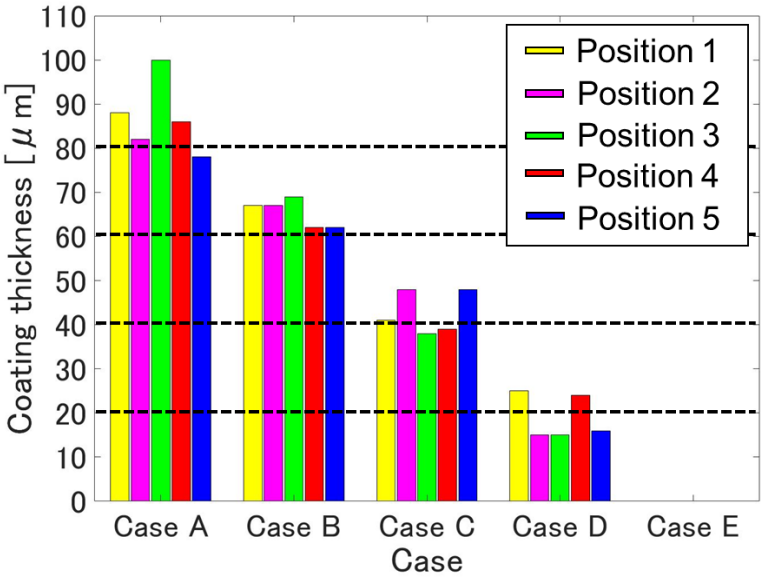

Figure 4.38 Coating thickness of 28 mm steel plate

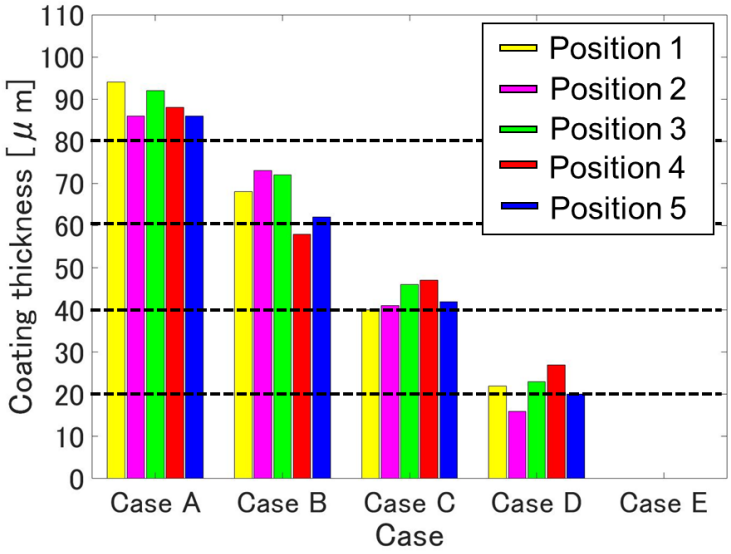

Figure 4.39 Coating thickness of 16 mm steel plate

Table 4.4 Mechanical properties of the specimen

Specimen	Steel type	Yield stress [N/mm^2]	Tensile strength [N/mm^2]
28 mm steel plate	SS400	286	437
16 mm steel plate		267	423

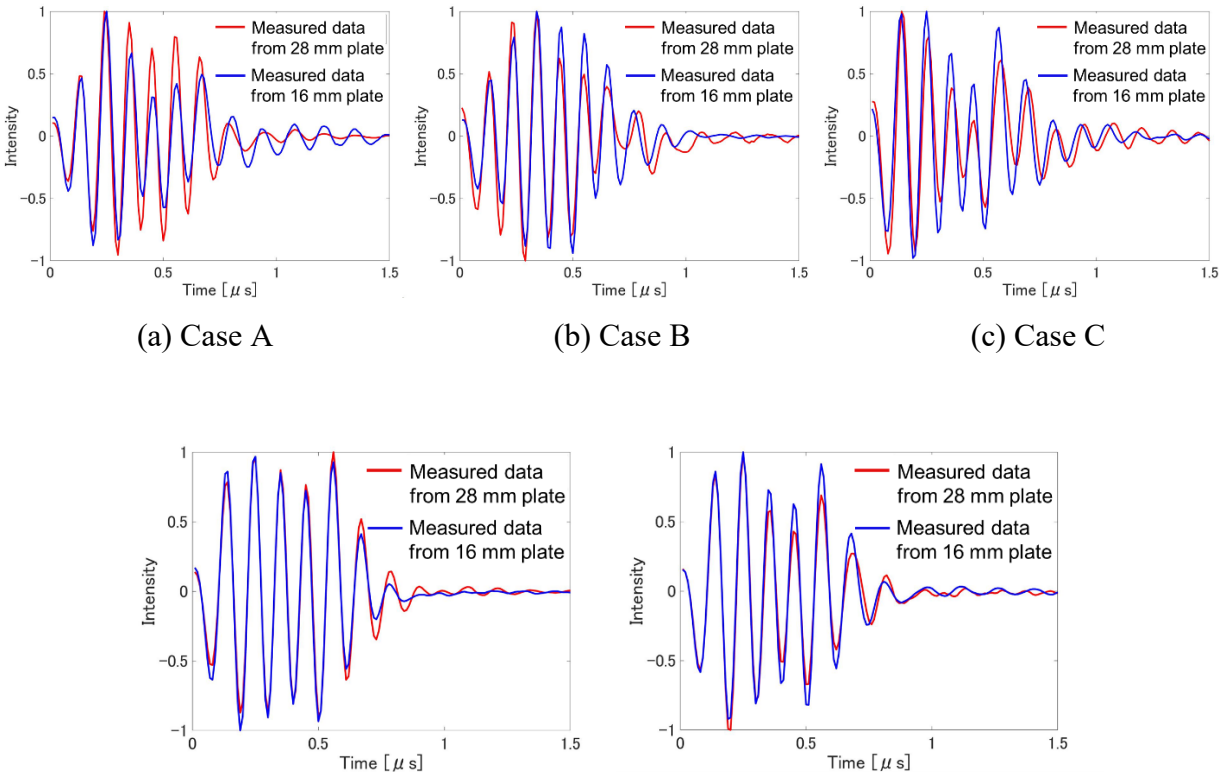

Figure 4.40 Comparison of normalized target waveforms obtained from a single plate

Table 4.5 Accuracy of the evaluation of the coating thickness on the backside of steel plate

Predicted value [μm]	Testing data				
	80μm [%]	60μm [%]	40μm [%]	20μm [%]	0μm [%]
80	100	8	0	0	0
60	0	92	12	0	0
40	0	0	60	9	0
20	0	0	0	55	44
0	0	0	28	36	56

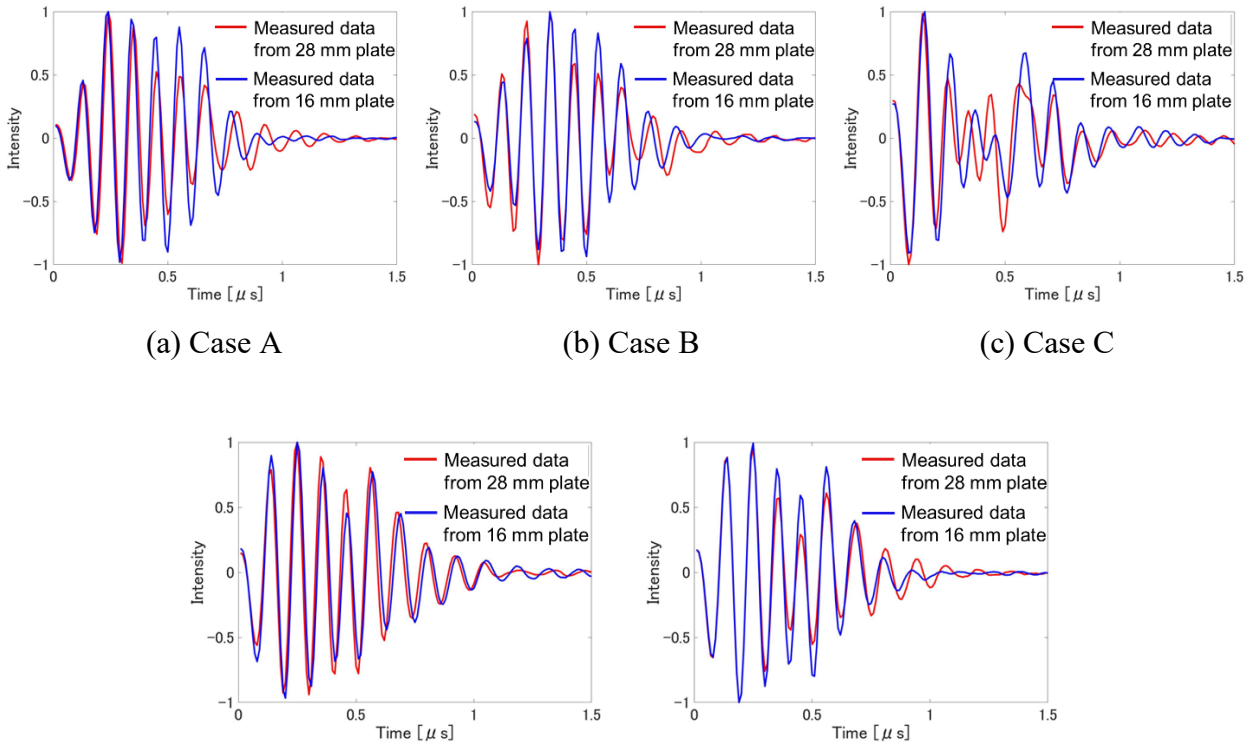

(a) Case A (b) Case B (c) Case C

(d) Case D (e) Case E

Figure 4.41 Comparison of normalized target waveforms obtained from 28 mm and 16 mm steel plates

Table 4.6 Accuracy of coating thickness evaluation of bolted joint faying surfaces

Predicted value [μm]	Testing data				
	80μm [%]	60μm [%]	40μm [%]	20μm [%]	0μm [%]
80	88	18	0	0	0
60	12	82	0	0	0
40	0	0	100	0	0
20	0	0	0	60	26
0	0	0	0	40	74

References (Chapter 4)

[1] Hutchings, I.M.: Leonardo da Vinci's studies of friction, *Wear An International Journal on the Science and Technology of Friction*, Lubrication and Wear, pp.51-66, 2016.

[2] Desplanques, Y.: Amontons-Coulomb Friction Laws, A Review of the Original Manuscript, *SAE International Journal of Materials and Manufacturing*, Vol.8, No.1, pp.98-103, 2015.1.

[3] Rubinstein, S.M., Cohen, G. and Fineberg, J.: Contact Area Measurements Reveal Loading-History Dependence of Static Friction, *Physical Review Letters*, Vol.96, No.25, pp.1-4, 2006.7.

[4] Rubinstein, S.M., Cohen, G. and Fineberg, J.: Dynamics of Precursors to Frictional Sliding, Physical Review Letters, Vol.98, No.22, pp.1-4, 2007.6.

[5] Matsukawa, H., Otsuki, M. and Nakano, K.: Breakdown of Amontons' Law and the Appearance of New Friction Law due to Local Precursor Slip, *The Surface Science Society of Japan*, Vol.36, No.5, pp.222-229, 2015.

[6] Matsukawa, H.: Physics of Friction, *The Surface Science Society of Japan*, Vol.24, No.6, pp.328-333, 2003.

[7] Minami, K., Mori, T. and Sugiya, T.: 摩擦面の状態が高力ボルト継手のすべり耐力に及ぼす影響, *JSCE* 第 59 回年次学術講演会, I-587, pp.1171-1172, 2004.9.

[8] Nishimura, N., Akiyama, H. and Kamei, Y.: Trend of Studies on High-Strength Friction Grip Bolt Joint, *Journal of the JSCE*, No.675, I-55, pp.1-14, 2001.4.

[9] Yamada, T., Kamei, Y., Nishimura, N. and Akiyama, H.: ジンクリッチペイントを塗布した高力ボルト摩擦接合継手の引張試験, *JSCE* 関西支部年次学術講演会講演概要集, I_109, 2000.6.

[10] Mori, N., Matsuda, N. and Kusaka, T.: Effect of Interfacial Adhesion on the Ultrasonic Interaction with Adhesive Joints: A Theoretical Study Using Spring-Type Interfaces, *The Journal of the Acoustical Society of America*, Vol.145, No.6, pp.3541-3550, 2019.6.

[11] Jerome, T.W., Shepherd, M.R. and Hambric, S.A.: Ultrasonic investigation of the pressure profile on the faying surface of fastened aluminum plates, *Mechanical Systems and Signal Processing*, Vol.150, pp.2-21, 2021.3.

[12] Minami, K., Tamura, H., Tsutsui, K., Fujino, D., Shirahata, H., Uchida, D. and Yoshioka, N.: A Study on Calibration tests for High Strength Bolts, Journal of Structural Engineering, A, Vol.67, pp.273-281, 2021.3.

[13] Murayama, R. Ayaka, K., Yamauchi, K. and Yoshida, K.: Harmonic Frequency Components Detection by a Guide Wave type Electromagnetic Acoustic Transducers [EMATs], Journal of Solid Mechanics and Materials Engineering, Vol.2, No.4, pp.437-444, 2008.

[14] Saitoh, T., Furuta, Y., Hirose, S. and Nakahata, K.: Simulation of Higher Harmonics on Nonlinear Ultrasonic Testing Using Convolution Quadrature Time-Domain Boundary Element Method in 2-D Elastodynamics, Journal of Japan Society of Civil Engineers, Ser. A2 (Applied Mechanics), Vol.67, No.2, pp.I_161-I_169, 2011.

[15] Tamura, H., Minami, K., Yoshioka, N., Uchida, D., Moro, M., Hama, T. and Hirao, K.: Applicability of Pretensioned Bolted Joints Including Different Contact Faces, *Journal of JSCE A1 (Structural Engineering & Earthquake Engineering)*, Vol.76, No.2, pp.255-274, 2020.4.

[16] Ishihara, Y., Kobayashi, G., Minada, O. and Nishimura, N.: Characteristic Investigation and Cyclic Slip Experiment of HSFG Bolted Joints Which were Damaged by Earthquake, *Journal of the JSCE A1*, No.745, I-65, pp.53-64, 2003.10.

[17] Mori, T., Minami, K., Inokuchi, S. and Yamaguchi, T.: Slip Coefficient and Contact Surface Condition of Friction Type of High Strength Bolted Connections, *Journal of JSCE A*, Vol.64, No.1, pp.48-59, 2008.1.

[18] 日本道路協会: 道路橋示方書・同解説-II鋼橋・鋼部材編, 2017.11.

[19] 土木学会: 鋼・合成構造標準示方書 総則編・構造計画編・設計偏 2016 年制定, 2016.8.

[20] Manifacier, J. C., Gasiot, J. and Fillard, J. P.: A Simple Method for the Determination of the optical constants n, k and the Thickness of a Weakly Absorbing Thin Film, *J. Phys. E: Sci. Instrum.*, Vol.9, No.11, pp.1002-1004, 1976.

[21] Sugaya, I.: Measurement of Paints-Thickness by Electromagnetic Meter, *Journal of the Surface Finishing Society of Japan*, Vol.28, No.11, pp.540-544, 1981.

[22] Yuuki, H.: Measurement of Coating Thickness by Eddy Current Equipment, *Journal of the Surface Finishing Society of Japan*, Vol.40, No.2, 1989.

[23] Hamada, S., Awai, K., Yamamoto, K. and Hirata, M.: Infrared Thickness Sensor of Paint Film, *Tetsu-to-Hagane, ISIJ*, Vol.70, No.16, pp.2289-2293, 1984.

[24] Zhao, Y., Lin, L., Li, X. M. and Lei, M. K.: Simultaneous determination of the coating thickness and its longitudinal velocity by ultrasonic nondestructive method, *NDT & E International*, Vol.43, No.7, pp.579-585, 2010.10.

[25] Tohmyoh, H. and Suzuki, M.: Measurement of the coating thickness on the back side of double-sided coated structures by means of acoustic resonant spectroscopy, *Surface and Coatings Technology*, Vol.204, No.4, pp.546-550, 2009.

[26] Tohmyoh, H. and Suzuki, M.: Precise measurement of thickness of thin coating at the back side of steel structure by utilizing acoustic resonant phenomenon, *The Proceedings of Autumn Conference of Tohoku Branch*, pp.115-116, 2009.9.

[27] Tohmyoh, H., Sunaga, T. and Suzuki, M.: Simultaneous observation of acoustic resonance phenomena at both surfaces of a plate coated with thin layers, *Review of Scientific Instruments*, Vol.83, No.3, 2012.3.

[28] Tohmyoh, H., Sunaga, T. and Suzuki, M.: Measurement of coating thickness utilizing acoustic resonance phenomenon: On the comparison of ultrasonic transducers, *Journal of JSNDI*, Vol.61, No.11, pp.597-604, 2012.

[29] Sunaga, T., Tohmyoh, H. and Suzuki, M.: Measurement of acoustic properties of coating on steel plate by acoustic resonant spectroscopy and imaging of distribution of coating thickness, *The Proceedings of the Materials and Mechanics Conference JSME*, 2012.9.

[30] Tsuji, Y., Hirokane, M. Hayashi, I. and Konishi, H.: Anal-ysis of characteristics for diagnosing axial force of high-strength bolts, *Journal of JSCE, Ser.F6*, Vol.72, No.2, pp.I_177-I_182, 2016.

[31] Kawashima, K.: ものづくりのための超音波非破壊材料評価・検査, 養賢堂, 2009.3.

[32] Okamoto, J., Nakayama, K. and Sato, M.: トライボロジー入門, 幸書房, 2014.3.

[33] Breiman, L.: Random forests, *Machine Learning*, Vol.45, No.1, pp.5-32, 2001.4.

[34] Breiman, L.: Bagging predictors, *Machine Learning*, Vol.24, pp.123-140, 1996.

[35] Wang, Y., Yan, J., Yang, Z., Wang, J. and Geng, Y.: A novel 1DCNN and domain adversarial transfer strategy for small sample GIS partial discharge pattern recognition, *Measurement Science and Technology*, Vol.32, No.12, 2021.

[36] Kohavi, R.: A study of cross-validation and bootstrap for accuracy estimation and model selection, *Proceedings of the 14th IJCAI*, pp.1137-1145, 1995.

[37] Yadav, S. and Shukla, S.: Analysis of k-fold cross-validation over hold-out validation on colossal datasets for quality classification, *2016 IEEE 6th International Conference on Advanced Computing (IACC), Bhimavaram*, pp.78-83, 2016.2.

Chapter 5
Conclusions and Recommendations

5.1. Conclusions

For the maintenance of steel structures, it is necessary to accurately evaluate the structural performance of existing high strength friction bolted joints. However, the problem is that the structural performance of existing bolts cannot be accurately evaluated because the bolted joints contain uncertain parameters that affect the structural performance [1-28]. In addition, in recent years, inorganic zinc-rich paint has been applied to the faying surface of bolted joints, which may increase the uncertain influential parameters. Slip resistance [29], which is one of the indices to evaluate the structural performance of bolted joints, is described below:

$$R_s = N_0 \cdot \mu_0 \cdot m \cdot n \quad (5\text{-}1)$$

This equation is determined mainly by the values of the designed bolt axial force N_0 and the slip coefficient μ_0. It is possible that these parameters are decreasing due to the effects of earthquakes and aging, but there is currently no method that can accurately evaluate them. Therefore, in this study, the effects of bolt axial forces, misalignment between washers and bolts, and bolted joint faying surface contact condition on the structural performance of bolted joints were considered analytically. Based on these considerations, a quantitative evaluation method using ultrasonic waves was proposed for bolt axial force and coating thickness on faying surface, which have the greatest influence on the structural performance of bolted joints.

Conclusions of this study are described as follows:

- To clarify the effect of uncertain parameters on the structural performance of bolted joints by numerical analysis

The analysis was conducted assuming actual phenomena that may occur. Firstly, an analysis considering the variation of the bolt axial force was conducted. In the above equation, R_s is determined by the total bolt axial force when the slip coefficient is constant. However, the stress distribution differs depending on the variation of the bolt axial force, which affects the order in which the bolts slip. Secondly, the misalignment of the bolt and washer was considered in the analysis. The results showed that the stresses concentrated in the bolt hole walls and that the distribution was not symmetrical but could be locally uneven. Finally, to clarify the actual faying surface contact condition, the distribution of contact pressure by tightening bolts was confirmed.

Based on the distribution, an analytical model that does not generate frictional force in the area with low contact pressure was considered. As a result, it was shown that the slip resistance may be determined almost entirely by the contact pressure around the bolt. This fact was clarified in the experiments in Chapter 4.

- To propose a non-destructive evaluation method of bolt axial force of bolted joints by applying machine learning

A quantitative evaluation method of bolt axial force, which is an important parameter to evaluate the slip resistance, was proposed. The conventional method of evaluating bolt axial force uses the correlation between bolt elongation and bolt axial force. However, since the performance of each bolt varies, there is still an issue of accuracy. In this study, a method for evaluating the bolt axial force using ultrasonic waves was proposed, focusing on the deformation shape of the bolt head. By applying an original signal processing to the waveform analysis, characteristic signals were extracted from the waveform in the initial time zone with a lot of noise. Furthermore, by combining machine learning, a highly accurate method for evaluating the bolt axial force has been developed.

- To propose an evaluation method for contact pressure distribution and coating thickness of inorganic zinc-rich paint

In Chapter 2, it was shown that most of the actual bolted joints are not in contact with the steel. In order to clarify the problem experimentally, a method using the characteristics of transmitted ultrasonic waves was used. As a result, the effectiveness of the analysis was demonstrated. In the case of unpainted plates with black skin, ultrasonic waves easily penetrated the interface, making it difficult to quantitatively evaluate the intensity of contact pressure. However, when the plate was coated with inorganic zinc-rich paint, the faying surface contact condition was in different condition due to the peeling of the inorganic zinc-rich paint, indicating the possibility of evaluating the contact pressure. In addition, a method for evaluating the thickness of inorganic zinc-rich paint, which is believed to have a direct effect on the slip coefficient, was proposed. In this experiment, a one-probe ultrasonic method was used to measure the thickness of inorganic zinc-rich paint under pressure. A highly accurate evaluation by machine learning was confirmed even in the raw waveform condition. Therefore, the capability to evaluate the coating thickness using ultrasonic waves was demonstrated.

Finally, the numerical analysis considered in Chapter 2 confirms that the most influential uncertain parameters on the slip resistance of bolted joints are the bolt axial force and the slip coefficient. Therefore, in Chapter 3, the method of evaluating bolt axial forces by combining ultrasonic waves, signal processing and machine learning was proposed, and its accuracy was confirmed. Furthermore, in Chapter 4, the combination of ultrasonic waves and machine learning was considered for faying surface contact conditions. First, an attempt was made to evaluate the contact pressure of bolted joints coated with Inorganic zinc-rich paint. Next, an evaluation of the coating thickness on the backside of steel plate and on faying surface was attempted. This study shows the possibility of quantitatively evaluating bolt axial forces and faying surface contact conditions, which are the most important parameters in the evaluation of the structural performance of bolted joints. The results of this study could enable quantitative evaluation of the structural performance of bolts in existing joints in the future, considering uncertain influential parameters.

5.2. Recommendations

Based on the conclusions of this study, the following suggestions are made for more accurate evaluation of the structural performance of high strength bolted friction joints.

I. The bolt axial force and the slip coefficient are important for evaluating the slip resistance. The accuracy of bolt axial force evaluation has been improved in recent years, including the results of this study. On the other hand, the slip coefficient is affected by the faying surface contact condition, which is difficult to measure, so there is still room for further study. However, since this study made it possible to evaluate the contact pressure distribution and the coating thickness of inorganic zinc-rich paint, it is necessary to revise the numerical analysis in the future. In particular, an analysis that represents a realistic contact surface is required. Furthermore, clarification of the deformation performance of inorganic zinc-rich paints, which have been used in recent years, on faying surfaces will enable accurate evaluation of the slip coefficient.

II. The evaluation of the bolt axial force in a bolted joint also remains to be studied. In this study, the ultrasonic waves showed a characteristic signal when the reflecting surface showed curvature. Thus, the evaluation can be made from the fact of the bolt head deformation caused by the introduction of bolt axial force. However, it is not clear how the characteristics of ultrasound reflected by curved surfaces affect the shape of the signal. Therefore, in the future, wave analysis will be carried out in order to clarify the characteristics of the reflected wave when the surface where the ultrasonic wave is as close as possible to the probe has a curvature. Furthermore, the evaluation of bolt axial forces in the case of corroded bolts needs to be considered. In fact, it is necessary to improve the accuracy of evaluating bolt axial force levels that consider the safety factor and other factors. In the future, it is planned to consider bolt axial force levels that should be evaluated in consideration of the safety factor, etc.

III. Slip testing of bolted joints by tensile testing is essential for evaluating the slip coefficient. However, the phenomena occurring on the faying surface may be uncertain and contain a huge amount of information. Since it is difficult to conduct experiments that reproduce all phenomena occurring on faying surfaces, it is desirable to develop machine learning that combines the results of many researchers, including the results of this study.

References (Chapter 5)

[1] Nishimura, A., Taido, Y., Sera, S., Hozumi, S. and Mitani, T.: On the Scattering of Clamping Forces of High-Strength Bolts in Actual Structural Joints, *Proceedings of the JSCE*, No.180, pp.1-9, 1970.8.

[2] Fukuoka, T. and Takai, T.: Mechanical Behaviors of Bolted Joint During Tightening Using Torque Control, *JSME International Journal Series A Solid Mechanics and Material Engineering*, Vol.41, No.2, pp.185-191, 1998.

[3] You, R., Ren, L. and Song, G.: A Novel Comparative Study of European, Chinese and American Codes on Bolt Tightening Sequence Using Smart Bolts, *International Journal of Steel Structures*, Vol.20, No.3, pp.910-918, 2020.

[4] Wang, Y.Q., Wu, J.K., Liu, H.B. and Xu, S.T.: Modeling and Numerical Analysis of Multi-Bolt Elastic Interaction with Bolt Stress Relaxation, *Proceedings of the Institution of Mechanical Engineers, Part C: Journal of Mechanical Engineering Science*, Vol.230, No.15, pp.2579-2587, 2015.

[5] Minami, K., Tamura, H., Uchida, D., Shirahata, H., Yoshioka, N., Tsutsui, K. and Fujino, D.: A Study on Initial Value Setting Method for Relaxation Tests in High Strength Bolted Joints, *Journal of JSCE A1 (Structural Engineering & Earthquake Engineering)*, Vol.76, No.3, pp.496-509, 2020.

[6] Abid, M., Khalil, M.S. and Wajid, H.A.: An Experimental Study on the Relaxation of Bolts, *IIUM Engineering Journal*, Vol.16, No.1, pp.43-52, 2015.

[7] Ishihara, Y., Kobayashi, G., Minada, O. and Nishimura, N.: Characteristic Investigation and Cyclic Slip Experiment of HSFG Bolted Joints Which were Damaged by Earthquake, *Journal of the JSCE A1*, No.745, I-65, pp.53-64, 2003.10.

[8] Wang, F., Ho, S.C.M. and Song, G.: Monitoring of Early Looseness of Multi-Bolt Connection: A New Entropy-Based Active Sensing Method Without Saturation, *Smart Materials and Structures*, Vol.28, No.10, pp.1-7, 2019.

[9] Marshall, M.B., Lewis, R., Howard, T. and Brunskill, H.: Ultrasonic Measurement of Self-Loosening in Bolted Joints, *Proceedings of the Institution of Mechanical Engineers, Part C: Journal of Mechanical Engineering Science*, 2011.

[10] Jiang, Y., Zhang, M. and Lee, C.H.: A Study of Early Stage Self-Loosening of Bolted Joints, *Journal of Mechanical Design, Transactions of the ASME*, Vol.125, pp.518-526, 2003.

[11] Tanihira, T., Kamei, M., Ishihara, Y. and Taido, Y.: Carrying Capacity Test for Friction Joint of High-Strength Bolt from a Removed Foot-Way Bridge Used Under 17 Years, *JSCE Journal of Structural Engineering*, Vol.36 A, pp.1087-1096, 1990.3.

[12] Kanou, M., Tanihira, T., Ishihara, Y., Kobayashi, G. and Nishio, H.: 高力ボルト軸力の経年変化に関する実験的研究, *JSCE* 第 56 回年次学術講演会, I-B162, pp.324-325, 2001.10.

[13] Ishihara, Y., Kobayashi, G., Kano, M., Kamei, M. and Tanihira, T.: The Influence of Reduction and Variation of Bolt Tensions by Aging on Limit States of HSFG Bolted Joint, *Journal of JSCE*, Vol.763, VI-63, pp.33-42, 2014.6.

[14] Temitope, S.J.: Condition Monitoring of Bolted Joints, Ph.D. *Thesis, University of Sheffield*, Sheffield, UK, 2015.6.

[15] Rafik, V., Combes, B., Daidié, A. and Chirol, C.: Experimental and Numerical Study of the Self-Loosening of a Bolted Assembly, *Advances on Mechanics, Design Engineering and Manufacturing II*, pp.85-94, 2019.

[16] Kikukawa, S., Murata, K. and Nishimura, A.: Secular Changes of Slip Resistance of Friction-Type Bolted Joints in Structural Members, *Kawasaki Steel Giho*, Vol.11, No.4, pp.127-135, 1979.

[17] Takai, T., Yamaguchi, T. and Yamashina, K.: Analytical Study on Influence of Irregularity on Slip Strength of High Strength Bolted Friction Type Joint, *JSCE Journal of Structural Engineering*, Vol.61 A, pp.605-613, 2015.3.

[18] Takai, T., Peng, X. and Yamaguchi, T.: An Analytical Study on Load Carrying Characteristic of High Strength Bolted Friction Type Joint with Thick Filler Plate, *Journal of JSCE A1 (Structural Engineering & Earthquake Engineering)*, Vol.71, No.1, pp.1-9, 2015.

[19] Tanaka, A., Masuda, H., Wakiyama, K., Tsujioka, S., Hirai, K. and Tateyama, E.: Experimental Study on High Strength Bolted Friction Joints with Oversized and Slotted Holes, *JSSC Steel Construction Engineering*, Vol.5, No.20, pp.35-44, 1998.12.

[20] Mori, T., Yamazaki, N. and Yamaguchi, J.: Slip and Yield Resistance of Friction Type of High Strength Bolted Connections with Over-Sized Holes, *Journal of the JSCE*, No.794, I-72, pp.157-169, 2005.7.

[21] Murakoshi, J., Sawada, M., Yamaguchi, T., Peng, X. and Ootake, A.: Slip Resistance Tests of Friction-Type High-Strength Multi Bolted Joints with Coated Contact Surfaces by Inorganic Zinc Rich Paint on Thick Plate, *Journal of JSCE A1 (Structural Engineering & Earthquake Engineering)*, Vol.70, No.1, pp.94-104, 2014.

[22] Peng, X., Yamaguchi, T., Takai, T., Murakoshi, J. and Sawada, M.: FEA Study on the Slip Behavior of High Strength Multi Bolted Friction Type Joints with Thick Plates by Structural Dimensions, *Journal of JSCE A1 (Structural Engineering & Earthquake Engineering)*, Vol.69, No.3, pp.452-466, 2013.

[23] Kamei, Y., Matsuno, M. and Nishimura, N.: An Analytical Study on Slip Strength of Multi HSFG Bolted Joints in Tention, *Journal of JSCE*, No.640, I-50, pp.49-60, 2000.

[24] Geoffrey, L.K., John, W.F. and John, H.A.S.: Guide to Design Criteria for Bolted and Riveted Joints, Second Edition, *American Institute of Steel Construction, Inc.*, 1987.

[25] Tamura, H., Minami, K., Yoshioka, N., Uchida, D., Moro, M., Hama, T. and Hirao, K.: Applicability of Pretensioned Bolted Joints Including Different Contact Faces, *Journal of JSCE A1 (Structural Engineering & Earthquake Engineering)*, Vol.76, No.2, pp.255-274, 2020.4.

[26] Murakoshi, J., Sawada, M., Yamashina, K., Yamaguchi, T. and Ishihara, D.: Study of Influence on Slip Coefficient of High Strength Bolted Friction Type Joints by Painting Condition and Exposure Term, *Journal of JSCE A1 (Structural Engineering & Earthquake Engineering)*, Vol.73, No.1, pp.40-53, 2017.

[27] Minami, K., Mori, T. and Sugiya, T.: 摩擦面の状態が高力ボルト継手のすべり耐力に及ぼす影響, *JSCE* 第 59 回年次学術講演会, I-587, pp.1171-1172, 2004.9.

[28] Tajima, J.: 高力ボルト摩擦接合概説, 第 2 版, 技報堂, 1966.11.

[29] 日本道路協会: 道路橋示方書・同解説-II鋼橋・鋼部材編, 2017.11.